TECHNISCHE UNIVERSITÄT WIEN
Vienna | Austria

Vienna University of Technology

Master's Thesis

Characterizing influences of specific miRNAs on phenotypic properties of mammalian cells

Lena Anna Leberbauer, Bakk. rer. nat.

Research was performed at the Department of Biochemical and Biomolecular Engineering at
Johns Hopkins University

supervised by
Prof. Dr. Michael J. Betenbaugh

Submitted to the Institute of Chemical, Environmental and Biological Engineering at
Vienna University of Technology

Advisor
Prof. Dr. Christoph HERWIG

March 7, 2017

Acknowledgments

There are a lot of people I need to thank for finishing this thesis. If I missed anyone please do not take it personally but ascribe it to stress.
First I would like to thank my thesis advisor, Prof. Christoph Herwig from the Institute of Chemical, Environmental and Biological Engineering at Vienna University of Technology who never stopped supporting me and who was incredibly patient on my journey to finishing this thesis. Thank you.
Of course I want to thank Prof. Michael J. Betenbaugh from the Department of Biochemical and Biomolecular Engineering at Johns Hopkins University. Thank you for opening the doors to your laboratory for me and giving me the all American experience in every aspect of life.
Regarding US colleagues, I would like to thank Jimmy Kirsch, Joey Priola, Su Xiao, Andrew Chung, Kelley Heffner and Christian Schroeder-Kaas who always had an open ear and a good answer to my many questions. I also want to mention friends I made along the way in the US: Rosie Yujin Wu, Leo Guedes da Silva, Koen Schipper, Sara Schroeder-Kaas, Paul Harry and many more. I will always look back fondly because of all of you.
The support I had back at home in Austria was endless. Of course I want to thank every member of my family who had to endure my many downs throughout the rough phases of this path. And there were many. Sigi, Mona, Christopher, Leni, Thomas, Phil, Berni, Sonja, Manu and so many more. Your time and friendship is absolutely invaluable to me and brings me joy in every life situation.
And last but not least, my love for 9 and best friend for 12 years, Andreas. You have been my rock during this difficult time and you kept me from falling when I struggled. You guided me when I needed guidance and you kept me grounded. You are my lifeline and my safe haven. Thank you for understanding me when no one else did and for loving me.

Declaration

I confirm that this Master's thesis is my own work and I have documented all sources and material used. This thesis was not previously presented to another examination board and has not been published.

Signed:

_____

Date:

_____

"*Yesterday is history, tomorrow is a mystery, today is a gift, that is why it is called the present.*"

Bill Keane

Contents

List of Figures

List of Tables

Abstract

MicroRNAs (miRNAs) are short, non-coding, hairpin shaped RNAs, that exhibit many functions within different cells. Their main function is to interfere with the post-transcriptional step of protein expression, called RNA interference. Development of diseases have been linked to the malfunction of these small molecules. As the requirement of recombinant therapeutic proteins rises continuously, every direction to increase production qualities and titers of active agents is pursued. Lately, miRNAs have also been investigated for this matter, as their abundance within cells across all species is well known and this could hold the key to new engineering procedures to enhance cellular productivity. Their potential to modulate complete biochemical pathways without burdening the metabolism could mean a highly advanced approach to modify complicated biochemical system of mammalian cells. This research aimed to investigate new ways to visualize effects of miRNAs on cell characteristics, by transiently transfecting HEK 293T cells with preselected miRNAs, and analyze the outcome using flow cytometry. Evaluation on the increase of protein expression, described promising trends in several specific miRNAs, pointing out that this line of research holds a reassuring future. An investigation into the possible involvement of specific miRNAs, stably cloned into the genome of Chinese hamster ovary cells, in cell metabolism was conducted, using metabolic flux analysis (MFA). This gave an opportunity to explore their effects on a complex mammalian biochemical network. Metabolic flux analysis, media development experiments and process parameter analysis of CHO cells with altered miRNA expression patterns did show significant differences in central metabolism. Especially extracellular measurable fluxes, like glucose and glutamine consumption, and glutamate and glutamine production decreased in anti-apoptotic cells, suggesting a more efficient handling of resources. Transient transfection of existing cell lines, parental, negative control and anti-miRNA cell line, with plasmids, carrying the sequences of complex glycoproteins, EPO and HubChe, facilitated the comparison of protein expression levels across cell clones. The production level of these proteins increased significantly in the anti-apoptosis cell line.

Chapter 1

Introduction

1.1 Structure of this work

Chapter 1 gives a short introduction to the history of recombinant protein production and development. It provides a quick overview of the discussed areas of biotechnology, developments in cell culture and process optimizations in the last few decades and therefore offer the fundamentals for the subsequent chapters.

Chapter 2 introduces the topic of using microRNAs as cell engineering tools to modify cells. Ten promising miRNAs were investigated on their abilities to enhance protein expression. By transfecting them into HEK 293Trex cells that carry a GFP encoding plasmid, the different microRNAs were introduced to the cells expression system. Their effects on protein production was subsequently monitored by detection of GFP related fluorescence using Flow Cytometry to compare the outcome in-between miRNAs.

Chapter 3 aims to confirm, assess and expand experiments based on the previous work of A. Druz, where apototic miRNAs were successfully identified and knocked out by stably integrating a complementary miRNA (anti-miRNA466h) strand into the genome of Chinese hamster ovary cells. This work comprises the analysis and confirmation of cell line specific new characteristics introduced by these modifications by repeating cellular growth and substrate usage experiments by mimicking the exact culture conditions. Media development investigations, necessary for subsequent labeled substrate metabolic flux analysis, gave further information about adaptability properties of the newly developed cell lines. Additional experiments with these cell lines, comparing the cellular flexibility on the extent of using diverse carbon substrate as a primary energy sources, delivers a metabolic substrate usage pattern that adds

to the information of phenotypical differences, created by the stable inhibition of mmu-miR-466h-5p. Metabolic flux analysis was performed to add supplementary information of the newly yielded cell line. Furthermore, MFA could identify if higher protein titers, produced by the knock out cell line, were just the result of higher biomass yield or could also be the product of metabolic shifts of intracellular fluxes. The capability of higher protein expression was investigated additionally. Druz, A. concluded that the miRNA modified cell line had a higher protein expression level using the reporter protein SEAP. This expression pattern was sought to be confirmed using other, partly more complex protein EPO and HubChe.

1.2 Background of protein production and cell engineering

1.2.1 Introduction and history

In a living organism thousands of different proteins are produced. They have the most important functions of controlling imperative chemical and biochemical processes, making them the actual active tools and components of a functioning cell. If this sensitive system malfunctions, diseases and illnesses are possible consequences (Lottspeich and Engels, 2012; Zimmer, 2015). Therefore, the importance of understanding the machinery, the role of proteins and their development within the cell *ex vivo* is obvious.

Protein production was revolutionized by Stanley Cohen and Herbert Boyer in 1973, who performed the first genetic engineering procedure by developing the technique of cloning DNA fragments into a different biological species (Cohen et al., 1973; Baeshen et al., 2014). Genetic engineering was born(Baeshen et al., 2014).

This way, the gene encoding the important, metabolic hormone insulin could be transfered and expressed using *E. Coli* as a host system (Baeshen et al., 2014). This whole new process reformed the direction of biological sciences. Today, the time when huge amounts of animal or plant tissues are necessary to harvest only small amounts of purified proteins are almost over, as more and more proteins are being produced using recombinant DNA or cell technology (Rosano and Ceccarelli, 2014). Insulin is a good example to outline this progress. The hormone, which has been used in medicine since 1928 for treating diabetes, was previously extracted from porcine and bovine pancreata. The insulin content of a single porcine or bovine pancreas only covered a diabetics demand for 3 days or 10 days, respectively (Schmid, 2016). Doubtless, the production of recombinant proteins using microbes as host factories changed biochemical research and medicine(Rosano and Ceccarelli, 2014).

1.2.2 Current state of the art

Today, projects that aim to express and purify proteins are designed using recombinant DNA technology. If successful, this technique allows for high yields of recombinant proteins applicable in industrial processes, in commercial goods and, of course, in the biochemical and biomedical field. In theory, the procedure is an easy task: First selecting the gene of interest, then choosing an available expression vector, followed by its transfection or transformation into the production host and after induction and expression finally, protein purification.

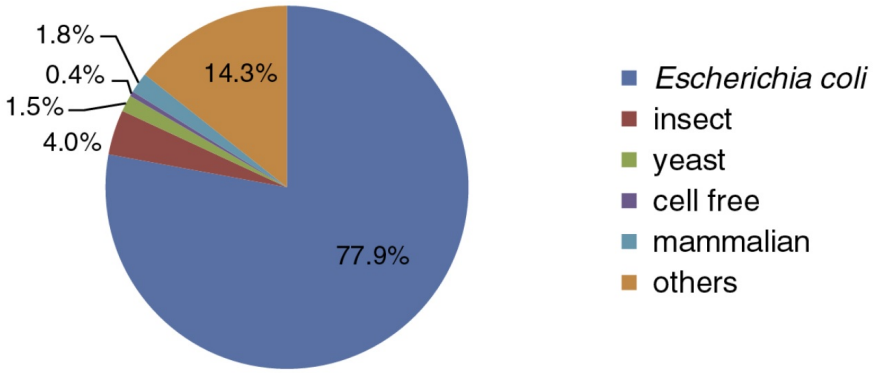

Figure 1.1: Current status of hosts used for recombinant protein production (Xiao, Joseph Shiloach, and Michael J Betenbaugh, 2014)

However, in actual practice, a lot of things can go wrong and hinder production (Rosano and Ceccarelli, 2014).

It is estimated that biopharmaceutical production will further increase in the next couple of years (Quek et al., 2010). Demands of recombinant proteins will rise disproportionally to meet diverse requests for new biological agents, better and safer proteins for diagnostics and therapeutic reasons and to lower costs in the production process based on operation improvements (Sobczyk, Carpentier, and Paris, 2008). Process optimization for recombinant protein production is therefore extremely important and has many faces. Genetic engineering, metabolic engineering, downstream harvest, and improvements of culture conditions are only some of the measurements taken to increase yields and lower production costs.

One strategy to overcome the bottlenecks of recombinant protein production is choosing the ideal host cell line (Xiao, Joseph Shiloach, and Michael J Betenbaugh, 2014; Rosano and Ceccarelli, 2014). Figure 1.1 depicts the percentages of hosts used for recombinant protein production in between the years 2004 and 2013 (Xiao, Joseph Shiloach, and Michael J Betenbaugh, 2014). The specific protein synthesis machinery of a chosen host cell will produce the protein of interest and will set all the steps necessary for the procedure. The host system therefore defines the technology, including reagents, molecular tools and equipment needed (Rosano and Ceccarelli, 2014).

As easy and fast as it is to produce proteins in non-mammalian expression hosts, it also has its disadvantages. However, compared to microbial systems, product yields of mammalian production hosts are still very low (Hackl, Borth, and Grillari, 2012). Today, using mammalian cells as an expression host of biopharmaceutical therapeutics is trending and has become a key technology,

creating revenue of approximately USD 150 billion in 2015 and is therefore one of the fastest growing segments in science, especially biotech (Xiao, Joseph Shiloach, and Michael J Betenbaugh, 2014; Jenkins, 2007; Bandaranayake and Almo, 2014; Dyson, 2016).

The efficacy and activity of proteins usually does not solely rely on the correct sequence of Amino Acids (AA) but also on a more or less complex expression pattern of alterations after protein translation, called post-translational modifications ($PTMs$). Insulin and albumin are two of the few examples of pharmaceuticals of biological origin that undergo simple alterations after translation and can be produced by yeast and bacteria (Jenkins, 2007). These PTM patterns can vary immensely in-between species and types of cells and can include carboxylation, hydroxylation, sulfation, amidation and proteolysis, along with the most common of them all: glycosylation (Walsh and Jefferis, 2006). Fig. 1.2 gives a quick overview of groups of some PTMs.

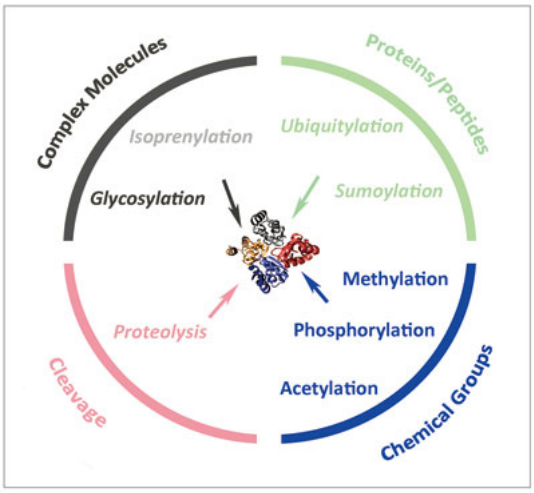

Figure 1.2: PTMs of Proteins. Small overview of possible post-translational modifications. Some of them are reversible, others are not (Wang, Peterson, and Loring, 2014).

The essential mechanisms of many PTMs to diversify protein functions are well known, as for other functions the exact purpose is not fully understood yet. However, generally PTMs contribute for stability, functionality, efficiency of secretion, cell signaling and can make or brake a successful production of a recombinant protein. These challenges have to be considered when designing a bioprocess to produce a desired agent. Incorrect PTMs could even pose as a risk for its field of application if there is no proven functionality, e.g. could provoke an immune response in patients if used as therapeutic proteins (Jenkins, 2007). All of this prooves that cell types should be wisely chosen and phenotypic

properties should be well-known before making them the production factory for important therapeutic biologicals.

The aim of this work was to highlight the new, exciting and very promising ways for improving, analyzing and characterizing mammalian cells as hosts for protein production.

1.2.3 Background metabolic engineering

Metabolic engineering is defined as the analysis and manipulation of metabolic pathways (George Stephanopoulos, Aristidou, and Nielsen, 1998). This is hard to achieve, especially in mammalian cells, this is incredibly hard to achieve(Jamey D Young, 2014b). The framework for basic knowledge of this field is the formulation of a quantitative biochemistry for the investigation of enzymatic reaction pathways. The overall aim with applying metabolic engineering is to improve cell line properties or product productivity by modifying or introducing new biochemical pathways using recombinant genetic technology (George Stephanopoulos, Aristidou, and Nielsen, 1998).

Biological organisms, and especially their metabolism, are complicated systems that create a biochemical network that can be compared to a spider's web, see Fig. 1.3. Every reaction interlocks perfectly with another one. Therefore engineering one pathway could have drastic consequences for the next one. However, driven by the goal to constantly improve the yields and quality of biopharmaceuticals, every possibility to do so is currently explored (Selvarasu et al., 2012). Traditionally, the focus of a metabolic engineering experiment was a specific biochemical reaction. This reaction was targeted and manipulated by identifying the corresponding gene and employing adequate genetic techniques to amplify, delete or deregulate associated enzymes (George Stephanopoulos, Aristidou, and Nielsen, 1998). However, methods to manipulate biochmemical reaction rates and intermediate concentrations have developed into a diverse field in the last few decades. One of which, microRNA (miRNA) engineering, will be introduced in section 2.1.

As this is one side of metabolic engineering, the more active *synthesis* side, there is another aspect of metabolic engineering that focuses on identifying the metabolic state of a cell. This includes the use of metabolic network modeling of biochemical processes. Detailed information about this method will be provided in chapter 3.

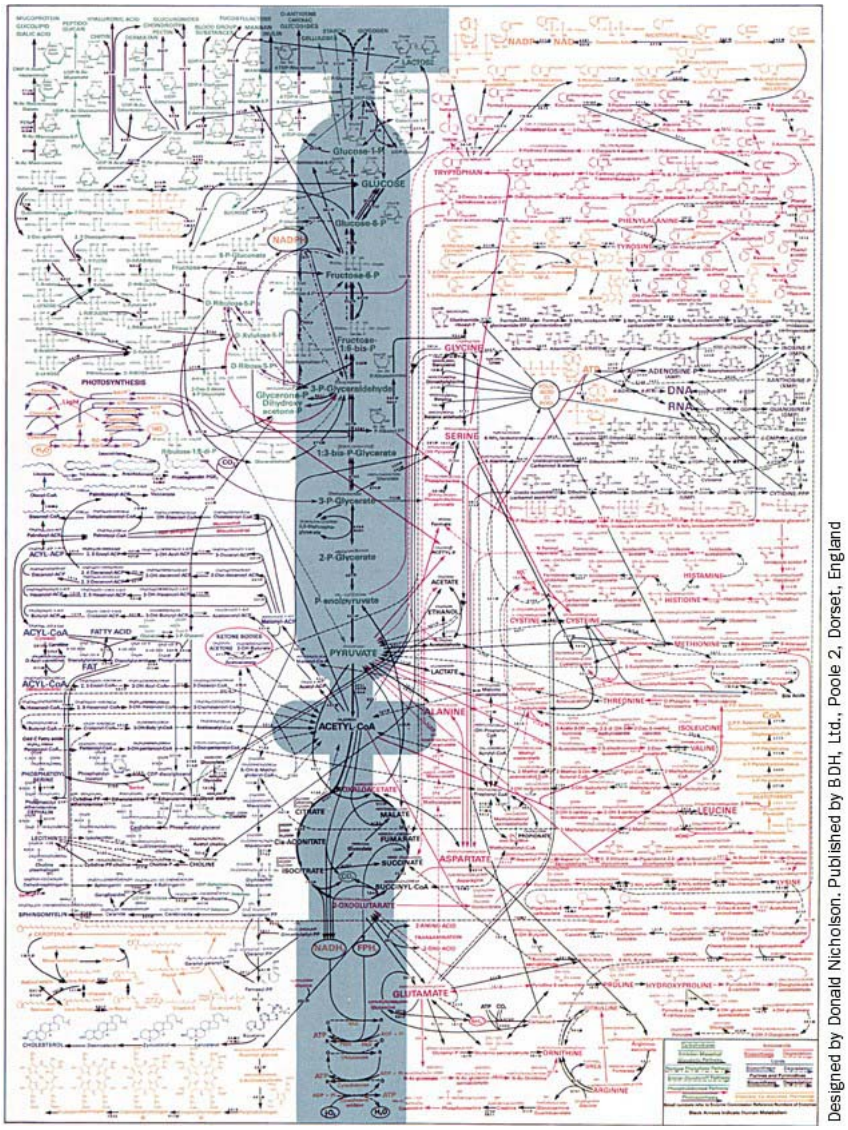

Figure 1.3: Overview of the complex biochemical pathway network within cells (D. Voet and J. G. Voet, 2011).

Chapter 2

Screening for potential miRNAs to enhance cellular protein production using HEK cells

2.1 Introduction

MicroRNAs (miRNAs) belong to a group of short, endogenous RNA molecules with a length between 18-24 nucleotides. To this day they have no known coding properties. Since their discovery in 1993, during genetic studies on nematodes, miRNAs have come a long way from unacknowledged short RNAs to powerful instruments that are studied widely for their implications on cell engineering and regulatory impacts on cellular pathways and gene expression (Jadhav et al., 2013; Wahid et al., 2010). MiRNAs are known to have a broad spectrum of functions, being highly conserved in-between species and cell types at the same time. These functions include implications in transcriptional gene regulation, cell growth and apoptosis, tumor development, cell differentiation and metabolism. Even more functions are expected to be influenced by these tiny, single stranded RNAs (Wahid et al., 2010; Niall Barron et al., 2012) Today, they are accepted as novel regulators, that can control entire networks of genes and other cellular pathways and thus achieve a switch of phenotypic properties (N. Barron et al., 2011; Hackl, Borth, and Grillari, 2012).

Currently, they are also used as biomarkers in clinical diagnostics as their expression profile of signature miRNAs may help with detection and even treat-

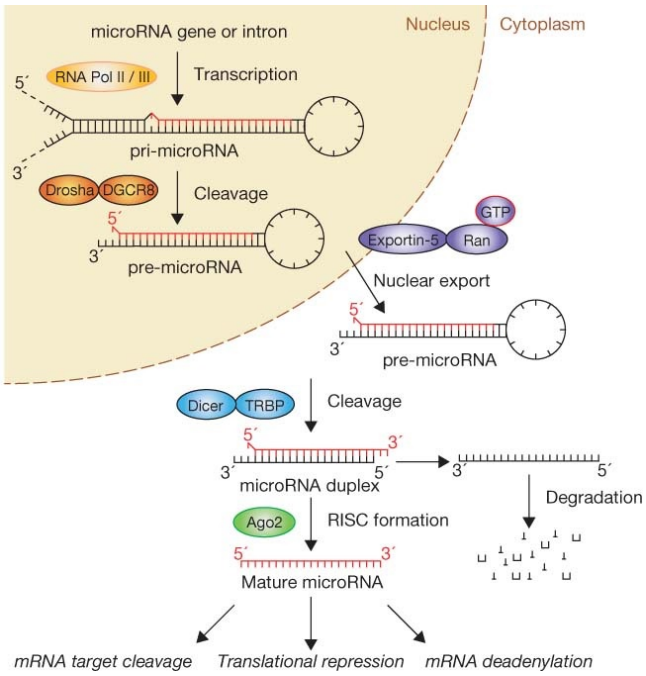

Figure 2.1: Biogenesis and processing of miRNAs in cells (Winter et al., 2009)

ment of diseases. Today, this new way of handling miRNAs still faces a lot of challenges (Lianidou, Markou, and Zavridou, 2015; Hackl, Heilmeier, et al., 2016). Understandably, researchers see the high potentials in investigating these small molecules to their full extent and to overcome the objections.

The miRNA development, see Fig. 2.1, starts in the nucleus. Following transcription, the primary RNAs (primiRNA) are enzymatically processed by a enzyme called Drosha to single stranded hairpin precursors (pre-miRNA). After being transported to the cytoplasm, pre-miRNAs are enzymatically cleaved by Dicer, a protein that produces the final mature miRNA with a length of about 22 nucleotides (Jadhav et al., 2013; Wahid et al., 2010). Subsequent loading into the so called RISC complex (RNA-induced silencing complex) activates the post-transcriptional inhibition function of miRNAs by being able to target the 3'-untranslated region of mRNAs, due to partial complementary sequences and thus, inhibition of translation or by degradation of mRNA by a RISC subunit. The outcome is an interference of the cells gene expression known as RNAi (RNA interference) (Müller, Katinger, and Grillari, 2008; Jadhav et al., 2013). There are other compounds that are part of the mechanism that control the sophisticated system of gene silencing. Small interfering RNAs (siRNA) play another big role in gene silencing and occur naturally in cells (*RNA Interference*

(RNAi) 2011). Today, the magnitude of importance of these small molecules guiding genomic expressions and biochemical pathways can only be assumed. A recent paper proposed that that miRNAs do not exclusively have inhibitory effects on protein translation but can also enhance their production by different effects (Vasudevan, 2012).

Hundreds of miRNAs can be encoded by the genome of mammalian cells, including humans, giving scientists a big new field to be discovered and researched (Felekkis et al., 2010). All of this created reasons to look further into this issue and investigate miRNAs regarding different directions, with varying cells. With this work the we aimed to show the versatility of miRNAs and prove that their engineering can create detectable alterations in cellular characteristics. The first approach was to establish a procedure to screen for miRNAS that actually have the capabilities to increase recombinant protein production. Due to the high number of different miRNAs, experimental volume-scales have become smaller to enable a cost efficient and high throughput system to get results fast (Vidugiriene et al., 2008). In this case microarrays were used to predetermine potential effective miRNAs for enhancement of protein expression. Using GFP and flow cytometry as a follow up enabled a subsequent analysis of miRNAs effects on protein expression. In flow cytometry different detectors are responsible to detect various of target fluorochromes and measures the emitted light (Herzenberg et al., 2006). Here, green fluorescent protein (GFP). Using GFP as a reporter protein has different advantages. On the one hand GFP can be rather simply utilized to determine optimal transfection conditions due to the fast and easy assay and detection via flow cytometry. On the other hand, detected GFP intensity directly relates to the number of GFP mRNA copy number in cells, which, in turn, gives clues about expression levels of other proteins in cells, e.g. by developing fusion proteins in plasmids. This gives reporter proteins like GFP the power to visualize differences of gene expression patterns and properties in-between cell populations (Vidugiriene et al., 2008; Soboleski, Oaks, and Halford, 2005). Thus, the decision of how to develop and proof effects of multiple miRNAs on protein expression levels *in vivo*, was easily made towards the powerful tool GFP.

2.1.1 HEK cell lines

Since its development, the human embryo kidney (HEK 293) cell line is one of the most frequently used mammalian cell lines in research. HEK293 were the first human cells being transformed with adenovirus DNA fragments (Thomas and Smart, 2005). There are many variants of the original cell line, such as 293N3S for suspension and 293S for culture in serum free media. To yield cell

lines with improved transient gene expression, 293-T line was created, which expresses the SV40 large T antigen, inducible by tetracycline (Xiao, White, et al., 2013; Bandaranayake and Almo, 2014). HEK cells are used predominantly as host cells when they are a closer match to human proteins regarding PTMs (Bandaranayake and Almo, 2014).

2.2 Materials and Methods

2.2.1 Cell culture of adherent 293T HEK cell line and determination of miRNAs used

The cells used for this experiment, HEK 293T GFP cells, which were transfected with pcDNA3.1/Zeo(+)GFplasmid carrying a GFP and a Zeocin resistance sequence, were kindly provided by Su Xiao, from the National Institution of Health (NIH). Cells were cultured in T-flasks in incubators maintained at 37°C and at 5% CO_2. DMEM media supplemented with 4.5mmol L-glutamine, 10% FBS and 200μg/ml Zeocin was used for cell culture. Cells were subcultured for at least two weeks after thawing before being used for miRNA transfection experiment. Ten microRNAs, tested with HEK 293T-GFP cells, were provided by NIH. Pre-selection of these miRNAs was performed by Su Xiao at NIH. Briefly, a library of 875 known human miRNAs was screened for enhancing neurotensin receptor (NTS1) expression by transfecting the short molecules into described cells. The results were screened for miRNAs that can most significantly enhance NTS1 production. For reasons of confidentiality names and sequences of miRNAs can not be revealed. .

2.2.2 Transfection and GFP expression analysis

Transient transfection was performed in 12-well plate format by using transfection reagent Lipofectamine® RNAiMAX (Life Technologies, Cat.No.: 13778-085) and human miRNA mimics (Qiagen). The optimized transfection condition has been determined by Su Xiao by varying miRNA concentration, transfection reagent concentration and the seeding cell density. Briefly, miRNAs were added to each well of a 12 well plate. Lipofectamin®RNAiMAX was diluted in Fetal Bovine Serum (FBS) free DMEM media and let sit for a few minutes; this mixture was incubated with the individual miRNAs for 20 - 40 minutes after adding the specific microRNA to each well. HEK 293T GFP cells were detached, washed and diluted to the ideal cell density; this suspension was added to each well, to allow transfection with each miRNA. The last two wells contained a positive control with "killer" siRNA, inhibiting cell viability and a negative control

siRNA respectively. These last two wells were used as positive and negative control for the transfection efficiency by checking the growth ratios. The last runs of green fluorescent protein expression assessment were performed with a slightly adjusted protocol: reducing the incubation time of miRNAs with Lipofectamine RNAiMAX transfection reagent due to higher occurrence of apoptosis shortly after transfection. After these slight modifications, performance of cell growth appeared to be regular again.

2.2.3 Harvesting and Flourescence Analysis

As soon as the transfected cells reached a confluence of around 70%, they were harvested and prepared for flow cytometry analysis to detect the green fluorescence intensity for each individual well by detaching cells followed by multiple washing steps with DPBS to remove all colored liquids and produce a single cell suspension, necessary for analysis. The assay itself was conducted with a FACSCalibur (Becton Dickinson, US) using DPBS as sheath fluids. Parameters were set to measure exactly 10 000 events for the preset gate for this cell type specific scattering patterns. Excitation was accomplished by laser with a wave length of 488nm and a detector at 530/30nm was used to capture the light signal. HEK TREx- 293 cell line without any GFP expression, used as a negative control to determine and compensate auto-fluorescence. HEK 293T cell lines were analyzed in parallel with every assay to minimize daily variations by the machine itself and by cell properties and growth conditions. At the last experimental run of this procedure the parental 293T HEK cell line without any miRNA transfection was analyzed additionally. Raw data was eventually analyzed using Flowing Software, Turku Centre for Biotechnology, Finland. Gating was done manually and individually for each cell line and each run based on 'dot plot' displays.

2.3 Results

2.3.1 Transfection step and cell culture

Cells were thawed less than two weeks prior to transfection with miRNAs to keep the passage number low. If cells did not fit the viability requirements, eventual findings were not included in final analysis. The transfection process with pcdna3.1-GFP plasmid, created 12 different cell pools, see Fig. 2.3. Information about transfection efficiency was obtained with microsopical anlysis, see Figure 2.2. Picture A presents adherent healthy 293T HEK cells transiently transfected with siRNA with no or little percentage of dead cells (negative control). B, on the other hand, shows a very high ratio of cells that are already

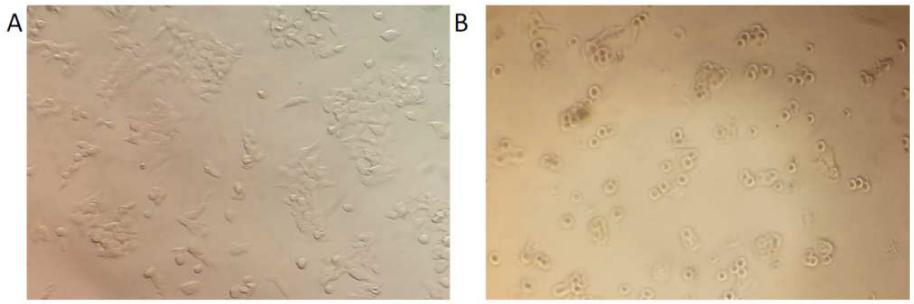

Figure 2.2: Comparison of negativ control siRNA and killer siRNA transfected into HEK 293T cells. (A) cells transfected with negative control siRNA; (B) cells transfected with killer siRNA.

rounded up and floating around, not being attached to the surface, transfected with "killer" siRNA (positive control).

2.3.2 Flow Cytometry Analysis

An overview of the final results of all summarized runs is given in Fig. 2.3. Values of Geometric Means (GeoMean) and Medians were chosen to demonstrate the outcome as both of them are equally utilized to present data for cellular fluorescence quantification. Opinions which parameter has more statistical power are strongly divided, thus both are presented in Fig. 2.3. GeoMean is commonly preferred over arithmetic mean as the latter one gives more statistical power to outliers and does not work well at describing log amplified data. Therefore, GeoMean was chosen to demonstrate the GFP fluorescence intensity (Davies, 2017; *Definition of Statistics* 2017; Reckermann, Mon Apr 6 07:24:04 EST 1998). Median is used, similar to GeoMean, as it does give outliers little or no influence on values and is considered at least as robust as GeoMean in describing a population of events (Best, 2014). The decision to present both parameters was made, not to raise any questions, but as the data shows, the relative difference between GeoMean and Median in comparing groups with each other are marginal and could be considered equal, or at least very similar. In contrast to GeoMean, the Median seems to have the ability to create slightly more reproducible data. All results are scaled relative to each other and do not display an absolute value. Green fluorescence intensity of the blank, serving as a negative control for auto-fluorescence, is almost basal with both parameters, GeoMean and Median. Although the results within a 'group' (set of data for different miRNAs used) vary quite a lot from experimental run, to the next one, a certain trend can still be detected. Picture D in Fig. 2.3, should represent the variation in fluorescence intensity created by single miRNAs. Shift of GFP

intensity can be seen on the x-axis which represents the GFP intensity. Considering the scale of the y-axis being the cell count, it is obvious that there is a shift of position of the peak (Mode) comparing both curves, demonstrating different effects of different miRNAs on cells. One single attempt was made to actually use a different cell line for this experiment in order to see if this protocol could be used with different cell lines. Time was too short though to actually modify and optimize the transfection method for this cell line. The cell line being 293TRex HEK transfected with an inducible pcDNA4 plasmid carrying a fusion protein of eGFP sequence and serotonin construct. Some adaption were made due to the cell line specific requirements as induction of protein expression with tetracycline, at a volumetric ratio of 1/1000, 48h after transfection and using a higher voltage of 485 at flow cytometry analysis. Results are presented in Fig. 2.4. The pattern of GFP intensity and thus the related expression of the fusion protein obviously differentiates from the first cell line, signaling that with different cell lines may come different results. Unfortunately, the washing step caused a huge loss of cells and would have to be improved to receive results for all sets of transfected cells.

2.4 Discussion

Flow Cytometry, as an easy applicable method, was used to relatively quantify GFP expression of cell populations, which are stably transfected with the mentioned reporter gene (*BD Biosciences Accuri C6 Personal Flow Cytometer - Applications - Gene Expression* 2014) By transfecting various miRNAs into the GFP expressing 293T HEK cell line, we hoped to acquire new cell populations with different cellular properties, especially with GFP expression. Improving production levels of recombinant proteins in mammalian cells has been a focus in in biomedical studies in academia (Xiao, Chen, et al., 2015). Proof that with this easy conductible experiment, aberrations in cellular components, system or metabolism can be achieved, would lay grounds for a more intense development towards a high throughput, cost effective method to investigate several miRNAs and their influence on cell types (Xiao, Chen, et al., 2015). Importantly, this could this could give an immense volume of additional information about complex cellular pathways, if promising results would be followed up with assays of protein patterns or even analysis of metabolic fluxes. An additional effect of this line of experiments, to establish and improve the reproducibility of the GFP expression intensity patterns using different miRNAs for transfection and thus creating a broadly applicable and cell type comprehensive protocol, was not entirely achieved due to time and material issues. The plan to create fully developed instructions to follow, which is also transferable to other cell lines

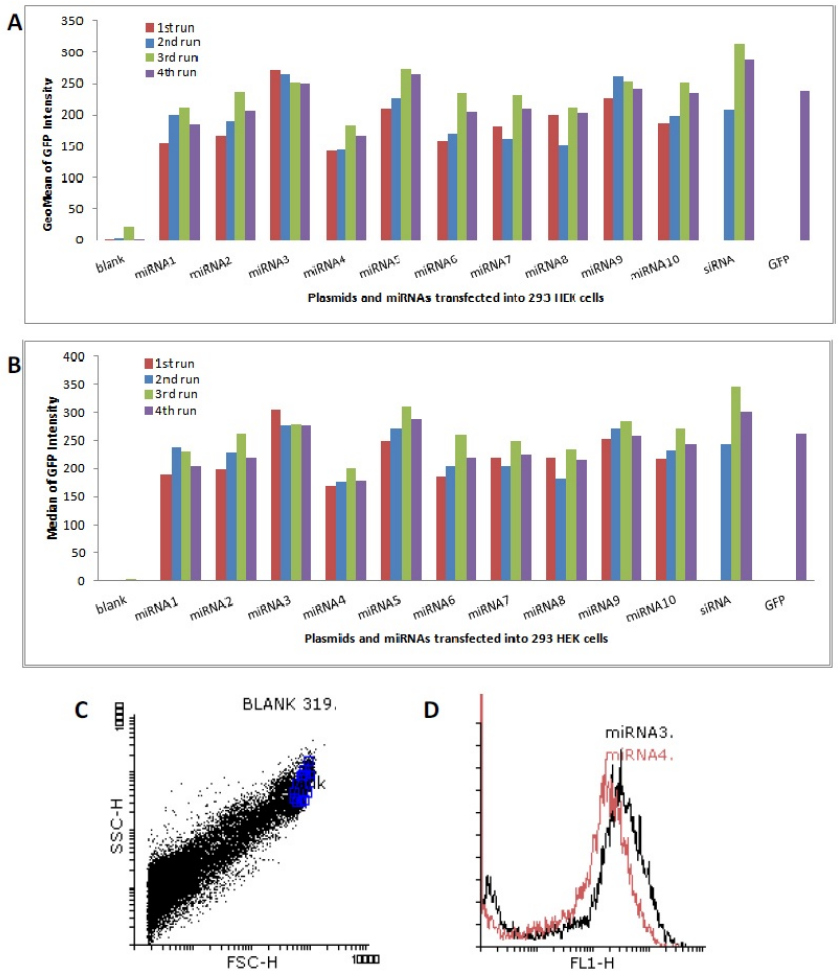

Figure 2.3: Overall View and comparison of Flow Cytometry (FC) Assay after Analysis(A) Shows the GeoMean results collected from all evaluable runs of HEK 293 cell transfection with different miRNAs and subsequent analysis with FC. The ordinate (vertical axis) represent the relative GeoMean intensity of the GFP signal, colors represent different dates of the eventual FC analysis. The abscissa (vertical axis) is defined by cell modifications;blank: negative control (TREx-293 HEK cell line) which was whether transfected with a GFP expressing plasmid nor any kind of miRNA;GFP: 'parental' cell line used for this line of experiments containing a constitutively expressed GFP plasmid; miRNAs 1-10:each group was the result of transfecting the 'parental' cell line with different kinds of miRNA; siRNA: 'parental' cell line transfected with a scramble RNA with nonsense- coding.(B)Shows similar data with the only difference of the ordinate showing the Median fluorescence intensity (C) demonstrates one example (Blank) of the dot plots received at data analysis, with the gate around the 293T HEK cell population, strikingly indicating a big count of dots excluded by the HEK gate probably created by a large amount of cell debris. y-axis being Side Scatter and x-axis being Forward Scatter(D) Shows an overlay histogram of one miRNA transfected cell line with the highest fluorescence intensity (miRNA3) and one with lower fluorescence intensity (miRNA4). Scale of the y-axis is the cell count, xaxis represents fluorescence intensity.

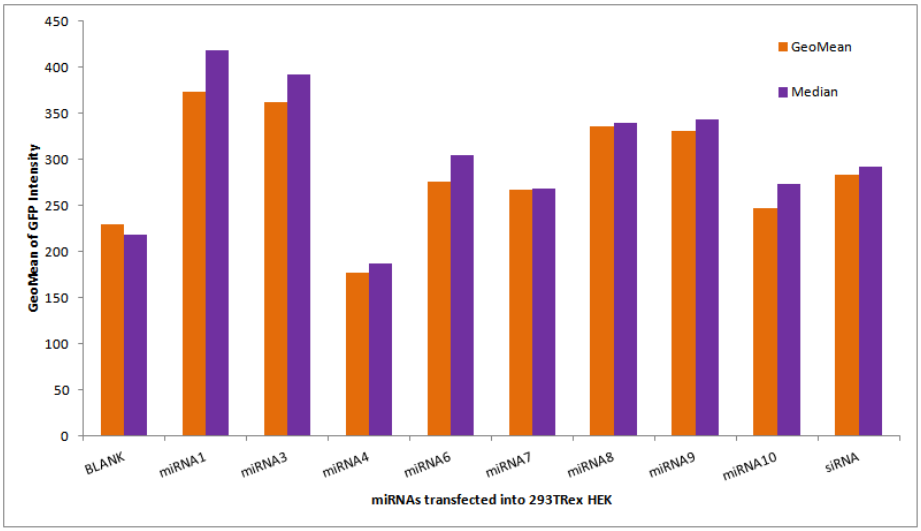

Figure 2.4: Results of GFP expression after miRNA transfection of 293T HEK cells. Due to a single experiment GeoMean and Median could easily be summarized within on figure. miRNA2 and miRNA5 cell pools are missing due to the loss of cells during washing steps. miRNA cell pools 1 and 4 had lower cell counts in Flow Cytometry analysis compared to others.

and types and of course miRNAs, was also made more complicated by no reproducible cell culture conditions with certain reruns of the experiment. However, although the absolute values of GFP expression profiles within a cell population, transfected with a specific miRNA, e.g. all different values for miRNA 1, are not comparable, it can be argued that there are certain trends within each group. One could claim that miRNAs 3, 5 and 9 seem to have an overall higher quality of green fluorescence protein expression, especially compared to miRNAs 4e, 6 and 8, that seem to have the lowest intensity of GFP fluorescence.Xiao, Chen, et al. reported successful enhancement of expression of NTSRI-GFP fusion protein following this method. One attempt to apply this scheme to a 293 TRex HEK cell line was made. Problems with cell culture of spontaneous cell lysis, due to unstable incubation temperatures, only allowed for one run, resulting in completely different patterns regarding miRNAs. Follow ups with this cell line and also cell lines, cultured inle surrounding conditions could give the crucial results. After all, possibilities to find a miRNA that is worth pursuing to enhance protein production seems very promising. As a conclusion, further investigations on this matter are certainly necessary to definitely evaluate this approach of investigation. Most importantly, standardization and constant cell culture conditions have to be given to go further, otherwise fluctuations in results will most certainly occur again and time and cost investment will be in vain.

Chapter 3

Detecting metabolic changes in CHO - cells caused by engineering miRNAs

3.1 Introduction

3.1.1 Background

Entering the keywords "CHO CELLS" into Pubmed delivers more than 13000 results and this the last 10 years. 144 of which are reviews giving a background and explaining why Chinese hamster ovary (*CHO*)) cells are as important and widely used in metabolic engineering as they are. When researching these papers about the characteristics of this cell type and the range of experiments they are used for, one realizes that almost every article starts with one or more of the following phrases similar to: "CHO cells are the most frequently used host in recombinant protein production"; "...allow a high titer production of recombinant therapeutic proteins..."; "...dominantly used cell factory for commercial production of therapeutics"; (J. Y. Kim, Y.-G. Kim, and Lee, 2012; Jadhav et al., 2013; Nakamura and Omasa, 2015) and this is only to name a few. However, before going into details about the application of CHO cells, a short look at the beginnings:

The Chinese Hamster Ovary cell or short CHO cells, as the name would suggest, was isolated from the species of *Cricetulus griseus, see Fig. 3.1.* A rodent native in the North of China. Initially using the hamsters initially in the laboratory to type pneumococci in 1919, they quickly became an important

tool in epidemiological research for being the carrier of the deadly parasite that causes black fever (Jayapal et al., 2016).

Figure 3.1: Chinese Hamster (*Chinese Hamster* 2016)

Subsequently, the animal was imported into the U.S. in 1948. In 1957, Dr. Theodor T. Puck from the University of Colorado Medical School conducted several cytogenetic studies and tissue culture experiments of various somatic mammalian cells, including CHO cells. Puck isolated the cells from the ovary of a female speciemen, establishing the original CHO cell line. These type of cells were of special interest to him and his team for performing genetic studies of cells karyotypes and their ploidy levels using radiation as a mutagen. The interest arose due to the relatively lower number of chromosomes ($2n = 22$) in CHO cells compared to the human set of chromosomes ($2n = 46$) (Jayapal et al., 2016; Puck, Cieciura, and Robinson, 1958). Culturing mammalian cells and/or their mutants was still in its nascency then, back then and had to face various difficulties that often ended in failure. In addition, mammalian cells have a limited count of cell generations before senescence occurs. However, with the CHO cells extracted from the Chinese Hamster, Puck et all managed to produce a stable cell line that gained some kind of immortalization by an unknown process, allowing them to proliferate indefinitely, while still keeping its diploid character (Wurm, 2013). Describing the developed cell line as "particularly hardy and reliable" by growing fast and well in their paper, the cells soon distributed all over the laboratories for further development and analysis (Puck, Cieciura, and Robinson, 1958).

It was still a long way from todays CHO cells, though. Despite the huge improvements in cultivation characteristics the cell line still needed a small amount of fetal bovine serum (FBS) in the culture medium (Wurm, 2013). As essential as FBS is for the cultivation of mammalian cells by stimulating metabolism, growth and proliferation ("mitogenic effect"), and therefore simulating the complexity of endogenous environment of an organism, there are some characteristics of this supplement in cell culture that call for alternatives. The reasons for this:

- FBS is not well defined chemically
- FBS has to be harvested by bovine fetuses causing ethical problems
- FBS has a high demand vs the possibilities of its global supply (Brunner et al., 2010)

Growing on serum- free media was successfully accomplished in 1977 when scientists declared effective cell line adaption of CHO cells to the new media without FBS (Gregory Hamilton and Ham, 1977; Neff, 2016).

This new property further established CHO cells status in the world of clinical science. In a interesting summary about the lineage development of modern CHO cells however, Wurm states that due to the extent of research of these cells, in different laboratories and under various growing conditions, and because of their ability to adapt, the immortalized CHO cell lines underwent a high degree of genetic and phenotypic diversity. Thus, creating quasispecies, differing quite significantly in their individual phenotypic characteristics. This produces drawbacks regarding platform selection, as it creates the necessity for a screening to detect the ideal cell clone presenting all the relevant phenotypic qualities that are essential for a successful production platform (Bandaranayake and Almo, 2014). Figure 3.2 shows that there are many different branches of sublines. Here, only the CHO S cell line is considered, as it was used in the experiments. Wurm states that little is known about its definite origin, although scientists Thompson, Gottesman and Tobey are considered as the pioneers in developing stable CHO cell lines capable to grow in single cell suspension cultures (Wurm, 2013).

CHO cells as the biotechnological workhorse of choice. In the 1980s, by approving CHO S derived *tissue plasminogen activator* (tPA) as the first therapeutic protein produced by mammalian cells, the U.S. Food and Drug Administration (FDA) set the framework for a reformation in the field of medical science. 30 years later this cell type is still the most favorable "production

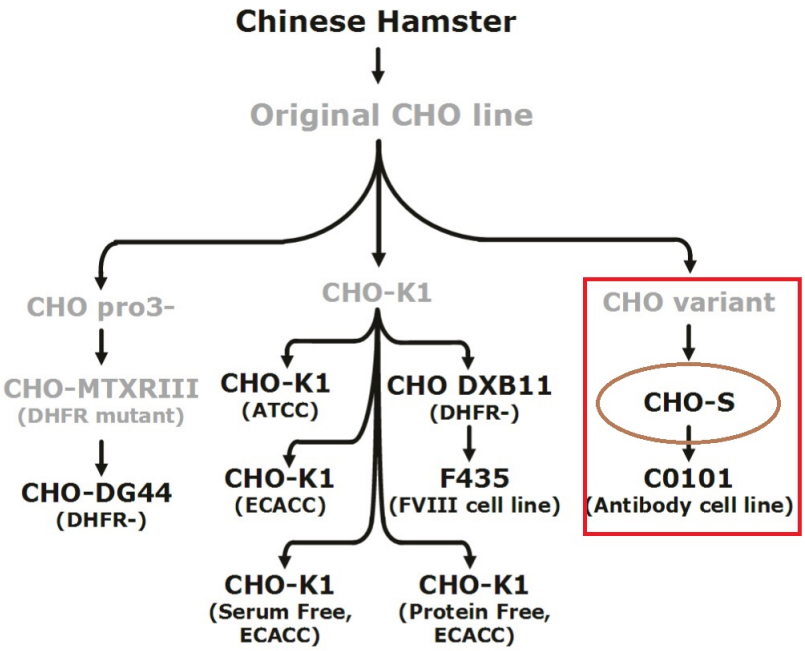

Figure 3.2: Overview of CHO cell lineage development As CHO S cells are the primary subject in this work, the branch of development has been highlighted. Figure adapted from (Schrøder Kaas, 2015)

factory" for biologics out there. The reasons are manifold (Lai, Yang, and Ng, 2013). These cells have several characteristic properties that are preferable compared to other cell types. The advantages of using mammalian cell lines over lower eukaryotic ot prokaryotic cells were already briefly discussed in section 1.2. Especially the fact that the valuable therapeutic proteins are highly compatible to humans due to similar post-translational modifications, such as proper glycosylation patterns to provide the correct functionality of the desired protein, make them very appealing for biotechnological causes. (Lewis et al., 2013; Riveros, 2012; Wurm, 2013). Other causes of their popularity have already been referred to,

- their ease of adaptability to suspension culture, which makes it easier for industrial upscaling,
- their growth on chemically defined, serum free and cheap media, guaranteeing reproducibility and sustainability (Lai, Yang, and Ng, 2013).

It has been reported that CHO cell have a restricted susceptibility to viral infections that are otherwise dangerous to humans (Berting, Farcet, and Kreil, 2010; Xu et al., 2011). Additionally, the transfection and amplification system

is well established and widely applied using the instability of the CHO cell genome to increase gene copies. Ultimately, these properties elevate the level of the desired product to a level facilitating recombinant protein titers of several grams per Liter. CHO cells also accomplished a certain status of regulatory approval in the production of therapeutic products (Xu et al., 2011; Lai, Yang, and Ng, 2013).

A brief description of prior work by Alex Druz. This paragraph introduces the topic of programmed cell death (PCD) and their unavoidable fate of apoptosis. Despite the progress of the last few decades and the previously described accomplishments to enhance biopharmaceutical production rates in mammalian cells, animal cell culture still faces obstacles as production platforms. Cell viability constitutes a key part in this endeavor. Previous efforts of improving capacity of cellular turnout rate mainly focused on media development and selection strategies to improve lifespan of cells (Xu et al., 2011; Aliaksandr Druz et al., 2011a). Apoptosis is also called "programmed cell death", describing the process quite appropriately. *In vivo,* apoptosis is a very important event, usually arising during cell aging and development and as a mechanism to check on the regular process of cell cycles to maintain homeostatic states of cell populations. In viable organisms, a defect in the apoptosis onset (either too much or too little) has been associated with many diseases including immunsystem dysfunctions, neurodegenerative events and cancer (Elmore, 2007). As important as programmed cell death is in viable organisms, to execute a certain way of health control, it can interfere in bioprocesses designed to yield a high amount of target protein. Mammalian cells have a high sensitivity to stressful conditions during cell culture like nutrient depletion, lack of growth factors, accumulation of metabolites, hypoxia and shear stress, to name a few (Aliaksandr Druz et al., 2011a). Contributing to 80% of cell death in bioprocess cultures Goswami et al., 1999 apoptosis is a major factor of production yields of recombinant proteins.

By publishing his paper “Stable Inhibition of Mmu-miR-466h-5p Improves Apoptosis Resistance and Protein Production in CHO Cells”, Aliaksandr Druz, Son, et al. reported a huge success in his field of research. The effective analysis and engineering of miRNAs in regard of their influence of the integrity and stability of mammalian cells, paved the way for a more reliable and sustainable way to improve and prolong cell viability and subsequently their productivity. As the principles of miRNAs were already discussed in section 2.1, detailed information about miRNAs will not be covered in this section. In his paper, Druz describes that the utilization of engineering miRNA expression patterns as an approach

of apoptosis delay in mammalian cells, might yield a better outcome compared to traditional methods. The conventional way is to manipulate a single gene and research its results. In previous studies Druz et al. investigated the expression of microRNAs in Chinese hamster ovary (CHO) cells during apoptotic conditions of nutrient depletion, finding that a cluster of miRNAs (mouse miR-297-669) was up-regulated caused by these inadequate nutritional conditions. Low glucose levels can lead to the onset of programmed cell death in different ways. Mitochondria mediated pathways caused by the lack ATP, reudce the rate of glycolysis leading to an impairment of the redox balance and oxidative stress and lastly, overexpression of transcriptionfactor Hif-1alpha inducing the p53 mediated onset of apoptosis (Sermeus and Michiels, 2011; Aliaksandr Druz et al., 2011a; Aliaksandr Druz, Son, et al., 2013). When inhibiting one member of this family of miRNAs (miRNA mmu- miR-466h-5p), which targets several genes with anti- apoptotic effects (dad1, bcl2l2, birc6, stat5a, smo), onset of apoptosis was delayed and cell viability increased. Briefly, after selecting the target miRNA Druz, A. created stable miRNA-466h-5p knockout cell clones, anti-miRNA-466h-5p, using short hairpin RNAs that target mature or pre-miRNAs of mmu-miRNA-466h-5p, due to base pair homology. Additionally, a negative control stable clone was created similar to the knockout cell line by using a short hairpin RNA with low homology to any relevant sequences. What he discovered was an equal growth rate of anti-miRNAs466h-5p, negative control and non transfected cell line in the beginning of culture but an increased maximum viable cell density of the knockout cell line anti-miRNa-466h-5p, and similar maximum cell densities for negative control cell line and non transfected cell line, respectively. Also, he detected a light shift in time point of apoptosis onset with the anti-miRNA-466h-5p clones, again with similar results for negative control and non transfected, parental CHO suspension cell line. Investigation of possible enhancement of protein production using secreted alkaline phosphatase (SEAP) concluded in determination of higher total titers and cell specific productivity of SEAP, especially in anti-miRNA-466h-5p engineered cells. It was mentioned that using miRNAs, instead of regulatory proteins, to create different intracellular properties has advantages, as it might not have the same metabolic burden on cells because miRNAs do not require any of part the translational machinery. This may give cells the opportunity to use more resources for recombinant protein production, ultimately leading to higher cell specific productivity, as seen in the results of Druz's study (Aliaksandr Druz et al., 2011b; A. Druz, M. Betenbaugh, and J. Shiloach, 2012; Aliaksandr Druz, Son, et al., 2013).

3.1.2 Background of metabolic mechanisms and process control

Ideally, in production bioprocesses, all glucose and amino acids consumed should mainly go into energy and recombinant product creation (Fan et al., 2015). Thus, major concerns of upstream process optimization are amino acid and glucose consumption, metabolism, cell growth and product titers (Fan et al., 2015). To ensure rapid cell proliferation, serum-free media usually contains high concentrations of glucose and glutamine. Evidence shows that there is a certain flexibility of metabolic pathways of glycolysis, glutaminolysis and oxidative phosphorilation as a response to micro-environmental changes and/or biosynthetic needs (Claudia Altamirano et al., 2013). Immortalized mammalian cells often exhibit inefficient characteristics of their metabolic phenotype by performing partial oxidation due to intense growth. Under batch conditions, high rates of glucose are converted to lactate instead of complete oxidation to H_2O and CO_2, even if oxygen is not the limiting factor. This phenomenon is known as the 'Warburg effect' (Zagari et al., 2013). Another biochemical process contributing to enhanced lactate concentration is the oxidation of glutamine (glutaminolysis) to malic acid, which converts into pyruvate and further into lactate (Zagari et al., 2013). Accumulation of lactate and ammonia in the culture medium is an undesired result of industrial processes as both of these substances can have toxic effects on cells at certain concentrations. Optimized feeding strategies, or classic genetic engineering approaches like knock-down of lactate dehydrogenase (LDH) or overexpression of pyruvate carboxlase (PC), as the missing link between glycolysis and TCA, were therefore natural targets to modification (Ahn and Antoniewicz, 2012; Niall Barron et al., 2012). Overall, monitoring glucose and glutamine as process substrates and lactate and glutamate as metabolic products in culture media routinely, can already provide substantial information about the quality of a bioprocess (Tsao et al., 2005) or the value of a newly developed cell line as a production host. For optimization of metabolic performance purposes, it can additionally implement the necessary background for feeding strategies to maintain substrate levels above critical concentrations and for reduction of by-product formation impedimental for high-productivity runs of culture processes (Le et al., 2012; Li et al., 2010). Furthermore, these parameter profiles can illustrate an overview of metabolism (Selvarasu et al., 2012) and hence contribute to the approach of genetic engineering (Niall Barron et al., 2012), or to visualize metabolic differences across cell lines. In this case: parental, negative control and anti-miRNA-466h-5p CHO cell lines.

Apoptosis is the result of a set of signals that are based on the source of stimuli: a) the endoplasmatic reticulum stress pathway b) the receptor mediated

pathway c) the intrinsic or mitochondria-mediated pathway (Majors, Michael J. Betenbaugh, and Chiang, 2007), all of which can be triggered in different ways and can cross-communicate, activating more than one pathway at a time (Arden and M. J. Betenbaugh, 2006). Only the most significant apoptosis related mechanism of molecules of the Bcl-2 (B-cell lymphoma) family should be mentioned here, as almost all of the anti-apoptotic-target genes (*bcl2l2, dad1, birc6, stat5a and smo*) are more or less involved in this cascade of reactions. Pro apoptotic (Bax, Bak, Bad, Bim) factors of this family are located in the cytosol in healthy cells and translocated and/or activated to target mitochondria during apoptotic signaling. This causes the release of the principal killing factor cytochrome *c*, that initiates the apoptotic cascade, and SMAC/DIABOLO, by creating a pore in the outer mitochandria membrane (Westphal et al., 2011; Majors, Michael J. Betenbaugh, and Chiang, 2007). Anti-apoptotic factors are set out to prevent the formation of this pore. Either directly by maintaining the potential of mitochondria or indirectly by binding apoptotic Bcl-2 components (Majors, Michael J. Betenbaugh, and Chiang, 2007). In terms of cell engineering, apoptosis genes have successfully been targeted in recent history to increase viability of industrial host cells (Chiang and Sisk, 2005; Figueroa et al., 2001), with the outlook of improving recombinant protein production as a result.

In recent years, several researchers have investigated the link between anti-apoptosis cells and changes in metabolism (Templeton et al., 2014; Dorai et al., 2009). In Fig. 3.3 apoptosis accounts for the major reason of cell death in bioreactor cultures and increased cell viability is proportional to improved product titer (Templeton et al., 2014), simultaneously investigating the connection to metabolism or changes thereof could point out the interdependence. The studies found that, while IVC was significantly higher, the nutrient consumption and production profiles were altered when the apoptosis pathways were modified. If this more classic way of overexpressing certain genes of anti-apoptotic proteins already influence the central carbon metabolism (Templeton et al., 2014; Dorai et al., 2009), what more could microRNAs do? They regulate mRNAs of whole apoptotic pathways and therefore influence more then one protein, while simultaneously avoid translational burdening of cells.

3.1.3 Assessing substrate usage characteristics using Omnilog

As differences in metabolism of the three different cell lines were a possibility, a quick and easy experiment to confirm this theory was performed. The Omnilog system, which was kindly provided by Biolog Inc. (Hayward, CA), creates the possibility to investigate patterns of energy producing pathway in various cell

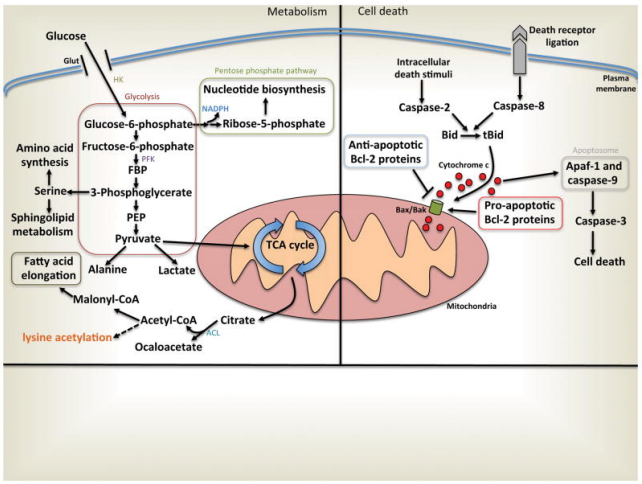

Figure 3.3: Overview of regional relevance of apoptotic pathways and metabolism (Andersen and Kornbluth, 2013)

lines, thus determining variations across cells. Basically, the system relies on dye reduction as a result of NADH production based on catabolism of biochemical substrates. It is well known that media supplements like glucose, glutamine and pyruvate are big supporters of cell growth. A broader understanding of universal but also unique potentials of energy production and substrate usage could help apply cell specific bioprocess optimization. It could also contribute to a better understanding of differences in metabolic patterns after application of cell engineering and its resulting effects on cell properties. In this case, cell engineering resulted in a higher protein production. If the modification due to the transfection resulted in a more effective metabolism and redistribution of energy in anti-miRNA-466h-5p cell line, using the Phenotypic microarray system could deliver first indications of this hypothesis. Profiling cell lines can be conducted in a high throughput manner by seeding cells in 96 well microplates (PM M1). These wells are coated with different substrates, mostly carbohydrates and carboxylates, that could be metabolized if the biochemical pathways of the cell lines can utilize the presented substrate as an energy resource (*The Phenotype MicroArray Assay Technology For Optimizing Clone Selection* 2016; Bochner et al., 2011).

3.1.4 Analysis of pathway flux alterations - ^{13}C MFA

In section 1.2.3, the subject of metabolic engineering, its influence in science and possibilities, was briefly mentioned.
The more we understand about cells and their functions and characteristics, the easier it is to find the perfect host cell line for protein production. Information

about network properties and patterns could be crucial for phenotypic determination which again conclude the fit for applications and quests. However, not only fields of metabolic engineering but also analysis of diseases, e.g. human metabolic diseases, can benefit from understanding metabolism and its alterations (Antoniewicz, Kelleher, and Gregory Stephanopoulos, 2006; Buescher et al., 2015).
Metabolism is subject to remarkably high conservation in all kingdoms of life, despite their immense differences in physiology and lifestyle. It took decades of many experiments like *in vitro* assembly of enzymatic data of singular reactions, mutant analysis and ILEs (isotopic labeling experiments), to gather information about metabolism that can now be found in countless textbooks. Due to this effort, the structure of metabolism is one of the best characterized arrangements in biological networks (Zamboni et al., 2009).

Metabolic flux analysis (MFA) is a powerful tool which makes make flux quantifications of major metabolic pathways possible, using a combination of mathematical concepts and experimental data (Selvarasu et al., 2012; Russmayer, 2016). The metabolic flux is described as the time dependent rate of intermediates through biochemical pathways that cannot be measured directly (D. Voet and J. G. Voet, 2011; Sauer, 2006).

One approach of analyzing intracellular biochemical fluxes is called *Flux Balance Analysis (FBA)* . A necessary assumption for this network is that the whole biological system is in a quasi- stationary state, meaning that the concentration of intracellular intermediates does not vary over time (W. Wiechert, 2001). Under this assumption the general term of intracellular metabolites $\frac{dX_met,i}{dt} = G^T v_met - \mu \cdot X$ applies. This equation and its derivation will be explained with a small example network to describe the mathematical methodology.

The method uses stoichiometric properties combined with optimization criterions to limit the solution space of the network in order to find a unique solution for the model and to minimize the degrees of freedom (Fernandez, Dustet, and Chico, 2012; Russmayer, 2016). Additional information on measured fluxes can further reduce the degrees of freedom to obtain an exacter model. Nevertheless, FBA is strongly limited in its capacity of finding a unique solution. (Chmiel, 2011) ^{13}C MFA has the possibility to overcome the limitations of FBA, that are (Chmiel, 2011):

- Parallel pathways cannot be concluded if none of the pathways are linked to a measurable variable (W. Wiechert, 2001)
- Stoichiometric approaches have no capability to generate information on

metabolic cycles or bidirectional reactions but can only give information about net fluxes (W. Wiechert, 2001; Wolfgang Wiechert, 2007)

- Correct stochiometric flux calculations in catabolic pathways like glycolisis, TCA- cycle, pentose phosphate pathway and other, is only possible if the energy metabolites ATP, NADH, NADPH are balances in the reactions, making the system extremely complex (W. Wiechert, 2001; Chmiel, 2011) Often these values have to be estimated as their stoichiometric is not known exactly for every physiological phase (Niklas and Heinzle, 2011).

^{13}C-Metabolic Flux Analysis uses the stoichiometric models in combination with in vivo isotopic labeling experiments to compute the exact value of fluxes. ^{13}C MFA results in a flux map of the considered metabolic pathways, illustrating the calculated rates of living cells in correspondence with their biochemical reactions(Fernandez, Dustet, and Chico, 2012; Noh, Droste, and W. Wiechert, 2015). This method was used here to identify and calculate fluxes of the three different cell lines obtained by A. Druz. G. N. Stephanopoulos, Aristidou, and Nielsen stated that the real value of flux maps are the observable flux differences that can be noticed within different cell lines under the same condition or same cell lines under varying conditions. By representing the current physiological status quo of the cells compared to the static, snap-shot-like concentrations of proteins or metabolites, other investigations provide as an outcome, this method establishes direct readouts of *in vivo* cellular metabolic activities (G. N. Stephanopoulos, Aristidou, and Nielsen, 1998a; Noh, Droste, and W. Wiechert, 2015; Sauer, 2006; McAtee, Jazmin, and Jamey D Young, 2015).

Carbon labeling experiments (CLE's) were developed in the 1990's, driven by the necessity of more information about the quantity of bidirectional steps (Wurzel and de Graaf, 1999). These experiments successfully unraveled new pathways, unexpected operations in pathways believed to be deciphered already and metabolic robustness to many genetic alterations (Zamboni et al., 2009). Under the assumption that cells do not differentiate in the usage of ^{13}C labeled glucose to unlabeled glucose, the principle behind the technique is that the labeled substrate is consumed and metabolized by the cell. Therefore the C marked molecules are distributed evenly throughout the network (Sauer, 2006; Chmiel, 2011). The labeled carbon reaches equilibrium at one point and creates characteristic ^{13}C patterns of metabolites. The carbon backbone of these metabolites can be labeled at any C position. The term isotopomers describes this possibility, see Fig. 3.4 (Zamboni et al., 2009; Wolfgang Wiechert, 2007).

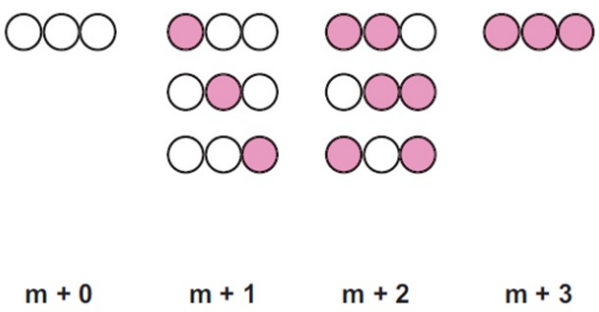

Figure 3.4: Mass isotopomer patterns. Circles demonstrate carbons. Pink color demonstrates labeling (Chmiel, 2011).

The isoptopomer data that results in the detection ^{13}C via mass spectometry (in this case), can then be used to calculate flux distributions by least square regression and elementary metabolite units (EMU) (Ahn and Antoniewicz, 2011).

For ^{13}C MFA to work, a few assumptions are applied. For better understanding the methodology, and underlying mathematics of MFA shall be explained in the following subsection. It also contains the underlying assumptions that are necessary to conduct this application:

MFA-Methodology

Basic assumptions. A cell, pro- or eukaryotic, is not a static construct but in a continuous exchange of material with its surroundings to produce and replenish necessary compounds and metabolites to maintain intracellular order. Cellular metabolism is the overall system in which energy is used to perform various sets of reactions to ultimately accomplish maintenance, growth, perform mechanical work, transport processes for input metabolites (*substrates*) or output metabolites (*products*) and biosynthesis of molecules. This principle, simplistically illustrated in the black box model seen in Fig. 3.5, is known as law of mass conservation (G. N. Stephanopoulos, Aristidou, and Nielsen, 1998c; D. Voet and J. G. Voet, 2011; Riveros, 2012).

This law can be generally apply to bioprocesses, presented in the following mathematical formulation called Mass Balance:

$$\frac{dM_i}{dt} = F_{i,IN} - F_{i,OUT} + v_i Z \tag{3.1}$$

Where: $\frac{dM_i}{dt}$ is the difference of metabolite i over time t; $F_{i,IN}$ and $F_{i,OUT}$ are the amount of input and output of metabolite i, respectively; the term $v_i Z$ is the reaction of metabolite i, v being the reaction rate and Z being the working

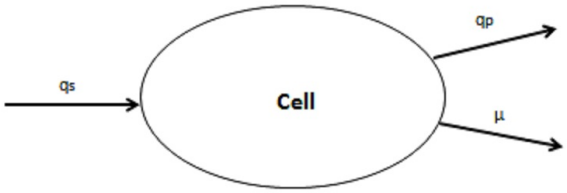

Figure 3.5: Black box model of the cell, adapted from (G. N. Stephanopoulos, Aristidou, and Nielsen, 1998c; Provost and Bastin, 2004)

volume.

This equation can now be solved for every reaction for substrate, metabolite, product and bioprocess model, batch, fed-batch and continuous culture designs. In this case, the equation has to be solved for batch culture with cells in exponential steady state, resulting in the following balances:

$$\frac{dX}{dt} = \mu \cdot X \tag{3.2}$$

$$\frac{dS}{dt} = -v_s X \tag{3.3}$$

$$\frac{dX_met, i}{dt} = G^T v_met - \mu \cdot X \tag{3.4}$$

$$\frac{dP}{dt} = -v_p X \tag{3.5}$$

The first equation, 3.2, being the classic growth balance.
The second one, 3.3, illustrates the rate at which cells consume substrates, using v_s as a vector of specific uptake rates of the given substrate.
Equation 3.4 is the most interesting in case of flux balancing. The right term contains the expression μX which describes the dilution of metabolites due to growth. Especially under the assumption of a pseudo-steady state this term can be easily neglected based on its very small effect compared to the much higher value of the second term $G^T v_{met}$. This term represents the general mass balance for intracellular metabolites, important for flux balancing. v_{met} can be described as the vector $v_{met}=(v_1, v_2, ..., v_6)$ of the specific velocity of change and G^T as the corresponding stoichiometric matrix. The last equation represents the product formation rate. V_p can illustrate the rate of intracellular product accumulation or secretion rate towards extracellular space (Henderson, 2016; Provost and Bastin, 2004; Fernandez, Dustet, and Chico, 2012; G. N.

Stephanopoulos, Aristidou, and Nielsen, 1998a).

At this point, it is very important to mention that due to their rapid turn over, intracellular metabolites are usually considered to be in a pseudo-steady state. Meaning, they do not accumulate in the cell and their concentration stays constant represented in formula 3.18. This fact is important for the mathematical definition or the cellular network system (Llaneras and Picó, 2007a; G. N. Stephanopoulos, Aristidou, and Nielsen, 1998b; Varma and Palsson, 1994).

Stochimetrics of reactions. With this background one can specify network stochiometrics, describing the reactions by which the substrates are metabolized into metabolic products and biomass components. For this cause it is most important to distinguish and characterize all molecules groups included in metabolism.

- *Substrates* are defined as compounds that are essential for cell function, providing energy, nitrogen or carbon sources and are usually present in the sourrouding media (e.g. Glucose and Glutamine)..
- *metabolic products* are described as materials produced by the cell and secreted to extracellular medium. This can be primary metabolits (e.g. Lactate) or secondary ones.
- *Biomass building blocks* are macromolecules that build up biomass. They include apparent substances like RNA, DNA, carbohydrates, lipids and proteins.
- The rest of the compounds within the cell are called*intracellular metabolites*. These are usually defined as consituents of the cellular pathways like glycolysis, but can also be components building macromolecules like amino acids (G. N. Stephanopoulos, Aristidou, and Nielsen, 1998b).

These definitions are necessary for the following description of the mathematical background of reaction stoichiometric Using rule of mass conservation a general model of the n reactions stoichiometric can be concluded as followed:

$$\sum_{i=1}^{n} \alpha_{ji} S_i + \sum_{i=1}^{m} \beta_{ji} P_i + \sum_{i=1}^{q} \gamma_{ji} X_{macro,i} + \sum_{i=1}^{k} \delta_{ji} X_{met,i} = 0 \qquad (3.6)$$

where α_{ji}, β_{ji}, β_{ji}, δ_{ji} are the corresponding stoichiometric coefficients for the ith constituent of the associated jth reaction. Considering that a regular metabolic network model has several more reactions than the sample network

that will be presented in the following, equation 3.6 can be rewritten in a compact form by using matrix notations:

$$AS + BP + DX_{macro} + GX_{met} \tag{3.7}$$

where A, B, D, G contain the stoichiometric constituents in matrix form. The following example, see Fig. 3.6, derived and modified from the actual network model, illustrates the last couple of paragraphs for better understanding. Part of the network, glycolysis to be exact, was remodeled. The overall reaction of the breakdown of glucose and other carbohydrates is Glucose + 2NAD$^+$ + 2ADP + 2Pi $\rightarrow$ 2NADH + 2 pyruvate + 2ATP + 2H2O + 4H$^+$. The individual reactions are split into the following equations:

$$\text{-Glucose + ATP + F6P} = 0 \tag{3.8}$$

$$\text{-F6P - ATP + DHAP + GAP} = 0 \tag{3.9}$$

$$\text{-DHAP + GAP} = 0 \tag{3.10}$$

$$\text{-GAP + 3PG + NADH + ATP} = 0 \tag{3.11}$$

$$\text{-3PG + Pyr+ ATP} = 0 \tag{3.12}$$

$$\text{-Pyr + NADH + Lactate} = 0 \tag{3.13}$$

Using the principle of equation 3.7 this can be displayed in a matrix formation like:

$$\underbrace{\begin{pmatrix} -1 \\ 0 \\ 0 \\ 0 \\ 0 \\ 0 \end{pmatrix}}_{A^T} \underbrace{\begin{pmatrix} S_{gluc} \end{pmatrix}}_{S} + \underbrace{\begin{pmatrix} 0 \\ 0 \\ 0 \\ 0 \\ 0 \\ 1 \end{pmatrix}}_{B^T} \underbrace{\begin{pmatrix} P_{Lact} \end{pmatrix}}_{P} + \underbrace{\begin{pmatrix} 1 & 0 & 0 & 0 & 0 \\ -1 & 1 & 1 & 0 & 0 \\ 0 & -1 & 1 & 0 & 0 \\ 0 & 0 & -1 & 1 & 0 \\ 0 & 0 & 0 & -1 & 1 \\ 0 & 0 & 0 & 0 & -1 \end{pmatrix}}_{G^T} \underbrace{\begin{pmatrix} X_{F6P} \\ X_{DHAP} \\ X_{GAP} \\ X_{3PG} \\ X_{Pyr} \end{pmatrix}}_{X_{met}} \tag{3.14}$$

Reaction rates or fluxes are defined as the velocity or forward flux v of a biochemical reaction. The previously defined stoichiometry of reactions declares the relative amounts of compounds consumed or produced in each of the J intracellular reactions by defining the corresponding their stoichiometric coefficients. However, it should be noted that this does not describe the velocity of their formation, secretion or consumption. This can be overcome by calculating

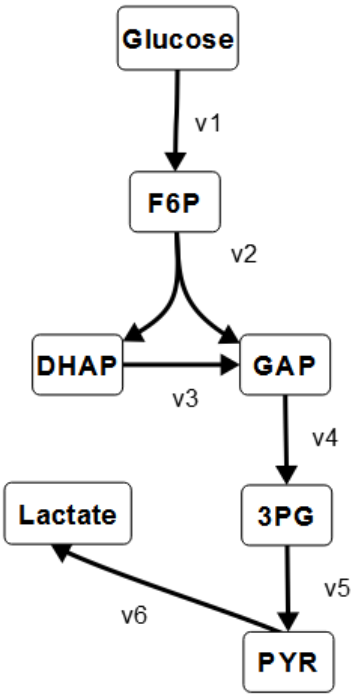

Figure 3.6: Example network for MFA: v = fluxes for specific reactions

fluxes of the individual reactions of change $\frac{dX_{met}}{dt}$. For example, an intracellular compound with the stoichiometric coefficient δ is produced or consumed with a rate of $\delta \cdot v$. Summarizing the rates for all reactions (J) and their compounds (i) we get an equation of

$$r_{met} = \sum_{j=1}^{J} \delta_{ji} v_j \tag{3.15}$$

specifying the formation rate of ith metabolite in the jth reaction. Ultimately, this balance can be converted to

$$\frac{d\boldsymbol{X_{met}}}{dt} = r_{met} \tag{3.16}$$

to

$$r_{met} = S^T \cdot v \tag{3.17}$$

Fluxes are not constant values but highly variable depending on their circumstances. Metabolic systems, however, will produce constant fluxes at constant input rates, meaning at steady states. This is how the pseudo-steady-state assumption is applicable here, yielding:

$$r_{met} = G^T \cdot v = 0 \tag{3.18}$$

$$G^T_{mes} \cdot v_{mes} + G^T_{calc} \cdot v_{calc} = 0 \tag{3.19}$$

$$v_{calc} = \frac{-(G^T_{mes} \cdot v_{mes})}{G^T_{calc}} \tag{3.20}$$

Transferring to example network means:

$$\frac{dS_{gluc}}{dt} = -v_1 \tag{3.21}$$

$$\frac{dF6P}{dt} = v_1 - v_2 \tag{3.22}$$

$$\frac{dDHAP}{dt} = v_2 - v_3 \tag{3.23}$$

$$\frac{dGAP}{dt} = v_2 + v_3 - v_4 \tag{3.24}$$

$$\frac{d3PG}{dt} = v_4 - v_5 \tag{3.25}$$

$$\frac{dPyr}{dt} = v_5 - v_6 \tag{3.26}$$

$$\frac{dP_{lac}}{dt} = v_6 \tag{3.27}$$

and further converting it into matrix format and splitting it up as presented in equation 3.19

$$\underbrace{\begin{pmatrix} v_1 \\ v_2 \\ v_3 \\ v_4 \\ v_5 \\ v_6 \end{pmatrix}}_{v_{calc}} = \underbrace{\begin{pmatrix} 1 & -1 & 0 & 0 & 0 & 0 \\ 0 & 1 & -1 & 0 & 0 & 0 \\ 0 & 1 & 1 & -1 & 0 & 0 \\ 0 & 0 & 0 & 1 & -1 & 0 \\ 0 & 0 & 0 & 0 & 1 & -1 \end{pmatrix}^{-1}}_{G^T_{calc}} \cdot \underbrace{\begin{pmatrix} v_1 \\ v_6 \end{pmatrix} \cdot \begin{pmatrix} -1 & 0 \\ 0 & 1 \end{pmatrix}}_{V_{mes} \cdot G^T_{mes}} \tag{3.28}$$

Now this equation can be solved for v_{calc} using linear algebra (G. N. Stephanopoulos, Aristidou, and Nielsen, 1998b; Zamboni et al., 2009; Chmiel, 2011; Riveros, 2012; Llaneras and Picó, 2007b; Provost and Bastin, 2004).
With these definitions one can calculate the degree of freedom (DOF). DOFs are important to conclude if there is a unique solution for the flux vector of

the system and informs of its determinability. With the formula $F = M - N$ the degrees of freedom are calculated. Where F is the degree of freedom, M is the number of independent linear reactions and N are the reaction fluxes (v) (Chmiel, 2011; Henderson, 2016; Niklas and Heinzle, 2011). There are three different possibilities of determination:

F = 0; determined system, meaning that same amount of M and N meaning that there is a distinct solution for the network, and there are no additional measurements necessary to determine the system.
F > 0: overdetermined system, meaning there is more information available than necessary to come to one definite resolution. This means that either additional measurements of secretion rates or uptake rates can be eliminated or the redundancies can be used to obtain better estimates of v_{calc} but also v_{mes} by using least square solution method. The additional information can also be used to control if the assumed pseudo steady state for intracellular metabolites even applies.
F < 0; underdetermined system, meaning that there are more Ns than Ms and there is no unique solution to the system. In realistic networks, models are usually underdetermined. Additional information is needed to determine the system. This can be achieved by further measurements to decrease the degree of freedom (Niklas and Heinzle, 2011; G. N. Stephanopoulos, Aristidou, and Nielsen, 1998a; Chmiel, 2011).

Using linear algebraic methods to solve the balance, the discussed example network would have a balance of $F = 7 - 6$, this means a positive the degree of freedom (+3) and an overdetermined system. This only applies to our example network. The realistic network used to model CHO cell metabolism would be underdetermined using only stochiometric approaches. Therefore a ^{13}C MFA experiment was conducted and the principle can be found in Fig. 3.7.

When cells reach a metabolic steady state (usually under balanced growth conditions), the cell specific, internal metabolic rates are regarded as constant and system information can be attained by measuring medium composition for extracellular substances. Calculations based on these measurements must account for accurate assessment of uncertainty (Taylor A Murphy and Jamey D Young, 2013) to continue with the input of data into the Metabolic Flux Tool (INCA).

These principles apply to every FBA and MFA. With ^{13}C labeling experiments however, additional to this information provided by measurable extracellular fluxes, the fate of labeled carbon can be determined with appropriate analytical methods. Proper intermediate modeling and suitable computer based analyzing tools can then predict (INCA, see 3.2.3) fluxes (Chmiel, 2011; Jamey D Young, 2014b).

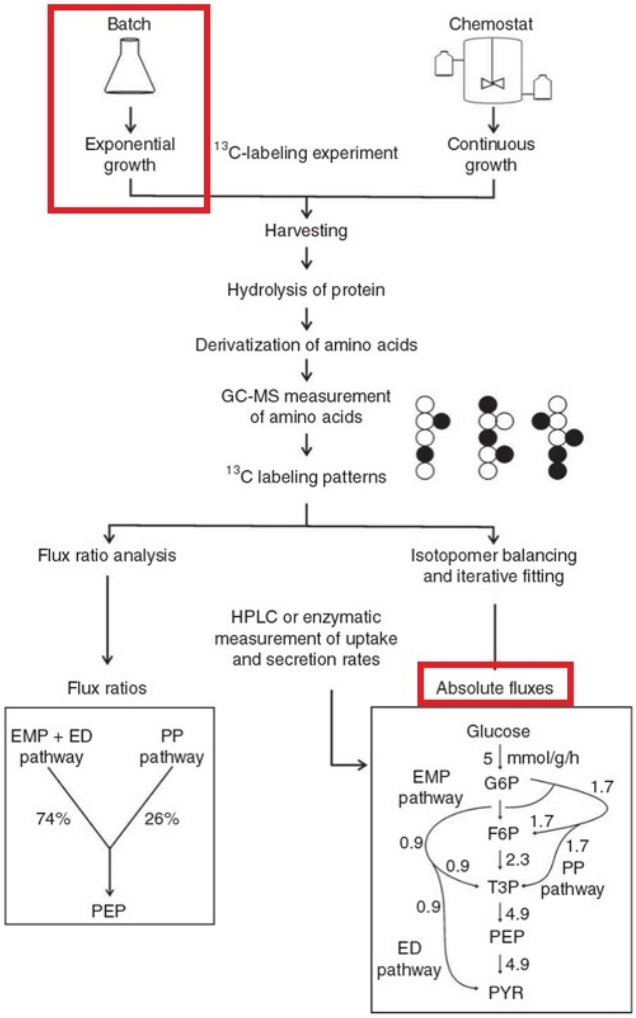

Figure 3.7: Principle of ^{13}C experiments Data analysis using INCA yielded absolute fluxes. Figure adapted from (Zamboni et al., 2009)

3.2 Materials and Methods

3.2.1 Cell cultivation and growth cultures

Chinese hamster ovary suspension cell lines (CHO S) were kindly provided by A. Druz at NIH, Bethesda, MD. Three different cell lines were used or developed, respectively, during Druz's PhD thesis. To do so, the parental cell line (here denominated as WT), purchased from Life Technologie, Gaitersburg, MD (Cat.no. 11619-012), was genetically modified (Aliaksandr Druz et al., 2011b; A. Druz, M. Betenbaugh, and J. Shiloach, 2012; Aliaksandr Druz, 2012; Aliaksandr Druz, Son, et al., 2013). For detailed information see section 3.1. Each cell line arrived at different passage numbers. Parental cell line (WT) exhibiting passage number of 8, the negative control (NC) exhibiting a passage number of 9 and the anti-miRA-466h-5p cell line (F9), exhibiting a passage number of 5. Media experiments and growth curves were conducted with different kinds of media. Medium (CD-CHO) is a chemically defined, serum free medium and commercially available at Gibco, Life Technologies (Ref. No.: 10743-011). It was supplemented with 8mM of glutamine to reproduce exact cell growth and viability studies were performed by A. Druz (Aliaksandr Druz et al., 2011a).
To recreate exact conditions for cell growth, cells were cultured at 37°C, 5% CO_2 in a humidified incubator, to simulate culture conditions used by A. Druz (Aliaksandr Druz et al., 2011a). Cell lines were seeded in triplicates at a concentration of 1 x 10^5cells/mL in a working volume of 40mL in 125mL shake flasks. Shaking platform was set to 130rpm, with flask lids loosened to optimize air flow. Sampling and cell counting was performed daily. Samples were counted manually by using a hemocytometer. Viability was determined by Trypan Blue exclusion method.

Media development for ^{13}C CD CHO, as a complete medium, could not be used for subsequent ^{13}C MFA experiments, due to the isotopically unlabeled glucose, therefore an alternate medium, providing identical growth conditions, had to be developed. CD OptiCHO medium (Ref. No.: ME120159L1), which misses some key nutrients, was used to perform quick media optimization experiments. Lacking nutrients were added considering the natural serum osmolarity of about 290 mOsmo/L. Stock solutions of 200 g/L glucose, 200 mM glutamine, 300 mg/L NaCl and 10 mM manganese were produced. Glucose and manganese concentrations were kept at a constant 5 g/L and 0,001 mM, respectively. Initial glutamine concentrations were varied for growth optimization reasons and NaCl was added at last to match up to an osmolarity of about 290mOsm/L. This media was tested with a glutamine concentration of 4 mM and 8 mM, respectively.

Subsequent culture conditions were performed identically to cell culture performed with CD CHO medium, in section 3.2.1.

Cell culture for ^{13}CMFA Data analysis of cell performance, in 4 mM and 8 mM medium, resulted in the decision to go forward with the media variation containing 4 mM glutamine. Glucose added contained 50% of unlabeled glucose and 50% ^{13}C of labeled glucose. Two different variations of ^{13}C labeled glucose were added. 25% of the total glucose consisted of U- ^{13}C D-glucose and 25% od 1,2 $^{13}C_2$ D-glucose, adding up to a total glucose concentration of 4.74 g/L glucose (experimentally measured values are around 4.5 g/L).

Well-growing, healthy cells of all cell lines were harvested, washed with PBS and reseeded in ^{13} media at a concentration of 1 $\times 10^5$ cells/mL in isotopically labeled media. The labeling process was executed in 2 consecutive batches with the prepared media to ensure isotopic steady-state within cells. The second run of batches being carried out in triplicates. Sampling for growth analysis was executed every 12 hours. No sampling was performed for the first batch. Culture conditions for all batches mimicked culture conditions used during growth and viability studies and media development experiments at 37°C, 5% CO_2 in vented 125 mL shake flasks on an orbital shaker at 130 rpm. To ensure cells were in a condition of metabolic steady-state, cells were harvested before transitioning into stationary phase and before reaching their maximal cell count. Thus, cell cultures of the parental cell line were harvested 83,5 h after seeding, the other two cell lines stayed in culture until hour 109 after seeding. The rest of the media was collected and analyzed for glucose, lactate, glutamate and glutamine concentration with the YSI 2700 Select analyzer.

Glucose and Lactate concentrations in media. Samples taken for growth studies were simultaneously probed for media concentration of glucose and lactose, to determine uptake and secretion rate, respectively. Samples were prepared by centrifugation at 3000 rpm for 10 minutes to receive a cell pellet and cell free supernatant that was subsequently tested for the substrate and product concentrations by YSI 2700 Select.

3.2.2 Assessing differences in substrate usage of the cell lines.

Providing a fast and simple way to predetermine differences in cellular energy metabolism pathways among the three cell lines, a quick Omnilog analysis experiment was executed. This tetrazolium-based redox assay resulted in parallel determinations of the ability of specific cells to use different substrates as their

main energy source.

Cells cultured under the same conditions as growth studies with CD CHO media were prepared simultaneously, each in triplicates, to perform the analysis. Cells were harvested and cell density was determined manually. Cell viability was established to guarantee ideal health for experimental conditions. Afterwards, cells were washed with DPBS and resuspended in experiment specific media IF M2, yielding a cell density of 500 000cells/mL. IF M2 is a method specific medium that was enriched with glutamine to reach a total concentration of 0,3 mM glutamine, but it was still lacking other amino acids and glucose. 50μ4L of this cell-media mixture was then dispensed into each well of the 96 well plate (PM M1) and subsequently incubated for 4 hours at 37°C and 5% CO_2, in an humidified incubator. After the incubation period, 10 μL of Redox Dye Mix MB was added to the wells and plates were immediately incubated in the Omnilog system chamber to monitor dye reduction by purple formazan formation inside the wells (Bochner et al., 2011). Formazan production was continuously detected every 5 minutes for a period of 4 hours.

3.2.3 Using Microarray assay to determine apoptosis onset under different nutritional conditions.

Like the previously described procedure with Omnilog's energy substrate usage analysis, this experiment was carried out in three parallel runs. Similar to before, cell viability was determined, cells were washed with DPBS and resuspended and seeded in specific Biolog medium. Other than before, seeding density, incubation time and redox dye were modified, resulting in different data provided by the system, after analysis. IF M2 media was replaced by IF M1 media. IF M1 media contains all important amino acids that the inoculation fluid M2 is lacking. Therefore IF M1 replaced IF M2 to avoid wrongful onset of apoptosis due to the lack of necessary amnio acids but to guarantee programmed cell death to be only dependent upon primary carbon source exhaustion.

Additionally, IF M1 was enriched with by adding 10 dialyzed FBS and 0.3 mM glutamine. Cells were resuspended to create a solution with a cell concentration of 4×10^4 cells/mL, resulting in a total cell count of 2 000 cells per well. A total of five PM M1 plates per cell line were seeded with these cell suspensions and incubated at 37°C, 5% CO_2. Incubation time added up to a total of 48 hours. Within this time frame every 12 hours, starting right after plating (hour 0), 10 μL/well of Redox Dye MB, containing 30 mM of glucose was added to only one of the incubate plates per cell line and sealed to avoid CO_2 loss. Subsequently, the plates were incubated with the Omnilog instrument system at 37°C to document change of color in the wells based on dye reduction.

Using glucose in the dye at low cell seeding densities can spike the signal for better detection and will not or very little influence the apoptosis results based on energy metabolism. This protocol was developed and conducted for a Biolog internal study and created fairly good results for Hep G2/C3A cells (Bochner, 2014; Bochner et al., 2011).

Sample preparation for subsequent GC/MS Analysis

Protein Extraction from Cell Cultures. In section 3.2.1 the development of the suitable medium and cell culture conditions of parental, negative control and anti-miRNA-466h-5p cell lines were already described for this experiment. After growing the cells until confluent, proteins and RNA were extracted by following a triphasic extraction protocol whereby RNA was obtained in the aqueous phase, DNA in the interphase and proteins in the organic phase. Protein extraction was accomplished using TRIzol® method (*TRIzol Reagent - Manuals & Protocols* 2016). At first cells were washed multiple times with PBS to remove isotopic labeled growth media. A pellet formation was sought by adding TRIzol® to the samples and vortex allowing the cells to lyse and homogenize. At this point the parental cell lines were frozen because they were confluent a day earlier than the miRNA engineered cell lines. The subsequent steps of the protocol were then again performed with all three cell lines simultaneously to allow the same preparation conditions.

Adding chloroform to the cell vials containing lyzed cells, shaking them vigorously and spinning them down at 4°C at 12 000 rpm yielded a separation of the homogeneous solution into three phases. For the purpose of this experiment, the only phase of interest was the one containing proteins.

For achieving purification of the protein biomolecules, the aqueous phase containing RNA was removed. Secondly, ethanol was added to the remaining inter- and organic phase, incubated and centrifuged to let DNA settle by centrifuging at 5000 rpm for 10 min at 4°C. Proteins remained in the supernatant solution. This supernatant was then treated with acetone, instead of isopropanol, to precipitate the contained proteins, followed by a centrifugation step to win a pellet of proteins (Taylor A. Murphy, Dang, and Jamey D. Young, 2013).

Tertbutyldimethylsilyl (TBDMS) derivatization of amino acids By using a variation of the protocol developed by Maciek R. Antoniewicz, derivatization of amino acids was accomplished. These proteinogenic amino acids were further analyzed by GC/MS. For preparation, proteins had to be hydrolyzed to produce single amino acids which could then be derivatized to receive less reactive molecules (Stenerson, 2015). This was attained by adding 6N HCl to

the protein pellet and by applying vaccuum and incubate at 110°C for 22h. Subsequent consecutive steps as removing of cell debris by centrifugation, drying samples under airflow at 60°C, resuspending samples in $dd\mathrm{H_2O}$ through sonication, filtration of samples through a0.2μm pore size filter, followed by re-drying samples under airflow at 60°C, prepares the samples for derivatization enabled GC/MS analysis.

To make resulting amino acids more volatile and produce tert-butyl dimethylsilyl (TBDMS) derivatives, the dried sample was dissolved in 50μL. 70μL of MTBSTFA + 1% TBDMCS were then added and incubated for 30 min at 60 °C. The last step was to centrifuge the samples and transfer the liquid phase to a GC/MS glass insert (Taylor A. Murphy, Dang, and Jamey D. Young, 2013).

Gas chromatography mass spectrometry analysis Gas chromatography mass spectrometry was done by using the Agilent 7890A gas chromatograph with DB-5ms (30m × 0.25mm ⌀ × 0.25μm; Agilent J&W Scientific) capillary column. The injection volume was 1 μL. Samples were run in split mode (ratio 1:10). The GC was linked to a ..... mass spectrometer. The GC inlet temperature and MS interface temperature were maintained at 250 °C. The helium flow was set to 1 mL/min and pressure- controlled electronically for the amino acid analysis. Mass spectra of amino acid fragments were assembled in SIR (selected iron recording) mode. Determined metabolite fragments can be seen in Table **??** (Ahn and Antoniewicz, 2011).

Calculation of growth related parameters Specific biomass related parameters like specific growth rate (μ) and extracellular rates including specific uptake (glucose q_{glc}, glutamine q_{gln}) and production rate (lactate[q_{lac}], glutamate[q_{glu}]) and metabolite specific biomass yields ($Y_{s/x}$) were calculated by using Excel for regression analysis of extracellular time-course analysis using the following equations, adapted from Glacken, Adema, and Sinskey:

$$\frac{dX}{dt} = \mu \cdot X \tag{3.29}$$

$$\frac{dS}{dt} = -v_s X \tag{3.30}$$

$$\frac{dP}{dt} = +v_p X \tag{3.31}$$

$$\frac{q_s}{\mu} = \mid -Y_{\frac{s}{x}} \mid \tag{3.32}$$

$$\frac{q_p}{\mu} = +Y_{\frac{p}{x}} \tag{3.33}$$

Integrating equation 3.29 generates the linear function $ln[X] = \mu t + ln[X]_0$,

Table 3.1: Isotopic fragments of essential amino acids measured by GC-MS

Metabolite	Fragment masses	Labeled carbons	Unlabeled Fragments
Alanine	232	2-3	$C_8H_{26}ONSi_2$
Alanine	260	1-2-3	$C_8H_{26}O_2NSi_2$
Glycin	218	2	$C_8H_{24}ONSi_2$
Glycin	246	1-2	$C_8H_{24}O_2NSi_2$
Proline	258	2-3-4-5	$C_{12}H_{28}ONSi_2$
Serine	288	2-3	$C_{12}H_{34}ONSi_2$
Serine	362	2-3	$C_{14}H_{40}O_2NSi_3$
Serine	390	1-2-3	$C_{14}H_{40}O_3NSi_3$
Aspartate	302	1-2	$C_{12}H_{32}O_2NSi_2$
Aspartate	376	1-2	$C_{14}H_{38}O_3NSi_3$
Aspartate	390	2-3-4	$C_{14}H_{40}O_3NSi_3$
Aspartate	418	1-2-3-4	$C_{14}H_{40}O_4NSi_3$
Glutamate	330	2-3-4-5	$C_{12}H_{36}O_2NSi_2$
Glutamate	432	1-2-3-4-5	$C_{14}H_{42}O_4NSi_3$

therefore μ can be determined as the slope of ln[X] plotted against corresponding time points.

Additionally to the manual identification, these values were calculated by using a MatLab based calculation framework ETA (extracellular time-course analysis). This robust software provides not only an additional way to check calculations, but also produces accurate quantifications of these cell specific parameters and their uncertainties, which are further needed for determination of intracellular fluxes in the MatLab based application, INCA (Taylor A Murphy and Jamey D Young, 2013).

Spontaneous degradation of glutamine to pyroglutamate and ammonium was not determined due to lab set up problem (Ahn and Antoniewicz, 2011; Ozturk and Palsson, 1990). Therefore the terms for spontaneous degradation were removed from the equations.

Another important descriptive parameter is the 'Integral of viable cell concentration' (IVC) . This parameter was calculated by integrating the area under the growth curves (AUC) for each discrete time interval of the different cell lines using the following equation:

$$IVC = \frac{(X_1 + X_2)}{2} \times (t_2 + t_1) \tag{3.34}$$

Variable X_1 and X_1 describe the cell concentrations of the corresponding parameters t_1 and t_2. The sum of all the integrals defines the AUC and can then be compared to other cell lines with the same specific productivity. The cells with the higher IVC can be declared as the ones with the greater overall product yield (de Lourdes Velez Suberbie, 2013; Pörtner, 2007).

Creating an metabolic network model for CHO-S cells. A detailed metabolic network model for CHO cell metabolism, comprising 105 fluxes total (72 net fluxes and 33 exch fluxes) was constructed and the complete network be found in the Appendix 6.2. The basis for this biochemical system were multiple descriptions in literature of mammalian metabolic networks (G. N. Stephanopoulos, Aristidou, and Nielsen, 1998a; Ahn and Antoniewicz, 2011; Miebach, 2012; Swarup et al., 2014; Metallo, Walther, and Gregory Stephanopoulos, 2009; Riveros, 2012) which were recombined to create this specific network. The network includes pathways of glycolysis, pentose phosphate pathway (PPP) , TCA cycle, , anaplerotic reactions, amino acid metabolism and biomass production. Cell compartmentalization was taken into account when defining the model. The compartments considered were: cytosol, mitochondrion and extracellular space. The network contains a total of n=72 net fluxes and comprises 47 intracellular metabolites. Four of which were extracellular uptake rates of glucose and glutamine and production rates of lactate and glutamate, as previously described. Cofactor balancing (e.g. NADH, ATP) was excluded because it can produce uncertainties in mammalian cell balancing systems (Taylor A. Murphy, Dang, and Jamey D. Young, 2013).

Metabolic flux analysis By using INCA, a MATLAB-based software, pathway fluxes could be estimated based on mass isotopomer measurements, pool size measurements and extracellular flux measurements. Using the elementary metabolite unit (EMU) method, INCA can simulate steady state and transient isotope labeling experiments. Here, the steady state flux analysis application was sought. The MFA calculations are completed by minimizing the variance-weighted sum-of-square residuals (SSR) between experimental measurements and simulated data of uptake and production rates, distributions of isotopomers of intracellular metabolites. The multistart option, starting with random initial guesses of the flux values, was used to improve the odds of a global solution. An included statistical test provided assessments of goodness-of-fit and accurate computations of 95% confidence intervals of all estimated fluxes (Jamey D Young, 2014b; Antoniewicz, Kelleher, and Gregory Stephanopoulos, 2007; Antoniewicz, Kelleher, and Gregory Stephanopoulos, 2006; Ahn and Antoniewicz, 2011).

3.2.4 Engineering non transfected, negative control and anti-miR-466h CHO cell lines for protein expression capabilities

To assess protein expression quality and differences between the cell lines two different protein expression assays were performed. One with the protein Human Butyrylcholinesterase (HuBChe), tetramer-glycoprotein with 574 amino acids per subunit, and one with recombinant Erythropoietin (rEPO), a complex glycoprotein with 165 amino acids and four glycan side chains (Jelkmann, 2007).

The gene encoding EPO was inserted into the plasmid pcDNA3.1-hygromycin, whereas the plasmid containing the HubChe sequence was called pCHO 1.0. Backbones of both plasmids kindly provided by A. Chung, who purchased them at Life Technologies (personal communication). EPO plasmids were amplified using E. Coli cultures, followed by a plasmid purification step using Qiagen®HiSpeed Plasmid Midi Kit procedure.

Plasmids were transfected using FreeStyle^{TM} MAX reagent (Life Technologies, Cat. No.: 16447-100) according to manufacturer's instructions in CD CHO medium. Speed of orbital shaker platform was reduced to 125 rpm and CO_2 level was adjusted to 8% in the incubator to match Life Technologies guidelines.

Cell lines transfected with EPO plasmid were cultured for 48 hours until they were harvested and the cell suspension was centrifuged at 200g for 10 min. Supernatant was obtained and stored at -20 °C until further investigations with ELISA were performed to assess EPO concentrations in media. A total of two of runs of this assay of EPO expression quality by the investigated cell lines, starting from transfecting cells with EPO plasmid to the ELISA investigation, were conducted. Cell counts and viability of the cells were investigated before plasmid transfection and at the time of cell harvesting.

Cell lines transfected with HubChe plasmid were cultured for 5 days (120 hours). A total of four samples were taken on four consecutive says starting 48 hours after transfection. Samples were centrifuged at 1800g for 5 min, followed by the analysis of the supernatant by Ellman Esterase Assay with Ellman's Reagent (Thermo Scientific, No. 22582). With each sample that was probed, cell count and viability was determined, simultaneously.

Indirect ELISA and Ellman Esterase Assay to determine protein production Abcam's®protocol for indirect ELISA was performed repeatedly to visualize and quantify possible cell line specific EPO expression differences across cell lines. Antigen containing supernatant of cell cultures transfected with EPO plasmid was suspended in 96 well plates in different concentrations. Afterwards,

the plates were incubated for 12 hours overnight at 4 °C. Negative controls were tested in parallel. AntiEPO was used as a primary antibody in a 1:2500 dilution in 1% BSA in BST solution. All washing steps were performed using PBST. 3,3',5,5'-tetramethylbenzidine (TMB) was used as the visualizing reagent. Its chemical reaction was quenched by adding H_2SO_4. Colorimetric results were obtained by a plate reader (Promega) measuring the optical density at 450nm. The best 2 dilution rates were used to repeat the analysis multiple times.

A single run of Ellman Esterase Assay was performed following the protocol of Thermo Fisher Scientific. The assay was conducted in 96 well plates, each cell line in duplicates.

3.3 Results

The following results contain color coded plots and specific abbreviations for valid throughout the rest of this thesis: Blue = parental cell line (WT); Red = negative control cell line (NC); Green = anti-miR-466h cell line (F9)

3.3.1 Comparison and reproduction of growth rate findings and kinetic analysis

To evaluate reproducibility of growth and viability stated by Aliaksandr Druz, Son, et al. the growth studies were recreated and results can be found plots Fig.3.8. Plots represent viable cell densities and cell viability.

Cells grown in medium CD CHO (Fig.(3.8 A)) exhibited a slightly different growth pattern than cells grown in CD OptiCHO (Fig. 3.8 B,C). The viable cell count peaks reached significantly different values across the two culture conditions. Genetically modified versions of the cell lines, anti-miR-466h and negative control cell lines, reached their maximum density 187h after seeding while the parental cell line reached their maximum at 139h, similar to Druz' results. Maximum viable cell densities were $5.6 \times 10^6 cells/mL$ for parental cell lines, $6.8 \times 10^6 cells/mL$ for the anti-miR-466h CHO cell line and $3.2 \times 10^6 cells/mL$. All differing significantly from each other. Interestingly, the parental cell line did not seem to start out with a lag phase or transition into stationary phase after the exponential growing stage with CD CHO medium, declining sharply in viable cell count after reaching the peak of cell density.

Considering Fig. 3.8 growth in CD OptiCHO medium containing 4mM L-glutamine, cells showed maximal cell densities of $5.9 \times 10^6 cells/mL$ for the parental cell line 90h after seeding, $9.4 \times 10^6 cells/mL$ for anti-miR-466h mu-

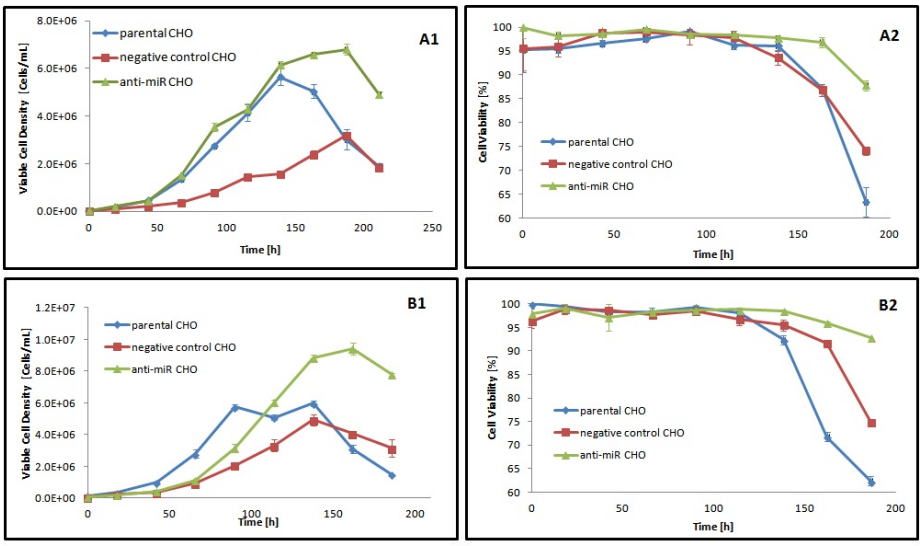

Figure 3.8: Growth charts and viability over time in different media (A) labeled charts depict data with CD CHO media; **(B)** labeled charts with CD OptiCHO medium and a L- Glutamine concentration of 4 mM; Cell density plots (A1, B1) only include viable cell data. A2, B2, B3 show percentage of cell viability data in the corresponding medium

tated cell line and $4.9 \times 10^6 cells/mL$ for NC-CHO cells, both 162h after seeding. Similar to the previously discussed medium, the parental cell line exhibited a short or no lag phase in this medium and last CD-Opti CHO medium containing 8mM L-glutamine (see Fig. 6.1 in Appendix) delivered maximal cell count results of $6.4 \times 10^6 cells/mL$ for the parental cell line at 116h, $9.0 \times 10^6 cells/mL$ for anti-miR-466h cell line 164.5h after starting cell culture and $5.8 \times 10^6 cells/mL$. For both media variations of CD-OptiCHO the significantly highest cell density peak was produced by the anti-miRNA-466h-5p cell line, with no significant difference being detected in between the parental cell line and negative control. Overall, growth profiles always showed a similar pattern with anti-miR-466h cells, scoring the highest cell densities and the negative control showing the lowest maximum cell densities.

Specific growth parameters μ, calculated for the complete growth phase, and μ_{max}, describing the growth rate during the exponential stage, outlined differences in between cell lines cultured in CD OptiCHO. To summarize, WT-CHO cells were growing slightly faster during exponential phase in all three media variations, followed by F9-CHO cell line, and last negative control cells (see values for CD-CHO and CD-Opti CHO 4mM glutamine in table 3.2). Regarding the total growth parameter however, F9-CHO cells reached a higher μ in CD-

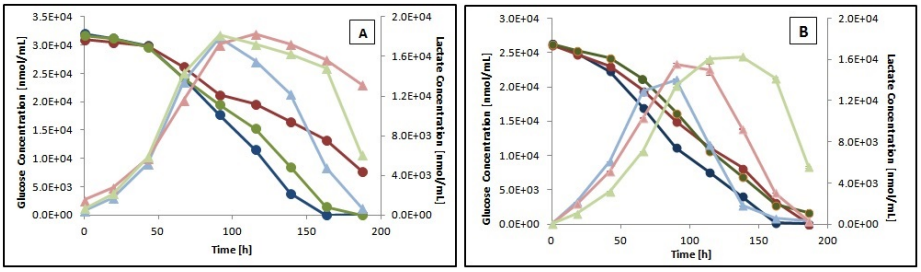

Figure 3.9: Time evolution of glucose and lactate concentrations for CHO cell lines Curves of lighter color show lactate curves, darker colored curves depict glucose curves. Chart (A) presents concentrations in CD CHO medium, whereas chart (B) presents concentrations in CD OptiCHO.

OptiCHO media. As for the CD-CHO medium, it was previously mentioned that there was no stationary phase in the parental cell line so in this case $\mu = \mu_{max}$. Relations between substrate consumption and product formation and growth are described in the following.

Viability of all cell lines, see plots (Fig.3.8 A2, B2 and C2), exhibited similar progression patterns across media variations. Differences were detected by the onset of cell death. One can observe that in all charts the anti-miR-466h cells stayed viable for a longer period of time, confirming Druz's findings that the first cell line decreasing in viability is the parental CHO S cell line, followed by the negative control cell line and, as already mentioned, at last the anti-miRNA-466h cell line. The timing of the onset of cell death, however, differs immensely from the timing stated in Druz's paper (Aliaksandr Druz, Son, et al., 2013). About 150h into the batch culture cells in all different variations of media started apoptosis. Viability declined faster in CD OptiCHO medium subsequently used for metabolic analysis.

Glucose and Lactose concentration in media To exclude a morphological influence over substrate usage, cell sizes were determined repeatedly using an automatic cell counter (Invitrogen Countess™Automated Cell Counter, Cat. No.: C10227). The average cell sizes were calculated to be 11.85μm for the parental cell line, 12.25μm for the negative control and 11.95μm for the anti-miR-466h CHO cell line and did not show any significant differences. Therefore, it can be assumed that there are no morphological deteriorations that could influence the substrate usage patterns.

In addition to the Omnilog's platform energy metabolism analysis, determination of glucose consumption and lactate production were measured with a YSI 2700 bioanalyzer. Nutrient assessments happened simultaneously to growth

curve analysis. Relations of substrate usage and product formation to biomass production were determined by calculating the yield coefficients as previously discussed in section 3.2.1. Figure 3.9 shows the evolution of substrate and product concentration within the media CD CHO and CD OptiCHO (4mM L-Glutamine). Table 3.2 presents the corresponding process parameters (specific growth rates, glucose consumption, lactate concentration and their related yield coefficients), of both media. Medium CD OptiCHO 8mM glutamine was excluded of detailed analysis due to occurring problems during culture conditions and consequently, inefficient data.

Glucose consumption profiles relate closely to cell growth curves, visible in chart 3.9. Experimental conditions investigated started out with a slightly higher glucose concentration in CD CHO media, in comparison with CD OptiCHO 4mM glutamine media. Nevertheless, substrate consumption of WT- and F9-cell lines show great similarities to each other. In both media, glucose was depleted around 160h into the batch culture with parental CHO cells and 1-2 days later with the anti-miRNA-466h-5p cells. Clearly, NC-cells differed in between culture conditions regarding the time course development. CD CHO media results of specific glucose consumption during exponential cell growth show that, the parental CHO cell line used more glucose in the growth process compared to the anti-miRNA-466h-5p cell line, but less compared to the negative control cell line. A conclusion that is confirmed by regarding the yield of amount substrate necessary for amount biomass built ($Y_{\frac{s}{x}}$). Usage yields of F9-CHO are located around 83% and negative control cells about 143% compared to WT-CHO, during exponential phase. A trend that can be also declared for the exponential phase of cell lines growing in CD-OptiCHO with a 83% yield for F9-CHO and 140% for NC-CHO cells compared to the WT-CHO cells. Absolute yield values however differ significantly over the two culture media conditions. Analyzing process performance of the complete growth phase in both media, including lag and stationary phase, these numbers shift in favor of the recombinant F9-cell line and negative control cell line. Even less glucose is needed to build a specific amount of cells. Overall, cell growing in CD CHO consumed more glucose and produced more lactate related to biomass production.

In general, the shapes of lactate concentration were similar to the profiles of cell growth curves (3.9). The peak of lactate concentration occurred earlier than the peak of cell density. Other than that, results of lactate production (or consumption) rates cannot be described as generically as glucose results.

Lactate production was uniformly high during exponential stage of biomass

Table 3.2: Descriptive parameters of growth analysis Parameters with white background are calculations including the complete growth phase. On the other hand, parameters in grey background only include values of exponential growth phase

	CD-CHO medium					
	Lactate			Glucose		
	WT	NC	F9	WT	NC	F9
μ [1/h]	0.0367	0.0237	0.0266	0.0367	0.0237	0.0266
qs [nmol/10^6cells/h]	84.22	87.65	36.60	208.46	172.71	115.06
Yield s/x [nmol/10^6cells]	$2.30e^{+03}$	$3.70e^{+03}$	$1.38e^{+03}$	$5.68e^{+03}$	$7.30e^{+03}$	$4.33e^{+03}$
μ_{max} [1/h]	0.0367	0.0323	0.0360	0.0367	0.0323	0.0360
qs [nmol/10^6cells/h]	67.91	355.57	82.45	181.99	230.22	148.40
Yield s/x [nmol/10^6 cells]	$1.85e^{+03}$	$1.10e^{+03}$	$2.29e^{+03}$	$4.96e^{+03}$	$7.13e^{+03}$	$4.12e^{+03}$
doubling time[h]	18.90	21.46	19.27	18.90	21.46	19.27
	CD-OptiCHO medium {4mM L-Glutamine}					
	Lactate			Glucose		
	WT	NC	F9	WT	NC	F9
μ [1/h]	0.0277	0.0288	0.0304	0.0277	0.0288	0.0304
qs [nmol/10^6cells/h]	26.91	59.51	46.79	91.45	105.82	68.95
Yield s/x [nmol/10^6cells]	$9.72e^{+02}$	$2.07e^{+03}$	$1.54e^{+03}$	$3.30e^{+03}$	$3.68e^{+03}$	$2.27e^{+03}$
μ_{max} [1/h]	0.0412	0.0288	0.0343	0.0412	0.0288	0.0343
qs [nmol/10^6cells/h]	99.50	59.51	64.15	108.50	105.82	74.91
Yield s/x [nmol/10^6cells]	$2.41e^{+03}$	$2.07e^{+03}$	$1.87e^{+03}$	$2.63e^{+03}$	$3.68e^{+03}$	$2.18e^{+03}$
doubling time [h]	16.813	24.091	20.209	16.813	24.091	20.209

formation. In CD OptiCHO medium the WT- and NC-cells started using lactate as a C-source at glucose concentrations of 2 g/L, whereas F9-cells only started to utilize lactate as a substrate at glucose values of 1.3 g/L. Otherwise, the beginning of lactate consumption correlated strongly with decrease of cell viability and with the transition into stationary phase. For all cell lines, peak values of lactate concentration were higher in CD CHO than in CD OptiCHO. Lactate peaks were highly dependent on cell culture medium. All CD CHO medium related lactate peaks unanimously exceeded 16 mM (1.45 g/L). CD OptiCHO media created different ranges of lactate peaks within the cell line variations. Peaks of lactate concentration were measured with values of 14 mM (1.26 g/L) for parental cells, 15.5 mM (1.40 g/L) for negative control cells and 16.3 mM (1.47 g/L) for anti-miR-466h-5p cells.

While absolute values of lactate production yields ($Y_{\frac{p}{x}}$) of both media ranked in the same dimensions during exponential growth, relative values (normalized to WT-CHO numbers) vary among cell lines and media, see 3.2.

Both recombinant cell lines (NC and F9) have a higher yield of lactate produced compared to the parental cell line in CD CHO medium. F9-cells produced 1.2 times the amount of lactate and NC-cells even generated almost 6 times as much with.

Relative numbers of $Y_{\frac{p}{x}}$ in CD-OptiCHO showed a different pattern by F9-cells producing only 0.78 times and NC-cells creating 0.85 times as much lactate related to WT-cells. This creates a representative difference of lactate production in-between the culture conditions.

Glutamine as another important C-source would have been an interesting factor to analyze here too, however the glutamine concentrations were not measured right away. Due to storage problems the samples could not be analyzed further.

3.3.2 Process parameters of ^{13}C-MFA batch cultures

The decision to use the medium variation of CD OptiCHO containing 4mM glutamine for labeling experiments had several reasons. First of all, the fact that there was no sufficient data of the experiment on the same medium containing 8mM glutamine, due to a variation of initial glucose concentration. Also, it was suggested that for recombinant mammalian cell lines, the concentrations of glutamine can influence phenotypic properties of cell lines immensely (Rajendra, Kiseljak, Baldi, David L. Hacker, et al., 2012).

Table 3.3 lists all regression analysis data calculated with Microsoft Excel and ETA (Extracellular Time-Course Analysis).

ETA, as a process data tool, was needed to gain additional information about the data required during the batch fermentations of all cell lines. It is capable to perform regression of extracellular exchange rates and provides specific metabolic rates and their uncertainties (Jamey D Young, 2014a; Taylor A Murphy and Jamey D Young, 2013), which are needed for further analysis in the metabolic flux software, INCA. Values in table 3.3 of Excel and ETA calculations are comparable but not an exact match.

Figure 3.10 shows the growth patterns, glucose and lactate profiles of cells in CD OptiCHO media with regular and one with glucose and one with ^{13}C labeled glucose. All clones in all media exhibited a high glucose to lactate transferring phenotype. Both media contained 4 mM glutamine. The culture with ^{13}C labeled glucose was stopped during the exponential growth phase to harvest cells while in metabolic steady state. Consequently, only the exponential growth phases can be studied. Comparing the cell density plots in figure 3.10, it is obvious that the cell densities grew to a higher level in a shorter period of time in unlabeled cell culture medium. Growth of WT-CHOs was stopped a day early in labeled medium as it was not clear, if the remaining glucose concentration would provide enough resource for further exponential growth, and ergo for metabolic steady state. Specific growth rates (μ), which in this case was equal to (μ_{max}), are slightly lower in labeled medium compared to maximum growth rates in unlabeled medium but present the same constellation, with the highest maximum growth rate yielded by WT-CHO cells, followed by F9-CHO cells and

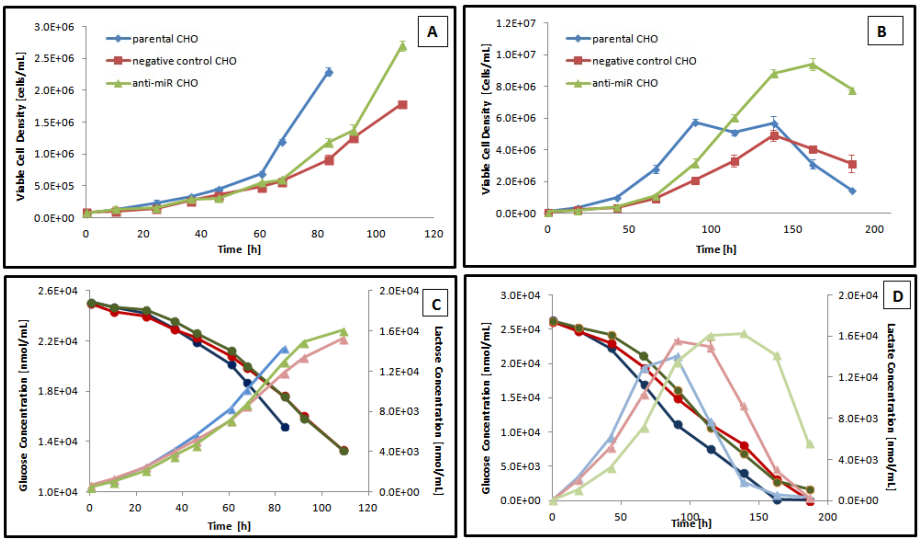

Figure 3.10: Growth in labeled and unlabeled media. Graphs (A, C) present growth patterns in C13 labeled media. Plots (B,D) show growth data of the media containing 4 mMol L-glutamine. Plots (E,F) depict glucose and lactate patterns in both media

lowest by NC-CHO cells, see 3.3. This mirrors previous results of μ_{max} in all media used for growth analysis. INCA analysis results (see section 3.3.5) of specific growth rates determined that each rate is significant from one another.

Initial glucose concentrations started out about the same in labeled and unlabeled media. Glucose curves of plots E and F of Fig. 3.10 were all comparable in-between media. However, analyzing specific consumption rates (q_s) of tables 3.2 and 3.3 one can deduce that relatively more glucose is consumed by cells growing in medium containing isotopic glucose, yielding less cells per glucose consumed. INCA analysis did find that the 95% confidence interval of glucose uptake rate of WT-CHO did not overlap with the confidence intervals of the other cell lines.

Although cell culture was stopped before the end of the exponential growth phase, one can estimate that the peaks of lactate concentration were similar of labeled medium to unlabeled medium. Differences in-between media were that NC-CHO cells seem to produce lactate slower. Yields of lactate on glucose ranged from 1.6 (nmol/nmol) for the control cell line to 1.8 (nmol/nmol) for parental and anti-microRNA cell line, which, according to literature, is the typical yield area for CHO cells (Ahn and Antoniewicz, 2012). Lactate production rates were re-calculated for the unlabeled medium data in order to match the time frame of labeled media. Though, the new values of lactate accumulation rates (129.18 nmol/10^6/h for WT-CHOs, 215.43 nmol/10^6/h for NC-CHOs and

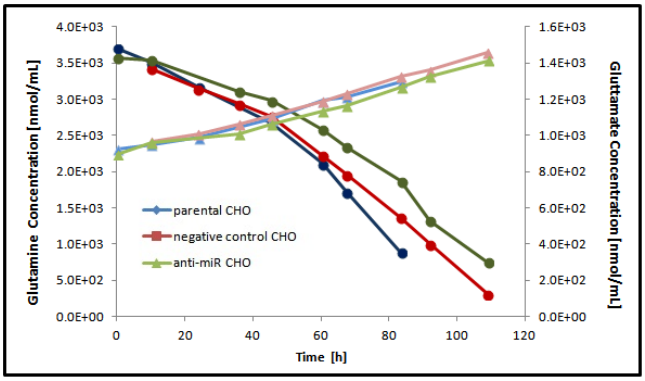

Figure 3.11: Media composition of glutamine and glutamate First data point of glutamine for NC-CHOs is missing as it could not be recovered from freezer

Table 3.3: Cell Specific Rates and Yields, based on biomass growth, determined by ETA software (white background) and by Excel calculations (grey background)

	Lactate			Glucose		
	WT	NC	F9	WT	NC	F9
Yield s/x *[nmol/10^6cells]*	1.26e+04	1.15e+04	1.13e+04	6.29e+03	7.89e+03	6.16e+03
Flux *[nmol/10^6cells/h]*	441.70	335.30	370.20	240.70	208.80	202.50
$\mu[1/h]$	0.0383	0.0265	0.0329	0.0383	0.0265	0.0329
Yield s/x *[nmol/10^6cells]*	1.27e+04	1.29e+04	1.02e+04	5.92e+03	7.34e+03	6.93e+03
Flux *[nmol/10^6cells/h]*	485.66	364.36	326.77	226.43	207.27	222.10
$\mu[1/h]$	0.0383	0.0282	0.0321	0.0383	0.0282	0.0321
	Glutamate			Glutamine		
	WT	NC	F9	WT	NC	F9
Yield s/x *[nmol/10^6cells]*	261.5	382.9	257.5	1.82e+03	2.42e+03	1.23e+03
Flux *[nmol/10^6cells/h]*	10.00	10.10	8.50	69.50	63.80	40.30
$\mu[1/h]$	0.0383	0.0265	0.0329	0.0383	0.0265	0.0329
Yield s/x *[nmol/10^6cells]*	270.5	324.5	259.9	1.77e+03	2.04e+03	1.46e+03
Flux *[nmol/10^6cells/h]*	10.35	9.17	8.33	67.92	57.68	47.12
$\mu[1/h]$	0.0383	0.0282	0.0321	0.0383	0.0282	0.0321

120.00 nmol/10^6/h for F9-CHOs) increased dramatically. Still, lactate production values of ^{13}C medium were significantly higher, see table 3.3. Glutamine and glutamate progress are presented in plot 3.11. Glutamate production was impressively equal comparing cell clones, whereas glutamine consumption followed the trend of glucose uptake rate.

Figure 3.12 shows the progress of media substance concentration plotted against cell density, producing the yield as the regression slope. Values of yields are also given in table 3.3. The plots visualize that, although the results are quite close, there is a trend of the anti-miRNA-cell line being the one with better usage yields and consumption or production rates. This goes hand in hand with findings in the previous section.

In general, the anti-miRNA cell line could be described as the cell line consuming less substrate and producing less byproduct in relation to biomass. Yields and flux rates are the lowest for F9-cells regarding production of lactate, glutamate and glutamine. INCA results suggest that almost all rates across

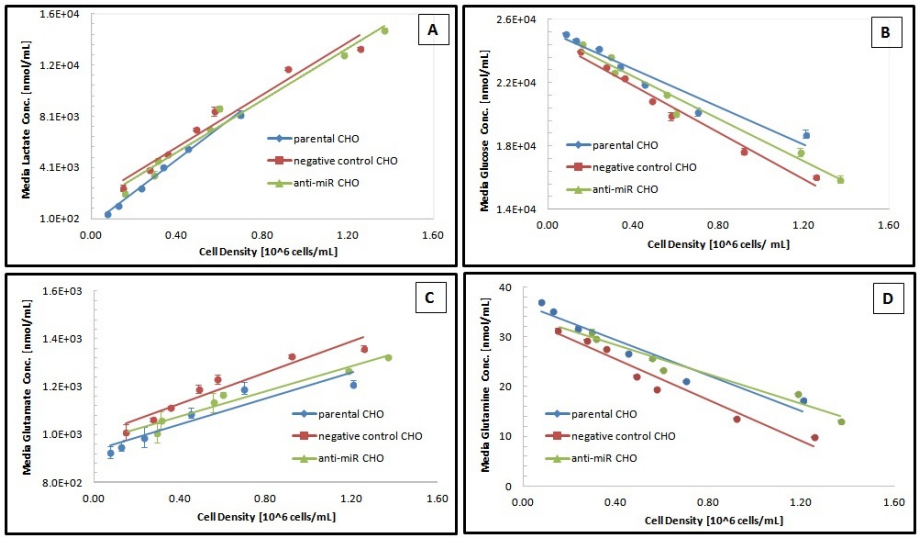

Figure 3.12: Biomass yields of different substrates during batch culture in ^{13}C substrate labeled medium. Cell lines are color coded: (A) Lactate over biomass; (B) Glucose over biomass; (C) Glutamate over biomass; (D) Glutamine over biomass

the cell lines exhibited significant differences to each other. Solely, glutamate secretion did not differ in-between WT-CHO and the control cell line.

3.3.3 Metabolic fingerprinting

The indications for possible different metabolic profiles were sought to be confirmed by Omilog's energy production assays, which was previously found to be effective to illustrate metabolic distinctions. If changes in extracellular energy metabolism occurred due to transfection with anti-miRNA-466h-5p, quick results could be provided by the system. Profiles of all three cell lines were easily collected and are presented in 3.13. After considering the kinetic background (curves in wells without any substrate) for calculations of the outcome, Dextrin, α-D- Glucose, D-Mannose, D-Galactose and D,L-Lactic acid still, had substantial growth curves to show for. Subsequent statistical analysis, including F-tests, ANOVA and students T-Test, using the initial rates of dye reduction and purple formazan production, led to the following results: Significant differences between the non transfected cell line and the anti-miRNA cell line are present with substrates α-D-Glucose and Dextrin, whereas the differences in-between the anti-miRNA cells and the negative control only occur with D-Mannose. Other metabolites that demonstrated significant distinctions in-between all cell lines, e.g. D-Fructose-6-Phosphate or citric acid, were excluded of the data representation because metabolism in general was too low for comparison (Bochner et al., 2011).

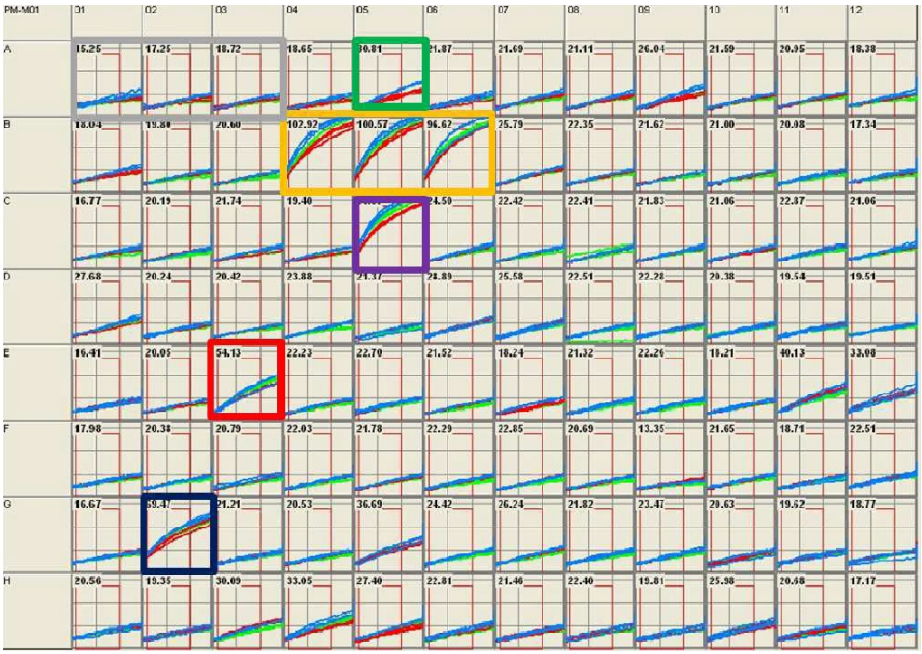

Figure 3.13: Kinetic graph of bioassay response of three cell lines in 96 well plates: Boxes (wells) are holding diverse substrates. Blue lines represent response of parental, non transfected cell line; red and green line show the negative control cell line and the anti-miRNA-466h-5p cell line, respectively. Numbers represent the initial rate of dye reduction. Substrates worth mentioning after subtracting kinetic background of negative control (grey frames) are Dextrin (green box), α-D-Glucose (yellow boxes), D-Mannose (purple box), D- Galactose (red box) and D,L-Lactic acid (dark blue box).

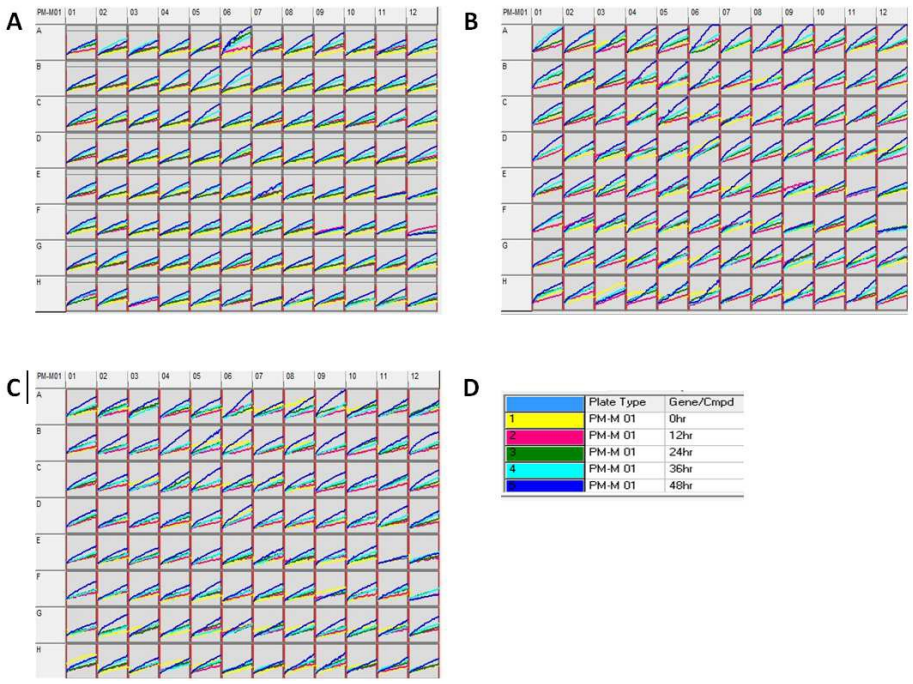

Figure 3.14: Growth and death assay (A) Results for parental, non transfected CHO suspension cell line, (B) non transfected, negative control CHO suspension cell line (C) anti-miRNA- 466h-5p CHO suspension cell line. Color key of lines can be found in picture (D).

3.3.4 Proliferation, stasis, cell death via Omnilog metabolic profiling

Having the possibility to approach the apoptosis study in a different way, previous cell death investigations could be supported and confirmed. Additionally, cell death profiles on other main energy sources than glucose could be investigated, giving an even better impression of possible newly developed cell properties. Conducting this experiment was suggested by Barry Bochner, CEO of Biolog, Inc., to demonstrate the effect of different nutritional influences on apoptosis onset.

Cells were incubated in Phenotypic MicroArray plates type one with no additional energy resource in their suspension solution, except for the substrates coated to the wells. The results of the first try of this experiment are presented in 3.14. Distinct colors of lines count as different incubation times of the plates before monitoring the formazan production via Omnilog platform. Wells A1, A2 and A3 are negative control wells with no exogenous substrate added. Other wells contain various substrates.

3.3.5 ^{13}C MFA Analysis

Solely using data of extracellular rates does not provide enough information to estimate fluxes through intracellular pathways. The intent was to uncover the fate of incoming glucose carbon and to map the flux differences of all three cell lines. For this purpose, a ^{13}C labeling study was performed with subsequent metabolic flux analysis (MFA) to define differences of intracellular metabolism of all clones. Especially, cyclic or parallel pathways can not be determined correctly without additional information, like a metabolic flux analysis using ^{13}C labeled glucose (Taylor A. Murphy, Dang, and Jamey D. Young, 2013; Templeton et al., 2014).

Isotopic tracers with a mix of 50% of unlabeled glucose, 25% of U-^{13}C D-glucose and 25% of 1,2-$^{13}C_2$ D-glucose were used to investigate possible differences in intracellular metabolism of all CHO cell lines. 1,2-$^{13}C_2$ tracer glucose was previously identified as the optimal tracer for flux analysis of the complete cellular metabolism (Metallo, Walther, and Gregory Stephanopoulos, 2009). During cell cultivation CO_2 production rate and oxygen uptake rate were not measured. As a result CO_2 had to be treated as an unbalanced metabolite in the metabolic network model (Ahn and Antoniewicz, 2011).

GC-MS results delivered mass isotopomere distributions of amino acids (Appendix 6.1). All data has been corrected by values of abundances of naturally occurring isotopes.

Inca determined flux results: The flux map depicting major pathways can be found in Fig. 3.15 and corresponding values can be seen in tables 3.4, 3.5, 3.6, 3.7, 3.8 and 3.9. Additionally to the net fluxes, a lot of reaction also comprised exchange rates that can be found in the complete network in the appendix (6.2). The tables also provide the 95% confidence intervals which overlapped in the majority of fluxes. Assuming the minimized sum of square residual has a χ^2, the expected upper and lower bounds of the 95% confidence range of SSR were [413;84.5] for WT-CHO, [86.3; 145.4] for NC-CHO and [81.1;138.7] for F9-CHO. Estimated fluxes resulted in minimized sum of square (SSR) of 75.6, 110.1 and 92.1, indicating that the fit was acceptable (Metallo, Walther, and Gregory Stephanopoulos, 2009; Ahn and Antoniewicz, 2011). All rates with overlapping confidence intervals are marked in bold. Only 10 out of a total of 41 intracellular net fluxes of central metabolism did exhibit significant differences of the 95% confidence interval in at least one cell line. Three of which (*v5, v11, v12*) account exclusively for differences of WT-CHO cells deviating from both other cell lines. Another three rates (*v16, v17, v18*) of F9-CHO cell rates differed significantly from parental and negative control cell line. And finally, fluxes *v8,*

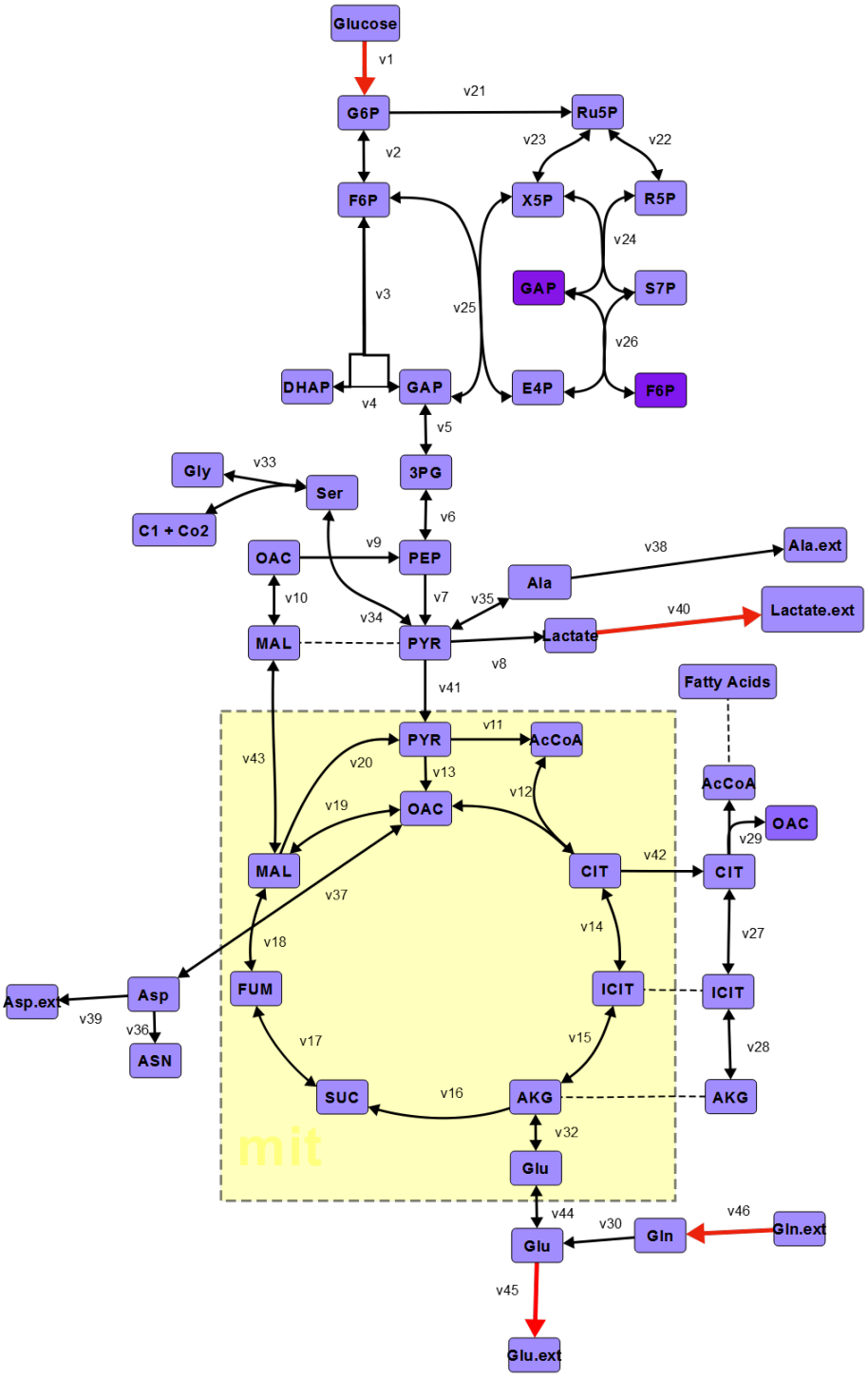

Figure 3.15: Metabolic Flux Map Diagram includes central metabolism pathways like glycolysis, oxidative and non-oxidative pathways, TCA cycle, anaplerotic and cataplerotic pathways and amino acid pathways. Red arrowed fluxes are externally measured rates

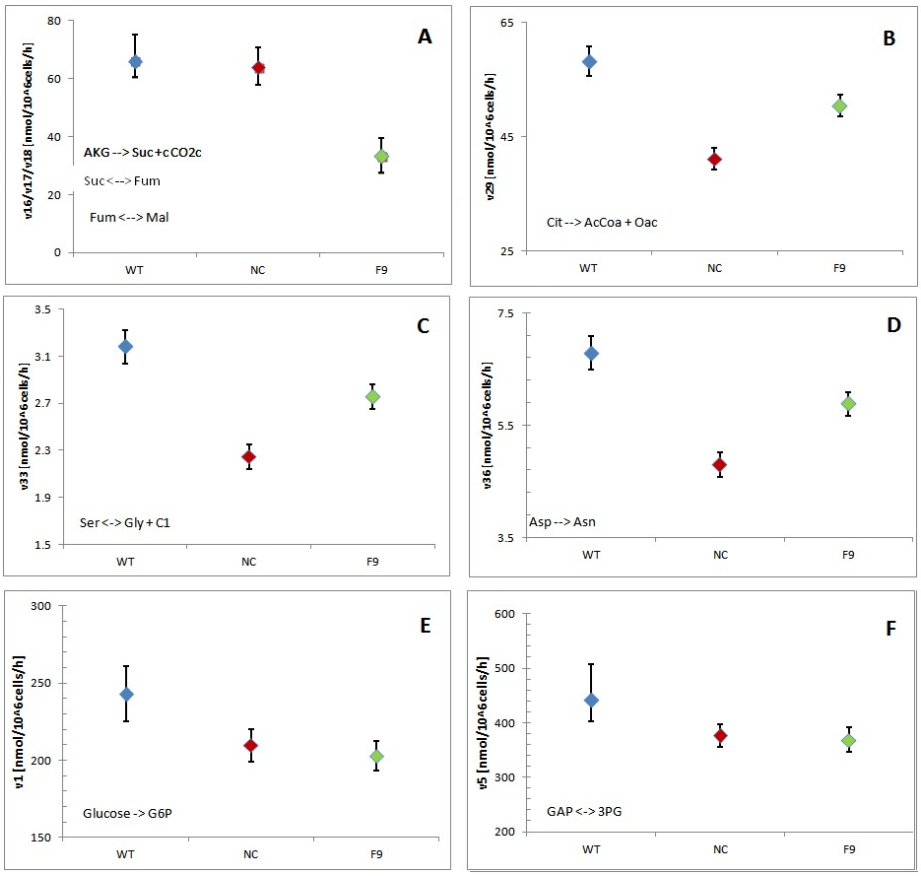

Figure 3.16: Significant different fluxes of anti-miR-466h cell line. WT is the parental cell line; NC describes the negative control cell line and F9 shows the fluxes of the anti-miRNA-466h cell line. (A, B, C and D) plots depict fluxes that have significant differences regarding the anti-miR-466h expressing cell. In (E, F) the anti-miRNA-466h cell line differentiates significantly from the parental cell line but not from the negative control cell line.

v29, v33 and v36 vary significantly across all cell lines, see Fig. 3.16.

Comparative flux analysis across cell lines There are some features of metabolism that were shared by all three clones: The pathway with the highest activity was glycolysis. As expected the major part of pyruvate produced by glycolysis was secreted as lactate. As a result TCA cycles were relatively low (30-33% for citrate synthase) and mostly driven by the anaplerotic reation of glutamine consumption and its glutamate dehydrogenase.

Results in glycolysis only show small changes regarding the metabolic state of engineered cell lines. Glucose consumption and the carbon transfered through enzymes *glyceraldehyde-phsophate dehydrogenase* (GAPDH) and phosphoglyc-

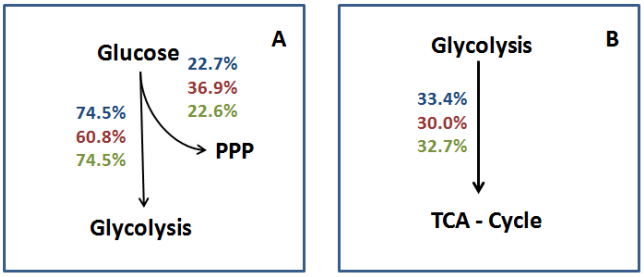

Figure 3.17: Metabolic flux ratios (A) Split between PPP and Glycolysis, (B) carbon shunt into TCA from glycolysis

erate kinase (PGK) was significantly lower in both engineered cell lines.

As pyruvate is a central metabolic node where pathways of fermentation and oxidation split up (Templeton et al., 2014), an analysis of incoming and outgoing fluxes can give interesting insights in metabolic variations. In WT-CHO ~25.4%, in NC-CHO ~30.5% and ~24.3% in F9-CHO cells all of the outgoing carbon from pyruvate hub entered into *pyruvate-dehydrogenase* and into *pyruvate-carboxylase*, whereas the rest went into lactate production. The absolute fluxes rates of pyruvate to lactate did produce significant fluxes for each cell line, see 3.5.

Total carbon consumption (glucose and glutamine) was diminished in both engineered clones. This only reflects in flux through reactions of α-ketoglutarate dehydrogenase/ succinyl-CoA-synthase, *succinate dehydrogenase* and *fumarase* of TCA cycle of the anti-apoptosis cells as these are significantly decreased. The control cell line was not effected in reaction rates through the citric acid cycle.

Approximately 23% of the carbon flux split into the pentose phosphate pathway in WT-CHO and F9 CHO clones, see figure 3.17. NC-CHO cells showed a higher shunt towards PPP with about 36% of glucose flux. All fluxes had overlapping 95% confidence intervals and therefore no significant differences.

Other significantly different fluxes through all three cell lines occurred in the fatty acid metabolism and amino acid metabolism. This generally reflects the pattern of specific growth rates.

As one can determine from table 3.9, the uptake rates of amino acids across all three cell lines all carry significance with the following pattern: highest uptake of amino acids was performed by parental cell line, followed by the uptake rates of the anti-apoptosis cell line and lastly by the negative control cell

line.

In general, the parental cell line seemed to have slightly higher flux rates across all pathways and exchange reactions compared to the anti-miRNA-466 cells. Despite these findings, there are a few exceptions including reactions in fatty acid metabolism. These findings however, can only be described as a trend. Based on the data available, significance is lacking. Also, in perspective of percentages of pathway splits, see Fig. 3.17, the naive and the anti-apoptosis cell lines tend to send the same amount of carbon through major pathways related to the incoming source of labeled glucose. Solely, the control cell line has a different distribution throughout the central metabolism.

Table 3.4: Experimentally determined net ($\longmapsto$) fluxes including 95% confidence interval for intracellular reactions of Anaplerosis and fates of pyruvate of parental, negative control and anti-466h-miRNA cell line. Flux IDs containing *net* included an exchange rate that can be found in the complete model in the Appendix, see 6.2

		WT		**NC**		**F9**	
Flux ID	***Biochemical Reaction***	**Flux Value**	**Interval**	**Flux Value**	**Interval**	**Flux Value**	**Interval**
Glycolysis							
v1	$Glucose + ATP \rightarrow G6P + ADP$	**243.27**	**[225.4, 261.1]**	209.77	[199.2, 220.3]	202.73	[193, 212.5]
v2	$G6P \rightleftharpoons F6P$	181.27	[137.5, 260.1]	127.54	[112.1, 160.7]	151.03	[128.1, 204.8]
v3 net	$F6P + ATP \rightleftharpoons DHAP + GAP + ADP$	214.40	[191.3, 256.4]	176.58	[166.3, 190.4]	178.40	[166.1, 201.8]
v4 net	$DHAP \rightleftharpoons GAP$	211.50	[188.4, 253.5]	174.53	[164.2, 188.3]	175.89	[163.6, 199.7]
v5 net	$GAP + NAD^+ \; ADP \rightleftharpoons 3PG + NADH + ATP$	**442.47**	**[403.3, 508.1]**	375.63	[355.3, 396.9]	367.98	[346.6, 391]
v6 net	$3PG \rightleftharpoons PEP + H_2O$	418.18	[381.1, 508.1]	360.48	[340.8, 381.8]	352.30	[330.4, 391]
v7 exch	$PEP + ADP \rightarrow ATP + Pyr$	418.18	[381.1, 535.7]	360.48	[340.8, 413.6]	352.30	[330.4, 380.8]
Anaplerosis and Pyruvate Fates							
v8	$Pyr + NADH \rightarrow LAC + NAD^+$	**442.00**	**[415.2, 469.5]**	**335.00**	**[316.8, 352.2]**	**370.00**	**[352.8, 387.2]**
v9	$OAC \rightarrow PEP + CO_2$	1.00E-07	[0, 32.7]	1.00E-07	[0, 32.3]	1.00E-07	[0, Inf]
v10 net	$OAC + NADH \rightleftharpoons MAL + NAD^+$	-50.1	[-55.2, 66.9]	-63.97	[-80.3, 6.3]	-28.60	[-40.2, 73.2]

Table 3.5: Experimentally determined net ($\longmapsto$) fluxes including 95% confidence interval for intracellular reactions of TCA- cycle of parental, negative control and anti-466h-miRNA cell line. Flux IDs containing *net* included an exchange rate that can be found in the complete model in the Appendix, see 6.2

		WT		**NC**		**F9**	
Flux ID	***Biochemical Reaction***	**Flux Value**	**Interval**	**Flux Value**	**Interval**	**Flux Value**	**Interval**
TCA-Cycle							
v11	$Pyr + NAD^+ + CoASH \rightleftharpoons AcCoA + CO_2 + NADH$	**81.31**	**[76.9, 89]**	62.95	[57.9, 69]	66.25	[60.4, 72.3]
v12 net	$AcCoA + OAC + H_2O \rightleftharpoons Cit + CoASH$	**81.31**	**[76.9, 89.0]**	62.95	[57.9, 69]	66.25	[60.4, 72.3]
v13	$Pyr + CO_2 \rightarrow OAC$	3.39	[0.7, 5.6]	9.44	[6.6, 11.8]	5.45	[2.5, 7.9]
v14 net	$Cit \rightleftharpoons Ict$	19.24	[-13.4, 25.3]	-7.41	[-11.5, 22.2]	-4.59	[-10.5, 15.8]
v15 net	$Ict + NAD^+ \rightleftharpoons AKG + CO_2 + NADH$	19.24	[-13.4, 25.3]	-7.41	[-11.5, 22.2]	-4.59	[-10.5, 15.8]
v16	$AKG + NAD^+ + GDP + Pi \rightarrow SUC + NADH + GTP + CO_2$	66.27	[60.6, 75.2]	63.97	[58, 70.7]	**33.29**	**[27.5, 39.4]**
v17 net	$SUC + FAD^+ \rightleftharpoons FUM + FADH_2$	66.27	[60.6, 75.2]	63.97	[58, 70.7]	**33.29**	**[27.5, 39.4]**
v18 net	$FUM \rightleftharpoons MAL$	66.27	[60.6, 75.2]	63.97	[58, 70.7]	**33.29**	**[27.5, 39.4]**
v19 net	$MAL + NAD^+ \rightleftharpoons OAC + NADH$	66.27	[10.2, 133.6]	6.36E-12	[0, Inf]	3.96E-13	[0, Inf]
v20	$MAL + NAD^+ \rightleftharpoons Pyr + CO_2 + NADH$	1.00E-07	[0, 13.4]	1.00E-07	[0, 12.2]	4.69	[0, 10.4]

Table 3.6: Experimentally determined net ($\longmapsto$) fluxes including 95% confidence interval for intracellular reactions of PPP and fatty acid biogenesis of parental, negative control and anti-466h-miRNA cell line. Flux IDs containing *net* included an exchange rate that can be found in the complete model in the Appendix, see 6.2

		WT		**NC**		**F9**	
Flux ID	***Biochemical Reaction***	**Flux Value**	**Interval**	**Flux Value**	**Interval**	**Flux Value**	**Interval**
Pentose Phosphate Pathway							
v21	$G6P + 2NADP + H_2O \rightarrow Ru5P + 2NADPH + CO_2$	55.19	[0, 97.8]	77.44	[45, 92.2]	45.81	[0, 67.7]
v22 net	$Ru5Pc \rightleftharpoons R5P$	22.06	[5.3, 36.3]	28.39	[17.6, 33.3]	18.44	[3.1, 25.7]
v23 net	$Ru5P \rightleftharpoons X5P$	33.13	[-3.9, 61.1]	49.04	[27.4, 58.9]	27.37	[-3.3, 41.7]
v24 net	$X5P + R5P \rightleftharpoons GAP + S7P$	16.57	[-1.9, 30.5]	24.52	[13.7, 29.4]	13.69	[-1.6, 20.9]
v25 net	$X5P + R5P \rightleftharpoons GAP + F6P$	16.57	[-1.9, 30.5]	24.52	[13.7, 29.4]	13.69	[-1.6, 20.9]
v26 net	$S7P + GAP \rightleftharpoons F6P + E4P$	16.57	[-1.9, 30.5]	24.52	[13.7, 29.4]	13.69	[-1.6, 20.9]
Fatty Acid Metabolism							
v27 net	$Cit \rightleftharpoons Ict$	3.91	[0.6, 39.2]	29.30	[0.5, 33.8]	20.48	[-0.7, 27.7]
v28 net	$Ict + NADP^+ \rightleftharpoons AKG + NADPH + CO_2$	3.91	[0.6, 39.2]	29.30	[0.5, 33.8]	20.48	[-0.7, 27.7]
v29	$Cit + CoA + ATP \rightarrow AcCoA + OAC + ADP$	**58.16**	**[55.6, 60.8]**	**41.05**	**[39.2, 42.9]**	**50.35**	**[48.5, 52.2]**

Table 3.7: Experimentally determined net ($\longmapsto$) and exchange ($\longleftrightarrow$) including 95% confidence interval for amino acid reactions of parental, negative control and anti-466h-miRNA cell line. Flux IDs containing *net* included an exchange rate that can be found in the complete model in the Appendix, see 6.2

		WT		NC		F9	
Flux ID	***Biochemical Reaction***	**Flux Value**	**Interval**	**Flux Value**	**Interval**	**Flux Value**	**Interval**
Amnio Acid Metabolism							
v30	$Gln \rightarrow Glu + NH_4^+$	62.20	[58.7, 302.7]	130.15	[55.7, 148.8]	79.18	[32.1, 121.5]
v31	$Glu \rightarrow Gln$	1.00E-07	[0, 196.3]	71.56	[0, 89.3]	45.41	[0, 87.6]
v32 net	$AKG + NADH + NH_4^+ \rightleftharpoons Glu + NAD$	-62.20	[-259.3, 96.4]	-73.11	[-148.8, 12.4]	-39.63	[-121.9, 31.7]
v33 net	$Ser \rightleftharpoons Gly + C1$	**3.18**	**[3, 3.3]**	**2.25**	**[2.1, 2.3]**	**2.76**	**[2.7, 2.9]**
v34 net	$Ser \rightleftharpoons Pyr + NH_4^+$	174.90	[103.8, 193.6]	121.11	[106.6, 133.1]	137.36	[125.8, 165]
v35 net	$Ala \rightleftharpoons Pyr$	-66.37	[-129.4, -13.9]	-74.21	[-111.2, -40.8]	-52.66	[-102.1, -12]
v36	$Asp + NH_4^+ \rightarrow Asn$	**6.79**	**[6.5, 7.1]**	**4.79**	**[4.6, 5]**	**5.88**	**[5.7, 6.1]**
v37 net	$Asp + AKG \rightleftharpoons OAC + Glu$	-58.16	[-113.5, 23.1]	-105.02	[-121.5, -19.1]	-78.95	[0, Inf]
v38	$Ala \rightarrow Ala.ext$	52.23	[0, 115.3]	64.23	[30.7, 101.2]	40.42	[0, 89.8]
v39	$Asp \rightarrow Asp.ext$	28.61	[0, 33.3]	38.87	[6.5, 43.4]	2.65	[0, 10.8]
v40	$Lactose \rightarrow Lactose.ext$	442	[415, 469]	335	[316.8, 353.2]	370.00	[352.8, 387.2]
v41	$Pyr \rightarrow Pyr.m$	151.07	[90.5, 268.5]	146.60	[108, 181.5]	119.66	[73.2, 171.9]

Table 3.8: Experimentally determined net ($\longmapsto$), including 95% confidence interval for internal exchange reactions of parental, negative control and anti-466h-miRNA cell line. Flux IDs containing *net* included an exchange rate that can be found in the complete model in the Appendix, see 6.2

		WT		NC		F9	
Flux ID	***Biochemical Reaction***	**Flux Value**	**Interval**	**Flux Value**	**Interval**	**Flux Value**	**Interval**
Exchange Reactions							
v42	*Cit.m* $\rightarrow$ *Cit.c*	62.07	[58.3, 97.9]	70.3586	[40-7. 75]	70.8333	[49.0, 78.2]
v43 net	*Mal.m* $\rightleftharpoons$ *Pyr.c*	50.9	[6.9, 55.3]	63.9685	[-6.2, 80.3]	28.5951	[-11.3, 42.9]
v44 net	*Glu.m* $\rightleftharpoons$ *Glu.c*	2.30E-12	[-174.2,177.4]	57.03	[-81.3, 71.3]	39.54	[-63.9, 75.3]
v45 net	*Glu.c* $\rightleftharpoons$ *Glu.e*	10.00	[9.43, 10.54]	10.10	[9.44, 10.75]	8.50	[8.06, 8.93]
v46 net	*Gln.e* $\rightleftharpoons$ *Gln.c*	69.78	[66.26, 73.31]	63.94	[61.01, 66.87]	40.34	[38.69, 41.98]
v47	*144.2*R5P + 83.6*C1 + 70*CO$_2$ + 76.14*DHAP + 178.9*G6P + 1528*AcCoA + 371.4*Ala + 233.4*Arg + 292*Asp + 178.3*Asn + 89.76*Cys + 199.3*Gln + 238.9*Glu + 450.1*Gly + 88.52*His + 200.6*Ile + 349.1*Leu + 352.8*Lys + 85.42*Met + 135.6*Phe + 193.7*Pro + 284.1*Ser + 238.9*Thr + 27.24*Try + 112.7*Tyr + 257.5*Val* $\rightarrow$ *Biomass*	**0.038**	**[0.036, 0.039]**	**0.027**	**[0.026, 0.028]**	**0.033**	**[0.032, 0.0234]**

Table 3.9: Experimentally determined net ($\longmapsto$) including 95% confidence interval with significant differences

. Flux IDs containing *net* included an exchange rate that can be found in the complete model in the Appendix, see 6.2

		WT	NC	F9			
Flux ID	*Biochemical Reaction*	Flux Value	Interval	Flux Value	Interval	Flux Value	Interval
Uptake1	*Arg.ext* $\rightarrow$ *Arg*	8.8838	[8.5, 9.3]	6.271	[6, 6.6]	7.6916	[7.4, 8]
Uptake2	*Cys.ext* $\rightarrow$ *Cys*	3.4165	[3.3, 3.6]	2.4117	[2.3, 2.5]	2.958	[2.8, 3.1]
Uptake3	*Gln.ext* $\rightarrow$ *Gln*	69.7886	[66.3, 73.3]	63.9412	[61, 66.9]	40.3376	[38.7, 42]
Uptake4	*Gly.ext* $\rightarrow$ *Gly*	13.9499	[13.3, 14.6]	9.8472	[9.4, 10.3]	12.0779	[11.6, 12.5]
Uptake5	*His.ext* $\rightarrow$ *His*	3.3693	[3.2, 3.5]	2.3784	[2.3, 2.5]	2.9171	[2.8, 3]
Uptake6	*Ile.ext* $\rightarrow$ *Ile*	7.6353	[7.3, 8]	5.3897	[5.1, 5.6]	6.6107	[6.4, 6.9]
Uptake7	*Leu.ext* $\rightarrow$ *Leu*	13.2876	[12.7, 13.9]	9.3796	[9, 9.8]	11.5045	[11.1, 11.9]
Uptake8	*Lys.ext* $\rightarrow$ *Lys*	13.4284	[12.8, 14]	9.4791	[9, 9.9]	11.6264	[11.2, 12.1]
Uptake9	*Met.ext* $\rightarrow$ *Met*	3.2513	[3.1, 3.4]	2.2951	[2.2, 2.4]	2.815	[2.7, 2.9]
Uptake10	*Phe.ext* $\rightarrow$ *Phe*	5.1613	[4.9, 5.4]	3.6433	[3.5, 3.8]	4.4686	[4.3, 4.6]
Uptake11	*Pro.ext* $\rightarrow$ *Pro*	7.3727	[7, 7.7]	5.2043	[5, 5.4]	6.3833	[6.1, 6.6]
Uptake12	*Tyr.ext* $\rightarrow$ *Tyr*	4.2896	[4.1, 4.5]	3.028	[2.9, 3.2]	3.714	[3.6, 3.9]
Uptake13	*Thr.ext* $\rightarrow$ *Thr*	9.0931	[8.7, 9.5]	6.4188	[6.1, 6.7]	7.8729	[7.6, 8.2]
Uptake14	*Val.ext* $\rightarrow$ *Val*	9.8011	[9.4, 10.2]	6.9185	[6.6, 7.2]	8.4858	[8.2, 8.8]

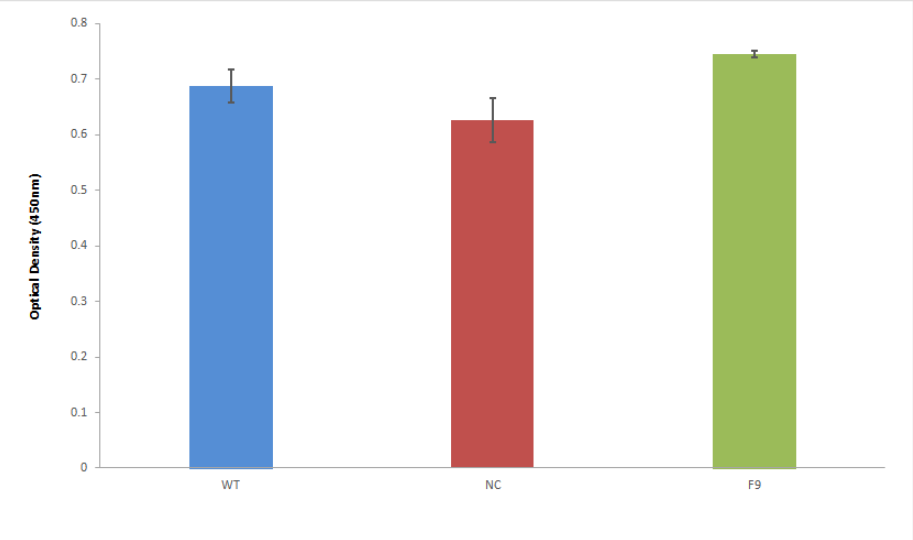

Figure 3.18: EPO expression levels of the 3 different cell lines. (blue) parental cell line; (red) negative control cell line; (green) anti-miRNA-466h cell line

3.3.6 EPO and HubChe production of CHO cell lines

Results for EPO and HuBChe expression differences can be explored in Fig. 3.18 and Fig. 3.19, respectively. The expectations were that, based on results published by Aliaksandr Druz, Son, et al., antimiRNA- 466h-5p cells would exhibit a higher expression of the proteins, EPO and HuBChe. Figure 3.18 shows the average results of all EPO determination assays, being supported by statistical evaluations that confirm the results presented as significant. Thus, the total EPO concentration of a cell population based the anti-mRNA-466h-5p cell line is higher. This only shows a relative comparison though and does not count as absolute values of cell specific productivity. Cells were counted before and at harvesting to establish the discrepancy in viability caused by transfection. Before transfection cells had a viability percentage higher than 95%. At harvesting, visual aberrations could be detected in-between each cell population. While the viability of antimiRNA-466h-5p population was still high with ranging around 83% viable cells, viability of parental cells were already diminished with around 72% and last the negative control cell line with about 65% of viability.

Protein expression results of HuBChe also turned out to be increased significantly with F9-CHOs, at all but one point of measurement, compared to both other cell lines. WT-CHOs and NC-CHOs did not differ substantially regarding the expression of HuBChe. Viability was first measured 48h after transfection at first point decreased in all cell lines over the course of the procedure. Viabil-

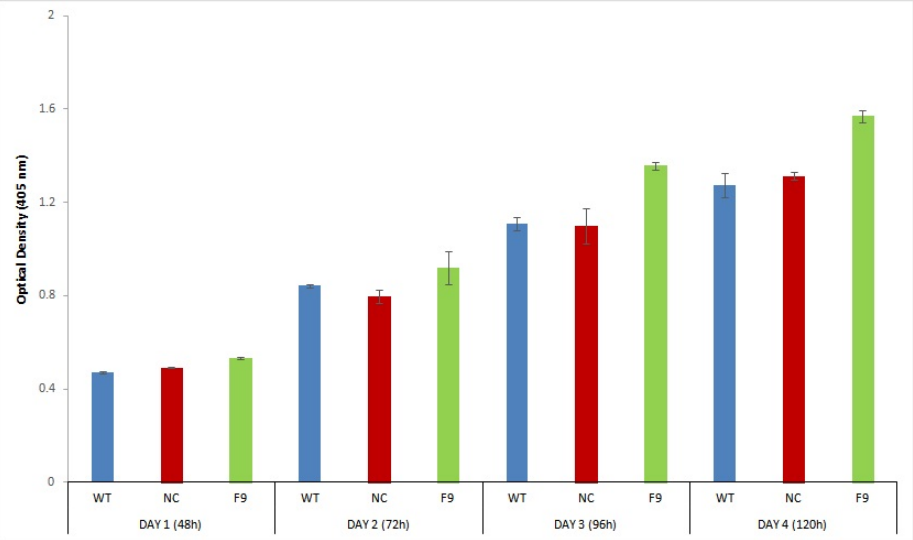

Figure 3.19: Progress of HubChe expression over time the course of four days. Cell lines are color coded. (Blue) - parental cell line; (Red) - negative control cell line; (Green) - anti-miRNA-466h cell line

ity of parental cells decreased from 78% to 69%. NC-CHOs showed even worse trend viability rates from 75.4% to 35%. In contrast, anti-miRNA-466h cells did not decrease as significantly, from 89,7% to 83,5% over the course of 4 days.

3.4 Discussion

3.4.1 Comparison and reproduction of growth rate findings Growth rate and Media development

The expression of recombinant proteins exerts an additional metabolic burden on the host cells metabolism. This means that metabolites like nucleotides and amino acids are drained from primary metabolism and redirected towards the production of the target protein (Nocon et al., 2016). Using miRNAs as cell engineering tools precisely targets this matter by, other than the classic approach of genetic engineering, not burdening the translational machinery and reducing the metabolic load on cells. The metabolic resources can then be better dispensed throughout metabolism, possibly resulting in higher recombinant protein titer (Aliaksandr Druz, Son, et al., 2013). This study aimed to visualize this exact "allocation" of resources, and interpret the arise of new metabolic phenotypic traits in terms of recombinant protein production, by comparing miRNA engineered cells with their naive parental cell. A key component of the overall cellular behavior is its metabolic phenotype (Metallo, Walther, and

Gregory Stephanopoulos, 2009). As Aliaksandr Druz, Son, et al. created cell clones that improved performance of recombinant protein secretion by interfering with programmed cell death (PCD), by using these novel compounds which target complete pathways, the question arose if there is a correlation between apoptosis signaling and metabolism.
Cell networks are complicated constructs that will not be fully understood for a long period of time because of the immense complexity of interlocking feedbacks and pathways. Recent findings link proteins involved in apoptosis with proteins necessary for metabolism and energy homeostasis. Metabolic and apoptotic pathways are distinguished within the cell but still share some important proteins (Majors, Michael J. Betenbaugh, and Chiang, 2007). Especially proteins from the Bcl-2 family, which were first discovered as over-expressed components in several different types of cancer, are of interest in their functions and influence in metabolic pathways (Templeton et al., 2014; Majors, Michael J. Betenbaugh, and Chiang, 2007). Research also found that varying expression patterns of apoptotic genes had effects on the lactate production and consumption of engineered cells (Dorai et al., 2009).

High viable cell densities are favorable for high product titers in bioreactors (C Altamirano et al., 2004). Aliaksandr Druz, Son, et al. found equal specific growth rates across cell lines and increased IVC levels for anti-466h-CHO cells in his experiments. These results could not be reproduced exactly, as we at least found significant growth rates for each cell line. With the result of the anti-miRNA cells only showing the second highest growth rate behind the parental cell line. Like with Aliaksandr Druz, Son, et al., the highest IVC could however be attached to anti-miRNA-466h cells, confirming the previous results and establishing it as a possible production cell line for high protein yields. IVC results also reflect the calculated biomass yields on glucose, that show major improvements of directing more carbon into biomass production rather than lactate. A result that was also reported by Templeton et al. Increased IVCs are attributed the characteristic of higher titers and better product quality (Niall Barron et al., 2012; Aliaksandr Druz, Son, et al., 2013). High concentrations of cells in culture rely on different factors. Supply of necessary nutrients and inhibition due to biochemical waste-/by-products are important influences (Ozturk, Riley, and Palsson, 1992). Interestingly, cell densities in self supplemented CD OptiCHO media increased dramatically compared to CD CHO. Combined with the smaller peak of lactate curiosity arises, if data can be validated, this could mean even better performances in recombinant protein production. This theory would be an interesting topic to investigate further.

Modern cell lines can exhibit metabolic pathway "disorders" by excessive

conversion of glucose into lactate and by glutamine constantly being shoved into tricarboxylic acid cycle (TCA), and as a result releasing huge amounts of ammonia in the process. It is well known that high concentrations of these by-products can trigger cell death and decrease quality of secreted product in terms of missing or incorrect glycosylation (Müller, Katinger, and Grillari, 2008; Li et al., 2010; Glacken, Fleischaker, and Sinskey, 1986; Klein et al., 2015). Inhibitory affects of lactate on bioreactor processes have broadly been investigated on mammalian cells and result of a combination of lowered pH (increase of media acidification) and increased osmolality at high lactate concentrations in the media (Ozturk, Riley, and Palsson, 1992; Glacken, Fleischaker, and Sinskey, 1986; Claudia Altamirano et al., 2013). Typical cellular behavior of high lactate production rates occurring during the exponential stage (Zagari et al., 2013) of biomass formation could be observed in all cell lines and both culture media. Curiously, in CD CHO medium, lactate was used simultaneously as a growth substrate when glucose concentrations were still sufficiently high, with residual glucose levels between 3-3.5 g/L. These findings are consistent with reports from Le et al., where researchers determined that the metabolic shift to lactate consumption, that correlates highly with increased production titers, does not necessarily depend on glucose concentration. Here, in both media, the switch to lactate usage in NC- and F9-clones did not appear as abruptly and as intense as the native counterpart cells. Reports of limits causing inhibitory effects for cell proliferation and protein production start around 10 mM (0.9 g/L) for specific hybridoma cell lines (Hassell, Gleave, and Butler, 1991) and 18 mM (1.6 g/L) for specific CHO cells lines (Kurano et al., 1990), suggesting that the inhibitory effect of lactate is cell type and cell line specific and can vary extensively (Lao and Toth, 1997). The results of this study would indicate that there was no inhibitory effects during cell culture as the highest concentrations of lactate never exceeded the limits provided by literature, see section 3.3.1. Incomplete oxidative metabolism and the resulting lactate production have been subject of many investigations of cell engineering by regulating key enzymes on the expression level (S. H. Kim and Lee, 2007; Zagari et al., 2013). Additionally to low lactate production rates, an increased lactate consumption rate is regarded as a favored metabolic trait and can improve bioprocess results (Li et al., 2010; Glacken, Fleischaker, and Sinskey, 1986; Klein et al., 2015). According to a study published in 2009, cells that have been genetically altered to delay onset the programmed cell death by different expressions of engineered anti-apoptosis genes (Aven, XIAP and E1B-19K) accumulated less lactate during early exponential phase and consumed the same metabolite much faster during stationary phase, compared to their un-engineered controls (Dorai et al., 2009). These findings, however, could not be confirmed beyond doubt in neither medium during

the course of this study as data on both of these traits have not been consistent across all media. Considering lactate production during exponential growth, i.e., the results seem to be medium dependent. The reason for this variation cannot be completely deciphered, as too little is known about the composition of purchased media.

3.4.2 Metabolic profiling with Phenotypic MicroArrays

Specific miRNAs may modify and control the metabolic pattern of cells and therefore increase or diminish specific biochemical pathways within cell metabolism. Alterations regarding these miRNAs are linked to diverse genotypic and phenotypic changes and can even cause serious diseases like cancer (Aliaksandr Druz et al., 2011a; A. Druz, M. Betenbaugh, and J. Shiloach, 2012). To see if the modification by stably transfecting a CHO suspension cell line caused aberrations to usual endogenous energy pathways, Phenotypic MicroArray was performed. Due to the procedure and materials used, by suspending the cells in 'energy-free' media, their only way of survival and energy sources is the exogenous material provided in the individual wells. During metabolism energy is converted to mitochondrial reducing equivalents (NADH), if the cell can metabolize the very substrate that is provided, and colorimetric reactions can be seen and measured (Inc., 2017). Kinetic background can be created due to remnant energy from intracellular resources. After considering this kinetic background in statistical calculations, not many substrates gave substantially different values of energy metabolism. The suspected variations in Dextrin, α-D-Glucose, D-Mannose, D- Galactose and D,L-Lactic acid usage were not as big as assumed but could still be detected. Overall, one could hypothesize that negative control cell line had slower metabolic rate by interpreting results seen in Fig. 3.13. Although, optimization runs were conducted to fine tune protocol steps to achieve optimal outcomes, more adjusting assays could lead to even better and more fitting protocols and improved results. More trials are needed to gather further experimental data to be able to give proper scientific evidence.

3.4.3 Viability and Apoptosis assays using Biolog's Phenotypic MicroArrays

Previous presented Omnilog data indicates that changes in metabolic patterns can be explored easily without an abundance of complicated experimental steps, that could influence the overall investigation by being prone to mistakes. This creates new possibilities to achieve reproducible data. However, fingerprinting of metabolic pattern variations is not the only investigation that can be conducted with the kinetic Omnilog assay. B. Bochner and colleagues illustrated rather

successfully that even proliferation, stasis and apoptosis can be detected with their phenotypic microarrays. By reducing the cell count seeded in each well, the well substrates will supply each individual cell with energy for a longer period of time. Apoptosis can occur due to many reasons but nutrient depletion is one that most certainly will result in cell death (Bochner et al., 2011; A. Druz, M. Betenbaugh, and J. Shiloach, 2012). Provoking nutrient depletion by incubating cells up to a point when intracellular resources and energy of the wells should be consumed and metabolized will mimic energy depletion and cause cell death. Running this experiment in parallel with all three cell lines should have been able to give information to the individual cell line apoptosis properties and resistance. In this case, however, the results are not what we hoped for. No real apoptosis was detectable after 48h of incubation. Although, in previous experiments with similar cell lines, the cell count and duration was ideal to gain proper results this time cells still seemed to be viable after the full incubation time and thus cannot provide information about differences in apoptosis onset in- between cell lines (Bochner et al., 2011; Bochner, 2014) Thus, again, optimization steps to create favorable and reproducible results should be conducted before experiments are repeated and any distinct declarations can be made.

3.4.4 Metabolic flux analysis

For a more detailed analysis of possible influences and differences in metabolism due to the engineered miRNA pattern, a steady state metabolic flux analysis was performed to illustrate potential variations. The flux rates through a pathway and the concentration of a specific metabolite relates sensitively to the needs and phase of an organism at a certain time point. Meaning, due to remarkably complex networks of control mechanisms, just enough flux is granted as actually needed (D. Voet and J. G. Voet, 2011).

As glucose is metabolized and converted into different intermediates in metabolism, it moves through pathways of glycolysis, TCA, and oxidative phosphorylation to provide energy but it also produces precursors including nucleic acid (Majors, Michael J. Betenbaugh, and Chiang, 2007). Glycolysis had the highest flux rates through central metabolism, as expected. Carbon distribution of parental cell line and anti-apoptosis cells show similar relative rates.

End-product of glycolysis and important node in central metabolism, pyruvate, is transfered into mitochondria and cycles through a series of reaction in the TCA cycle (Andersen and Kornbluth, 2013). These consecutive rates of oxidative reactions, that ultimately result in the production of ATP and NADH, were relatively low compared to glycolysis across all cell lines. These

results were expected as mammalian cells usually show little connection from glycolysis to TCA (Ahn and Antoniewicz, 2012). In the anti-apoptotic cell line, however TCA was mainly fed by glutamine consumption, entering mitochondria as glutamate and subsequently being converted into α-ketoglutarate. Interestingly, a flux toward citrate from isocitrate was observable for the two engineered cell lines which suggests that these cell lines undergo reductive carboxylation of α-ketoglutarate, which can often be observed in cancer cells (Mullen, Hu, et al., 2014). There, this reaction is used to overcome mitochondria impairment and use the glutamine-dependent reductive carboxylation to produce citrate, which is an important intermediate in lipid synthesis and TCA related macromolecular precursors and therefore supports growth (Mullen, Wheaton, et al., 2012). How far this could have supported growth of the miRNA-engineered cell lines cannot be determined here. However, looking at the reactions towards fatty acid metabolism, miRNA enigneered cell lines indeed transfered more citrate into the cytosol, but a huge fraction of this did not proceed into fatty acid biosysnthesis. Examining the parental cell line, there was less citrate leaving the mitochondria but more than 90% of this was shunt into fatty acid biogenesis. The most prominent implications of a connection between TCA cycle metabolism and apoptosis is of course the common localization within the cell, see figure 3.3 (Andersen and Kornbluth, 2013). There are some suspected or even confirmed associations of anti-apoptotic proteins: Bcl-2, for example, can regulate cell death by blocking the activation of the permeability transition pore (PTP) of the mitochondrial membrane $\triangle \Psi_m$ and therefore maintaining the transmembrane potential functions (Gupta et al., 2010) as a blocker of the release of cytochrome c, which in turn stops the caspase cascade (Templeton et al., 2014). The same protein has been found to regulate Ca^{2+} uptake and these effects can be expected to simultanousley influence activities of metabolic pathways, since some mitochondrial enzymes are controlled by alterations of $\triangle \Psi_m$ and Ca^{2+} (Templeton et al., 2014; Majors, Michael J. Betenbaugh, and Chiang, 2007). There is no definite change of TCA pathways here that can be declared favorable towards recombinant protein production that would not have to be investigated further.

The split into pentose phosphate pathway (PPP) showed great differences in reaction rates (although no significance could be determined) of CHO cell lines. Considering that PPP is an important pathway during rapidly proliferating cells, as it provides the key precursor for nucleotide synthesis, (Ahn and Antoniewicz, 2012) one would assume that the cell line with the highest specific growth rate (WT-CHO) would also have the highest activity of PPP. However, the exact opposite seems to be the case. The lowest proliferating cell line did exhibit the highest rate of PPP with about 37% during the exponential growth phase 3.17.

Parental and anti-apoptosis cell lines have similar distribution results with about 22% each. In their review Ahn and Antoniewicz describe that the oxidative part of the pentose phosphate pathway (oxPPP) was not only important for synthesis of biomolecules but also to reduce oxidative stress. One can hypothesize now that there might be a reason for the negative control cell lines to be more prone to stress, having gone through the procedure of genetic modification but not expressing apoptosis reducing miRNAs. According to (Jamey D Young, 2013) usual rates of carbons that are diverted into pentos phosphate pathway lie around 10%. Others report shunts of up to 40% into oxPPP.

As an essential component of culture media glutamine is often used as an alternative substrate for cell growth along with glucose. Metabolism of glutamine, glutaminolysis, induces ammonia accumulation in culture media. High concentrations of ammonia (>2 mM) can be toxic for cells and inhibit cell growth and production of recombinant proteins (Rajendra, Kiseljak, Baldi, David L Hacker, et al., 2011) Ammonia concentrations were not measured during the batch cultures. Uptake rates of all modeled amino acids (exception glutamine) were of substantial difference across all cell lines, see 3.9. Mammalian cells need to consume essential amino acids to produce proteins and biomass (Ahn and Antoniewicz, 2012). With only few exceptions the parental cell line had the highest uptake rate of amino acids, followed by the anti-apoptosis cell line and negative control respectively. This agrees with biomass production rates during exponential growth. First, one might consider the consumption rates to be conform with the decreased metabolic burden on the translational machinery, however negative control shRNA has limited homology to any known sequences (Aliaksandr Druz, Son, et al., 2013) and would not lessen the burden on the translational machinery.

Many of these alterations in reaction rates could be interpreted as metabolic shift towards a phenotype with improved protein expression qualities. However, all of these alterations could also be explained with adjustments to shifts in growth rates. Therefor, decisive arguments and declarations cannot be made here.

3.4.5 Protein production of EPO and HuBChe

Investigating the protein production with complex recombinant proteins could give more information of the new possible phenotypic capacities that may have been developed by transfecting cells with an inhibitor of a specific miRNA. Previous results for increased production capacities of anti-miRNA-466h cells using secreted alkaline phosphatase (SEAP) yielded positive outcomes (Aliaksandr Druz, Son, et al., 2013). If the metabolic burden was lowered as an implication

of transfection, higher protein productions rates could also apply to very complex proteins like EPO or HubChe. An overall enhanced production of target proteins in anti-miRNA engineered cells was discovered. Further investigations are needed to confirm these findings and check protein quality and cell specific protein productivity. Pertinent arguments, that a metabolic shift towards a more productive host cell line occurred, cannot be made as metabolic flux results did not provide confirming data on this matter.

Chapter 4

Overall Conclusion and Outlook

Engineering mammalian cells by alteration of miRNA patterns has high potential to successfully improve expression of recombinant proteins. Transient transfection of HEK 293T cells with various miRNAs did not bring conclusive results to either: deduce capabilities towards protein expression enhancement or develop a protocol for screening for this power. Investigations into cell lines with varying miRNA expression pattern did show slight adjustments with phenotypic properties. Prolonged cell viability and IVC, previously reported by Aliaksandr Druz, Son, et al. could be confirmed. Media experiments showed drastic opportunities to improve cellular performance. GLucose, lactate, glutamine and glutamate consumption and secretion rates showed significant variations but these differences could not be determined to have substantial impact on process achievements. Still, improved yields on all of these substances for anti-apoptotic cells do suggest less 'waste' of resources. However, the reason for this revised efficiency could not be clarified here with absolute certainty. More analysis will be needed to give more statistical information of ideal process set ups, e.g. metabolic flux analysis of exponential and stationary phase, as stationary phase is the actual time of product formation. Future applications for this line of research could include further optimizations of media, possibly in combination with Biolog's phenotypic microarrays, where various substrates could show cell line specific usage profiles. Subsequently, a industrially scaled application could be investigated. All of the experiments focused on a stable or transient transfection of a single miRNA. A worthwhile approach could be to combine alterations of promising miRNAs or even miRNA clusters, to enhance positive effects like robustness or expression capacities.

Chapter 5

References

Ahn, Woo Suk and Maciek R. Antoniewicz (2011). "Metabolic Flux Analysis of CHO Cells at Growth and Non-Growth Phases Using Isotopic Tracers and Mass Spectrometry". en. In: *Metabolic Engineering* 13.5, pp. 598–609.

— (2012). "Towards Dynamic Metabolic Flux Analysis in CHO Cell Cultures". en. In: *Biotechnology Journal* 7.1, pp. 61–74.

Altamirano, Claudia et al. (2013). "Advances in Improving Mammalian Cells Metabolism for Recombinant Protein Production". In: *Electronic Journal of Biotechnology* 16.3.

Altamirano, C et al. (2004). "Strategies for Fed-Batch Cultivation of t-PA Producing CHO Cells: Substitution of Glucose and Glutamine and Rational Design of Culture Medium". en. In: *Journal of Biotechnology* 110.2, pp. 171–179.

Andersen, Joshua L. and Sally Kornbluth (2013). "The Tangled Circuitry of Metabolism and Apoptosis". In: *Mol Cell* 49.3, pp. 399–410.

Antoniewicz, Maciek R., Joanne K. Kelleher, and Gregory Stephanopoulos (2006). "Determination of Confidence Intervals of Metabolic Fluxes Estimated from Stable Isotope Measurements". en. In: *Metabolic Engineering* 8.4, pp. 324–337.

— (2007). "Elementary Metabolite Units (EMU): A Novel Framework for Modeling Isotopic Distributions". In: *Metabolic engineering* 9.1, pp. 68–86.

Arden, Nilou and M. J. Betenbaugh (2006). "Regulating Apoptosis in Mammalian Cell Cultures". en. In: *Cytotechnology* 50.1-3, pp. 77–92.

Baeshen, Nabih A. et al. (2014). "Cell Factories for Insulin Production". In: *Microbial Cell Factories* 13, p. 141.

Bandaranayake, Ashok D. and Steven C. Almo (2014). "Recent Advances in Mammalian Protein Production". en. In: *FEBS Letters* 588.2, pp. 253–260.

Barron, Niall et al. (2012). "MicroRNAs as Potential Engineering Targets for Improvement of CHO Cell Production Phenotypes". en. In: *Proceedings of the 21st Annual Meeting of the European Society for Animal Cell Technology (ESACT), Dublin, Ireland, June 7-10, 2009*. Ed. by Nigel Jenkins, Niall Barron, and Paula Alves. ESACT Proceedings 5. Springer Netherlands, pp. 3–11.

Barron, N. et al. (2011). "Engineering CHO Cell Growth and Recombinant Protein Productivity by Overexpression of miR-7". en. In: *Journal of Biotechnology* 151.2, pp. 204–211.

BD Biosciences Accuri C6 Personal Flow Cytometer - Applications - Gene Expression (2014). `https://www.bdbiosciences.com/instruments/accuri/applications/geneexpression.jsp`.

Berting, Andreas, Maria R. Farcet, and Thomas R. Kreil (2010). "Virus Susceptibility of Chinese Hamster Ovary (CHO) Cells and Detection of Viral Contaminations by Adventitious Agent Testing". en. In: *Biotechnology and Bioengineering* 106.4, pp. 598–607.

Best, Adam (2014). *Understanding MFI in the Context of FACS Data*.

Bochner, Barry R. (2014). *Private Communication*.

Bochner, Barry R. et al. (2011). "Assay of the Multiple Energy-Producing Pathways of Mammalian Cells". en. In: *PLoS ONE* 6.3. Ed. by Daniel Tomé, e18147.

Brunner, Daniel et al. (2010). "Serum-Free Cell Culture: The Serum-Free Media Interactive Online Database". In: *Altex* 27.1, p. 53.

Buescher, Joerg M. et al. (2015). "A Roadmap for Interpreting 13 C Metabolite Labeling Patterns from Cells". In: *Current opinion in biotechnology* 34, pp. 189–201.

Chiang, Gisela G. and William P. Sisk (2005). "Bcl-xL Mediates Increased Production of Humanized Monoclonal Antibodies in Chinese Hamster Ovary Cells". en. In: *Biotechnology and Bioengineering* 91.7, pp. 779–792.

Chinese Hamster (2016). en. Page Version ID: 728965598.

Chmiel, Horst, ed. (2011). *Bioprozesstechnik*. ger. 3., neu bearb. Aufl. OCLC: 846492080. Heidelberg: Spektrum, Akad. Verl.

Cohen, Stanley N. et al. (1973). "Construction of Biologically Functional Bacterial Plasmids in Vitro". In: *Proceedings of the National Academy of Sciences* 70.11, pp. 3240–3244.

Davies, Derek (2017). *Data Analysis*. `http://www.cyto.purdue.edu/cdroms/cyto3/8/data/icrf/stats.htm`.

de Lourdes Velez Suberbie, Maria (2013). "Characterisation of the Bioreactor Environment and Its Effect on Mammalian Cell Performance in Suspension

Culture during Antibody Production". PhD thesis. University College London.

Definition of Statistics (2017). `http://www.flowjo.com/v76/en/statdefinitions.html`.

Dorai, Haimanti et al. (2009). "Expression of Anti-Apoptosis Genes Alters Lactate Metabolism of Chinese Hamster Ovary Cells in Culture". In: *Biotechnol. Bioeng.* 103.3, pp. 592–608.

Druz, A., M. Betenbaugh, and J. Shiloach (2012). "Glucose Depletion Activates Mmu-miR-466h-5p Expression through Oxidative Stress and Inhibition of Histone Deacetylation". en. In: *Nucleic Acids Research* 40.15, pp. 7291–7302.

Druz, Aliaksandr (2012). "Utilizaton of MicroRNAs to Engineer Apoptosis in Mammalian Cells". PhD thesis.

Druz, Aliaksandr, Young–Jin Son, et al. (2013). "Stable Inhibition of Mmu-miR-466h-5p Improves Apoptosis Resistance and Protein Production in CHO Cells". en. In: *Metabolic Engineering* 16, pp. 87–94.

Druz, Aliaksandr et al. (2011a). "A Novel microRNA Mmu-miR-466h Affects Apoptosis Regulation in Mammalian Cells". en. In: *Biotechnology and Bioengineering* 108.7, pp. 1651–1661.

— (2011b). "A Novel microRNA Mmu-miR-466h Affects Apoptosis Regulation in Mammalian Cells". en. In: *Biotechnology and Bioengineering* 108.7, pp. 1651–1661.

Dyson, Michael R. (2016). "Fundamentals of Expression in Mammalian Cells". en. In: *Advanced Technologies for Protein Complex Production and Characterization*. Ed. by M. Cristina Vega. Advances in Experimental Medicine and Biology 896. Springer International Publishing, pp. 217–224.

Elmore, Susan (2007). "Apoptosis: A Review of Programmed Cell Death". en. In: *Toxicologic Pathology* 35.4, pp. 495–516.

Fan, Yuzhou et al. (2015). "Amino Acid and Glucose Metabolism in Fed-Batch CHO Cell Culture Affects Antibody Production and Glycosylation". en. In: *Biotechnol. Bioeng.* 112.3, pp. 521–535.

Felekkis, K et al. (2010). "microRNAs: A Newly Described Class of Encoded Molecules That Play a Role in Health and Disease". In: *Hippokratia* 14.4, pp. 236–240.

Fernandez, Osman, Julio C. Dustet, and Ernesto Chico (2012). "Modelo Matematico Del Metabolismo de Las Celulas CHO En La Sintesis de Eritropoyetina Humana Para Aplicar La Tecnica de Analisis de Flujos Metabolicos". In: *Biotecnologia Aplicada* 29.4, pp. 246–252.

Figueroa, Bruno et al. (2001). "Comparison of Bcl-2 to a Bcl-2 Deletion Mutant for Mammalian Cells Exposed to Culture Insults". en. In: *Biotechnology and Bioengineering* 73.3, pp. 211–222.

Glacken, M. W., E. Adema, and A. J. Sinskey (1988). "Mathematical Descriptions of Hybridoma Culture Kinetics: I. Initial Metabolic Rates". en. In: *Biotechnology and Bioengineering* 32.4, pp. 491–506.

Glacken, M. W., R. J. Fleischaker, and A. J. Sinskey (1986). "Reduction of Waste Product Excretion via Nutrient Control: Possible Strategies for Maximizing Product and Cell Yields on Serum in Cultures of Mammalian Cells". en. In: *Biotechnol. Bioeng.* 28.9, pp. 1376–1389.

Goswami, J. et al. (1999). "Apoptosis in Batch Cultures of Chinese Hamster Ovary Cells". en. In: *Biotechnol. Bioeng.* 62.6, pp. 632–640.

Gregory Hamilton, W. and Richard G. Ham (1977). "Clonal Growth of Chinese Hamster Cell Lines in Protein-Free Media". en. In: *In Vitro* 13.9, pp. 537–547.

Gupta, Sanjeev et al. (2010). "Mechanisms of ER Stress-Mediated Mitochondrial Membrane Permeabilization". en. In: *International Journal of Cell Biology* 2010, pp. 1–9.

Hackl, Matthias, Nicole Borth, and Johannes Grillari (2012). "miRNAs–pathway Engineering of CHO Cell Factories That Avoids Translational Burdening". In: *Trends in biotechnology* 30.8, pp. 405–406.

Hackl, Matthias, Ursula Heilmeier, et al. (2016). "Circulating microRNAs as Novel Biomarkers for Bone Diseases – Complex Signatures for Multifactorial Diseases?" en. In: *Molecular and Cellular Endocrinology* 432, pp. 83–95.

Hassell, T., S. Gleave, and M. Butler (1991). "Growth Inhibition in Animal Cell Culture. The Effect of Lactate and Ammonia". eng. In: *Appl. Biochem. Biotechnol.* 30.1, pp. 29–41.

Henderson, Nicholas Wayne (2016). "Carbon Labeling for Metabolic Flux Analysis". In:

Herzenberg, Leonore A. et al. (2006). "Interpreting Flow Cytometry Data: A Guide for the Perplexed". In: *Nature immunology* 7.7, pp. 681–685.

Inc., Biolog (2017). *Phenotype MicroArrays for Mammalian Cells.* `http://www.biolog.com/products-static/phenotype_mammalian_cells_overview.php`.

Jadhav, Vaibhav et al. (2013). "CHO microRNA Engineering Is Growing up: Recent Successes and Future Challenges". en. In: *Biotechnology Advances* 31.8, pp. 1501–1513.

Jayapal, KP et al. (2016). "Recombinant Protein Therapeutics from CHO Cells - 20 Years and Counting". In: *Chemical Engineering Progress* 103, p. 40.

Jelkmann, W. (2007). "Recombinant EPO Production Points the Nephrologist Should Know". en. In: *Nephrology Dialysis Transplantation* 22.10, pp. 2749–2753.

Jenkins, Nigel (2007). "Modifications of Therapeutic Proteins: Challenges and Prospects". en. In: *Cytotechnology* 53.1-3, pp. 121–125.

Kim, Jee Yon, Yeon-Gu Kim, and Gyun Min Lee (2012). "CHO Cells in Biotechnology for Production of Recombinant Proteins: Current State and Further Potential". eng. In: *Appl. Microbiol. Biotechnol.* 93.3, pp. 917–930.

Kim, Sung Hyun and Gyun Min Lee (2007). "Down-Regulation of Lactate Dehydrogenase-A by siRNAs for Reduced Lactic Acid Formation of Chinese Hamster Ovary Cells Producing Thrombopoietin". en. In: *Appl Microbiol Biotechnol* 74.1, pp. 152–159.

Klein, Tobias et al. (2015). "Quantification of Cell Lysis during CHO Bioprocesses: Impact on Cell Count, Growth Kinetics and Productivity". en. In: *Journal of Biotechnology* 207, pp. 67–76.

Kurano, N. et al. (1990). "Growth Behavior of Chinese Hamster Ovary Cells in a Compact Loop Bioreactor. 2. Effects of Medium Components and Waste Products". In: *Journal of biotechnology* 15.1, pp. 113–128.

Lai, Tingfeng, Yuansheng Yang, and Say Ng (2013). "Advances in Mammalian Cell Line Development Technologies for Recombinant Protein Production". en. In: *Pharmaceuticals* 6.5, pp. 579–603.

Lao, Mio-Sam and Derek Toth (1997). "Effects of Ammonium and Lactate on Growth and Metabolism of a Recombinant Chinese Hamster Ovary Cell Culture". In: *Biotechnology progress* 13.5, pp. 688–691.

Le, Huong et al. (2012). "Multivariate Analysis of Cell Culture Bioprocess Data—Lactate Consumption as Process Indicator". en. In: *Journal of Biotechnology* 162.2-3, pp. 210–223.

Lewis, Nathan E et al. (2013). "Genomic Landscapes of Chinese Hamster Ovary Cell Lines as Revealed by the Cricetulus Griseus Draft Genome". In: *Nature Biotechnology* 31.8, pp. 759–765.

Li, Feng et al. (2010). "Cell Culture Processes for Monoclonal Antibody Production". In: *MAbs* 2.5, pp. 466–477.

Lianidou, Evi, Athina Markou, and Martha Zavridou (2015). "MicroRNA Signatures as Clinical Biomarkers in Lung Cancer". English. In: *Current Biomarker Findings*.

Llaneras, F. and J. Picó (2007a). "An Interval Approach for Dealing with Flux Distributions and Elementary Modes Activity Patterns". In: *Journal of Theoretical Biology* 246.2, pp. 290–308.

— (2007b). "An Interval Approach for Dealing with Flux Distributions and Elementary Modes Activity Patterns". en. In: *Journal of Theoretical Biology* 246.2, pp. 290–308.

Lottspeich, Friedrich and Joachim W. Engels (2012). *Bioanalytik*. de. Google-Books-ID: RQxstwAACAAJ. Spektrum Akademischer Verlag.

Majors, Brian S., Michael J. Betenbaugh, and Gisela G. Chiang (2007). "Links between Metabolism and Apoptosis in Mammalian Cells: Applications for Anti-Apoptosis Engineering". In: *Metabolic Engineering* 9.4, pp. 317–326.

McAtee, Allison G, Lara J Jazmin, and Jamey D Young (2015). "Application of Isotope Labeling Experiments and 13C Flux Analysis to Enable Rational Pathway Engineering". en. In: *Current Opinion in Biotechnology* 36, pp. 50–56.

Metallo, Christian M., Jason L. Walther, and Gregory Stephanopoulos (2009). "Evaluation of 13C Isotopic Tracers for Metabolic Flux Analysis in Mammalian Cells". en. In: *Journal of Biotechnology* 144.3, pp. 167–174.

Miebach, Stephan (2012). "Charakterisierung Und Validierung Der 13C-Stoffflussanalyse Im Parallelansatz". PhD thesis. Universitätsbibliothek Bielefeld, Hochschulschriften.

Mullen, Andrew R., Zeping Hu, et al. (2014). "Oxidation of Alpha-Ketoglutarate Is Required for Reductive Carboxylation in Cancer Cells with Mitochondrial Defects". In: *Cell Rep* 7.5, pp. 1679–1690.

Mullen, Andrew R., William W. Wheaton, et al. (2012). "Reductive Carboxylation Supports Growth in Tumour Cells with Defective Mitochondria". en. In: *Nature* 481.7381, pp. 385–388.

Müller, Dethardt, Hermann Katinger, and Johannes Grillari (2008). "MicroRNAs as Targets for Engineering of CHO Cell Factories". en. In: *Trends in Biotechnology* 26.7, pp. 359–365.

Murphy, Taylor A., Chi V. Dang, and Jamey D. Young (2013). "Isotopically Nonstationary 13C Flux Analysis of Myc-Induced Metabolic Reprogramming in B-Cells". en. In: *Metabolic Engineering* 15, pp. 206–217.

Murphy, Taylor A and Jamey D Young (2013). "ETA: Robust Software for Determination of Cell Specific Rates from Extracellular Time Courses". In: *Biotechnology and bioengineering* 110.6, 10.1002/bit.24836.

Nakamura, Tsuyoshi and Takeshi Omasa (2015). "Optimization of Cell Line Development in the GS-CHO Expression System Using a High-Throughput, Single Cell-Based Clone Selection System". eng. In: *J. Biosci. Bioeng.* 120.3, pp. 323–329.

Neff, A. (2016). *Fetal Bovine Serum RNA Interferes with Cell-Culture-Derived Extracellular RNA*. `http://exrna.org/fetal-bovine-serum-rna-interferes-with-cell-culture-derived-extracellular-rna/`.

Niklas, Jens and Elmar Heinzle (2011). "Metabolic Flux Analysis in Systems Biology of Mammalian Cells". In: *Genomics and Systems Biology of Mammalian Cell Culture*. Ed. by Wei Shou Hu and An-Ping Zeng. Berlin, Heidelberg: Springer Berlin Heidelberg, pp. 109–132.

Nocon, Justyna et al. (2016). "Increasing Pentose Phosphate Pathway Flux Enhances Recombinant Protein Production in Pichia Pastoris". In: *Appl Microbiol Biotechnol* 100, pp. 5955–5963.

Noh, K., P. Droste, and W. Wiechert (2015). "Visual Workflows for 13C-Metabolic Flux Analysis". en. In: *Bioinformatics* 31.3, pp. 346–354.

Ozturk, Sadettin S. and Bernhard O. Palsson (1990). "Chemical Decomposition of Glutamine in Cell Culture Media: Effect of Media Type, pH, and Serum Concentration". en. In: *Biotechnology Progress* 6.2, pp. 121–128.

Ozturk, Sadettin S., Mark R. Riley, and Bernhard O. Palsson (1992). "Effects of Ammonia and Lactate on Hybridoma Growth, Metabolism, and Antibody Production". en. In: *Biotechnology and Bioengineering* 39.4, pp. 418–431.

Pörtner, Ralf (2007). *Animal Cell Biotechnology: Methods and Protocols*. en. Google-Books-ID: oqs7CyFj0FUC. Springer Science & Business Media.

Provost, A. and G. Bastin (2004). "Dynamic Metabolic Modelling under the Balanced Growth Condition". en. In: *Journal of Process Control* 14.7, pp. 717–728.

Puck, Theodore T., Steven J. Cieciura, and Arthur Robinson (1958). "Genetics Of Somatic Mammalian Cells: III. Long - Term Cultivation Of Euploid Cells From Human And Animal Subjects". In: *J Exp Med* 108.6, pp. 945–956.

Quek, Lake-Ee et al. (2010). "Metabolic Flux Analysis in Mammalian Cell Culture". en. In: *Metabolic Engineering* 12.2, pp. 161–171.

Rajendra, Yashas, Divor Kiseljak, Lucia Baldi, David L Hacker, et al. (2011). "Influence of Glutamine on Transient and Stable Recombinant Protein Production in CHO and HEK-293 Cells". In: *BMC Proc* 5.Suppl 8, P35.

Rajendra, Yashas, Divor Kiseljak, Lucia Baldi, David L. Hacker, et al. (2012). "Reduced Glutamine Concentration Improves Protein Production in Growth-Arrested CHO-DG44 and HEK-293E Cells". en. In: *Biotechnol Lett* 34.4, pp. 619–626.

Reckermann, Marcus (Mon Apr 6 07:24:04 EST 1998). *Mean, Geo-Mean, Median - Summary*.

Riveros, Francisca Zamorano (2012). "Metabolic Flux Analysis of CHO Cell Cultures". PhD thesis. Université de Mons.

RNA Interference (RNAi) (2011). *RNA Interference (RNAi): By Nature Video*.

Rosano, German L. and Eduardo A. Ceccarelli (2014). "Recombinant Protein Expression in Escherichia Coli: Advances and Challenges". In: *Front Microbiol* 5.

Russmayer, H. (2016). "The Impact of Amino Acid Metabolism on Recombinant Protein Production in Pichia Pastoris". PhD thesis. BOKU Wien.

Sauer, Uwe (2006). "Metabolic Networks in Motion: 13C-Based Flux Analysis". In: *Molecular Systems Biology* 2.

Schmid, Rolf D. (2016). *Taschenatlas der Biotechnologie und Gentechnik*. de. Google-Books-ID: ziDSCwAAQBAJ. John Wiley & Sons.

Schrøder Kaas, C (2015). "Characterization of Chinese Hamster Ovary Cells Producing Coagulation Factor VIII Using Multi-Omics Tools". PhD thesis. Technical University of Denmark.

Selvarasu, Suresh et al. (2012). "Combined in Silico Modeling and Metabolomics Analysis to Characterize Fed-Batch CHO Cell Culture". en. In: *Biotechnol. Bioeng.* 109.6, pp. 1415–1429.

Sermeus, A and C Michiels (2011). "Reciprocal Influence of the P53 and the Hypoxic Pathways". In: *Cell Death and Disease* 2.5, e164.

Sobczyk, André, Flavien Carpentier, and Sébastien Paris (2008). "Transiently Produced Recombinant Proteins to Speed up the Decision-Making Process and Limit Risks". en. In: *Nature Methods* 5.11.

Soboleski, Mark R., Jason Oaks, and William P. Halford (2005). "Green Fluorescent Protein Is a Quantitative Reporter of Gene Expression in Individual Eukaryotic Cells." In: *FASEB J* 19.3, pp. 440–442.

Stenerson, Katherine K. (2015). *The Derivatization and Analysis of Amino Acids by GC-MS*. `http://www.sigmaaldrich.com/technical-documents/articles/reporter-us/the-derivatization.html`.

Stephanopoulos, George, Aristos A. Aristidou, and Jens Nielsen (1998). "The Essence of Metabolic Engineering". In: *Metabolic Engineering: Principles and Methodologies*. Academic press.

Stephanopoulos, Gregory N., Aristos A. Aristidou, and Jens Nielsen (1998a). "CHAPTER 8 - Metabolic Flux Analysis". In: *Metabolic Engineering*. San Diego: Academic Press, pp. 309–351.

— (1998b). "Comprehensive Models for Cellular Reactions". In: *Metabolic Engineering*. San Diego: Academic Press, pp. 81–114.

— (1998c). "Review of Cellular Metabolism". In: *Metabolic Engineering*. San Diego: Academic Press, pp. 21–79.

Swarup, Aditi et al. (2014). "Metabolic Network Reconstruction, Growth Characterization and 13C-Metabolic Flux Analysis of the Extremophile Thermus Thermophilus HB8". en. In: *Metabolic Engineering* 24, pp. 173–180.

Templeton, Neil et al. (2014). "The Impact of Anti-Apoptotic Gene Bcl-2d Expression on CHO Central Metabolism". en. In: *Metabolic Engineering* 25, pp. 92–102.

The Phenotype MicroArray Assay Technology For Optimizing Clone Selection (2016). `http://www.biolog.com/products-static/phenotype_mammalian_cells_bioprocess_improvement.php`.

Thomas, Philip and Trevor G. Smart (2005). "HEK293 Cell Line: A Vehicle for the Expression of Recombinant Proteins". In: *Journal of Pharmacological and*

Toxicological Methods. Electrophysiological Methods in Neuropharmacology 51.3, pp. 187–200.

TRIzol Reagent - Manuals & Protocols (2016). https://tools.thermofisher.com/content/sfs/manuals/trizol_reagent.pdf.

Tsao, Y.-S. et al. (2005). "Monitoring Chinese Hamster Ovary Cell Culture by the Analysis of Glucose and Lactate Metabolism". eng. In: *J. Biotechnol.* 118.3, pp. 316–327.

Varma, Amit and Bernhard O. Palsson (1994). "Metabolic Flux Balancing: Basic Concepts, Scientific and Practical Use". In: *Bio/Technology* 12.10, pp. 994–998.

Vasudevan, Shobha (2012). "Posttranscriptional Upregulation by MicroRNAs". en. In: *Wiley Interdisciplinary Reviews: RNA* 3.3, pp. 311–330.

Vidugiriene, Jolanta et al. (2008). "Getting the Most from Your Transfections: Increasing Throughput and Sensitivity". In: *Signal* 1.10, T14.

Voet, Donald and Judith G. Voet (2011). *Biochemistry*. 4th ed. OCLC: ocn690489261. Hoboken, NJ: John Wiley & Sons.

Wahid, Fazli et al. (2010). "MicroRNAs: Synthesis, Mechanism, Function, and Recent Clinical Trials". en. In: *Biochimica et Biophysica Acta (BBA) - Molecular Cell Research* 1803.11, pp. 1231–1243.

Walsh, Gary and Roy Jefferis (2006). "Post-Translational Modifications in the Context of Therapeutic Proteins". In: *Nature Biotechnology* 24.10, pp. 1241–1252.

Wang, Yu-Chieh, Suzanne E. Peterson, and Jeanne F. Loring (2014). "Protein Post-Translational Modifications and Regulation of Pluripotency in Human Stem Cells". In: *Cell research* 24.2, pp. 143–160.

Westphal, Dana et al. (2011). "Molecular Biology of Bax and Bak Activation and Action". In: *Biochimica et Biophysica Acta (BBA) - Molecular Cell Research*. Mitochondria: The Deadly Organelle 1813.4, pp. 521–531.

Wiechert, W. (2001). "13C Metabolic Flux Analysis". In: *Metabolic Eng* 3, pp. 195–206.

Wiechert, Wolfgang (2007). "The Thermodynamic Meaning of Metabolic Exchange Fluxes". In: *Biophys J* 93.6, pp. 2255–2264.

Winter, Julia et al. (2009). "Many Roads to Maturity: microRNA Biogenesis Pathways and Their Regulation". In: *Nature Cell Biology* 11.3, pp. 228–234.

Wurm, Florian (2013). "CHO Quasispecies—Implications for Manufacturing Processes". en. In: *Processes* 1.3, pp. 296–311.

Wurzel, Michael and Albert A. de Graaf (1999). "Bidirectional Reaction Steps in Metabolic Networks: III. Explicit Solution and Analysis of Isotopomer Labeling Systems". In: *BIOTECHNOLOGY AND BIOENGINEERING* 66.2.

Xiao, Su, Yu-Chi Chen, et al. (2015). "MiRNA Mimic Screen for Improved Expression of Functional Neurotensin Receptor from HEK 293 Cells: MiRNAs Improve Neurotensin Receptor Expression". en. In: *Biotechnology and Bioengineering* 112.8, pp. 1632–1643.

Xiao, Su, Joseph Shiloach, and Michael J Betenbaugh (2014). "Engineering Cells to Improve Protein Expression". en. In: *Current Opinion in Structural Biology* 26, pp. 32–38.

Xiao, Su, Jim F. White, et al. (2013). "Transient and Stable Expression of the Neurotensin Receptor NTS1: A Comparison of the Baculovirus-Insect Cell and the T-REx-293 Expression Systems". en. In: *PLoS ONE* 8.5. Ed. by Sadashiva Karnik, e63679.

Xu, Xun et al. (2011). "The Genomic Sequence of the Chinese Hamster Ovary (CHO)-K1 Cell Line". In: *Nature Biotechnology* 29.8, pp. 735–741.

Young, Jamey D (2013). "Metabolic Flux Rewiring in Mammalian Cell Cultures". en. In: *Current Opinion in Biotechnology* 24.6, pp. 1108–1115.

— (2014a). "13C Metabolic Flux Analysis of Recombinant Expression Hosts". en. In: *Current Opinion in Biotechnology* 30, pp. 238–245.

— (2014b). "INCA: A Computational Platform for Isotopically Non-Stationary Metabolic Flux Analysis". eng. In: *Bioinformatics* 30.9, pp. 1333–1335.

Zagari, Francesca et al. (2013). "Lactate Metabolism Shift in CHO Cell Culture: The Role of Mitochondrial Oxidative Activity". en. In: *New Biotechnology* 30.2, pp. 238–245.

Zamboni, Nicola et al. (2009). "13C-Based Metabolic Flux Analysis". In: *Nature Protocols* 4.6, pp. 878–892.

Zimmer, Marc (2015). *Illuminating Disease: An Introduction to Green Fluorescent Proteins*. en. Google-Books-ID: jX4ZBQAAQBAJ. Oxford University Press.

Chapter 6

Appendix

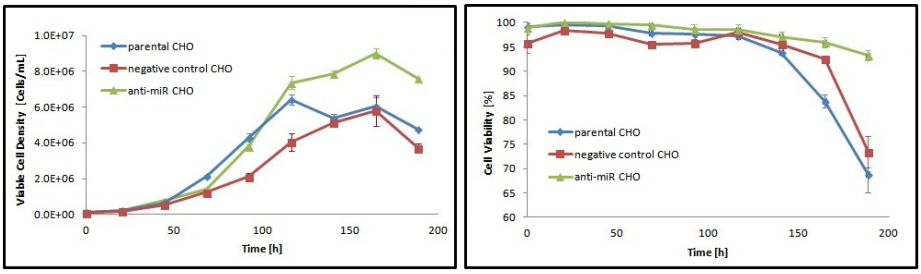

Figure 6.1: Growth and viability charts of CHO cell in CD OptiCHO with 8mM glutamin This media was not used due to immense alterations in initial glucose concentrations and therefore insufficient process data.

Table 6.1: Raw GC/MS results of massisotopomer distribution of essential amino acids

Ala260	0.5267	0.5159	0.5141	0.5139	0.5117	0.5371	0.5265	0.5302	0.7451
Ala261	0.1433	0.1537	0.1567	0.1483	0.1489	0.1468	0.1465	0.1435	0.1717
Ala262	0.1297	0.1325	0.1328	0.1344	0.1328	0.1266	0.1321	0.1291	0.0704
Ala263	0.1502	0.1489	0.1504	0.1549	0.1559	0.1458	0.1506	0.1504	0.0107
Ala232	0.5474	0.545	0.5409	0.5385	0.5359	0.5539	0.548	0.5439	0.7551
Ala233	0.1393	0.1415	0.1439	0.1398	0.1395	0.1399	0.1388	0.1414	0.1655
Ala234	0.2469	0.2468	0.2517	0.2537	0.2537	0.2409	0.2459	0.2473	0.0679
Gly246	0.7284	0.7241	0.7324	0.7245	0.7269	0.7316	0.7302	0.7266	0.7535
Gly247	0.1684	0.17	0.1674	0.1738	0.1703	0.168	0.1699	0.1712	0.1652
Gly248	0.0858	0.0897	0.0843	0.0866	0.0869	0.0834	0.0841	0.0846	0.0693

Ion	WT		NC			F9			Theory
Gly218	0.7289	0.7339	0.738	0.7346	0.7351	0.741	0.7377	0.7368	0.7636
Gly219	0.185	0.1829	0.1789	0.1793	0.18	0.176	0.1753	0.1784	0.1588
Pro286	0.7152	0.7097	0.7135	0.7103	0.708	0.7178	0.703	0.7333	0.7289
Pro287	0.1936	0.1966	0.1944	0.1915	0.192	0.1836	0.1847	0.1809	0.1842
Pro288	0.0727	0.0716	0.0724	0.0737	0.0743	0.0731	0.0762	0.0704	0.0726
Pro289	0.0185	0.0183	0.0183	0.0192	0.0171	0.0185	0.021	0.0155	0.012
Pro290	0	0.0038	0.0015	0.0053	0.0086	0.0066	0.0131	0	0.0021
Pro258	0.7398	0.7417	0.7387	0.7363	0.7321	0.7361	0.7391	0.735	0.7386
Pro259	0.1803	0.1775	0.1798	0.1816	0.183	0.18	0.1775	0.1799	0.1783
Pro260	0.0689	0.0717	0.0699	0.0706	0.0715	0.07	0.0708	0.071	0.0701
Pro261	0.0104	0.0091	0.0116	0.0104	0.012	0.0119	0.0115	0.0119	0.011
Pro262	0.0006	0	0	0.0011	0.0014	0.0018	0.0011	0.0015	0.0018
Pro184	0.8132	0.8106	0.8156	0.8119	0.8131	0.8136	0.8135	0.8149	0.7447
Pro185	0.1364	0.1384	0.1353	0.1372	0.137	0.1358	0.1382	0.1369	0.1979
Pro186	0.0419	0.0441	0.0412	0.0423	0.0404	0.0407	0.0403	0.0411	0.0494
Pro187	0.0054	0.0054	0.0051	0.0049	0.0049	0.0048	0.0055	0.0053	0.0072
Ser390	0.6082	0.6055	0.6074	0.6049	0.6087	0.6136	0.6097	0.605	0.6408
Ser391	0.2182	0.2217	0.2245	0.2266	0.2208	0.2208	0.2238	0.2247	0.224
Ser392	0.1138	0.1136	0.1128	0.1123	0.1148	0.113	0.1122	0.1149	0.1043
Ser393	0.0428	0.0431	0.0398	0.0405	0.04	0.0378	0.0398	0.0406	0.0242
Ser288	0.6834	0.6803	0.7441	0.7252	0.6858	0.6919	0.6964	0.7717	0.7221
Ser289	0.2004	0.1949	0.2207	0.2143	0.2056	0.1978	0.1965	0.2239	0.1907
Ser290	0.0957	0.0947	0.0333	0.0512	0.0885	0.091	0.0885	0	0.0726
Ser362	0.6173	0.6166	0.6136	0.6144	0.6153	0.6224	0.6178	0.6169	0.7205
Ser363	0.2175	0.2179	0.2208	0.2246	0.222	0.2189	0.2221	0.2222	0.1904
Ser364	0.1233	0.1238	0.1241	0.1208	0.1224	0.1198	0.1207	0.1209	0.0739
Ser302	0.8181	0.6898	0.7009	0.6913	0.703	0.7047	0.8617	0.98	0.7205
Ser303	0.0878	0.1873	0.178	0.1855	0.1821	0.1817	0.0647	0	0.1904
Ser304	0.0763	0.0981	0.0937	0.0983	0.0902	0.0894	0.0639	0	0.0739
Ser305	0.0072	0.0186	0.0183	0.0196	0.0177	0.0147	0.0035	0	0.0127

Ion	WT		NC			F9			Theory
Asp418	0.5613	0.5579	0.5517	0.5491	0.5437	0.5514	0.543	0.5378	0.6323
Asp419	0.2224	0.2267	0.2274	0.2263	0.2263	0.2227	0.2263	0.2256	0.2282
Asp420	0.1434	0.1424	0.1436	0.1443	0.148	0.1462	0.148	0.1489	0.1068
Asp421	0.0499	0.0496	0.0527	0.0543	0.0553	0.0532	0.055	0.0583	0.0255
Asp422	0.0171	0.018	0.0185	0.0193	0.0197	0.0195	0.0201	0.0216	0.0061
Asp423	0.0046	0.0046	0.0049	0.0054	0.0055	0.0055	0.0061	0.006	0.001
Asp424	0.0011	0.0008	0.0011	0.0012	0.0014	0.0013	0.0014	0.0015	0.0002
Asp390	0.5833	0.5773	0.5733	0.5705	0.5669	0.5738	0.5649	0.5612	0.6408
Asp391	0.2316	0.2349	0.235	0.236	0.2373	0.2316	0.2359	0.2362	0.224
Asp392	0.131	0.1322	0.1356	0.1368	0.1365	0.1361	0.1376	0.1392	0.1043
Asp393	0.039	0.0398	0.0408	0.0408	0.0423	0.0411	0.0433	0.0446	0.0242
Asp394	0.0122	0.013	0.0126	0.0129	0.0133	0.0135	0.0141	0.0145	0.0057
Asp395	0.0028	0.0026	0.0025	0.0027	0.0033	0.0033	0.0037	0.0036	0.0009
Asp396	0.0001	0.0002	0.0001	0.0002	0.0003	0.0005	0.0004	0.0007	0.0001
Asp376	0.5887	0.5884	0.5862	0.5783	0.5784	0.5818	0.5792	0.5729	0.648
Asp377	0.2337	0.2351	0.2382	0.235	0.2348	0.2359	0.236	0.2352	0.2192
Asp378	0.1318	0.1348	0.1365	0.1377	0.1379	0.1374	0.1408	0.1409	0.103
Asp379	0.0315	0.0322	0.0277	0.0361	0.0344	0.032	0.0321	0.036	0.0233
Asp380	0.0108	0.0095	0.0109	0.0112	0.0112	0.0099	0.0104	0.0117	0.0055
Asp302	0.6712	0.6758	0.6733	0.6645	0.6654	0.6685	0.6616	0.6589	0.7205
Asp303	0.1964	0.1943	0.1943	0.1974	0.1953	0.1963	0.1996	0.2009	0.1904
Asp304	0.1044	0.1035	0.1051	0.109	0.1091	0.1067	0.1086	0.1101	0.0739
Asp305	0.0214	0.0208	0.0216	0.0229	0.023	0.022	0.0229	0.0239	0.0127
Asp306	0.0055	0.0055	0.0057	0.0061	0.0059	0.0061	0.0062	0.0061	0.0022
Glu432	0.5256	0.5287	0.5142	0.4949	0.493	0.5228	0.5092	0.4985	0.6253
Glu433	0.2175	0.2156	0.2159	0.2148	0.2152	0.2141	0.2128	0.215	0.2327
Glu434	0.162	0.1623	0.1683	0.1754	0.176	0.1658	0.1713	0.173	0.1081
Glu435	0.0575	0.0566	0.0604	0.0674	0.0675	0.0576	0.0628	0.0661	0.0264
Glu436	0.0261	0.026	0.0288	0.033	0.033	0.0277	0.0304	0.0325	0.0063
Glu437	0.0084	0.0081	0.0092	0.0107	0.0111	0.0088	0.0098	0.0107	0.0011
Glu438	0.0023	0.0024	0.0027	0.0031	0.0033	0.0026	0.003	0.0032	0.0002
Glu439	0.0005	0.0004	0.0005	0.0007	0.0008	0.0006	0.0007	0.0008	0

Ion	WT		NC			F9			Theory
Glu330	0.5922	0.5958	0.5776	0.5561	0.5574	0.5882	0.5757	0.5653	0.7046
Glu331	0.2028	0.2014	0.2039	0.2093	0.2067	0.2	0.2009	0.2038	0.202
Glu332	0.1408	0.1405	0.1482	0.1557	0.1561	0.1449	0.1506	0.1536	0.0766
Glu333	0.0445	0.0434	0.0486	0.0544	0.0546	0.0457	0.0495	0.0523	0.0141
Glu334	0.0156	0.015	0.017	0.019	0.0195	0.0167	0.0182	0.0194	0.0024
Glu335	0.0035	0.0034	0.0039	0.0047	0.0047	0.0038	0.0042	0.0045	0.0003

Table 6.2: Complete set of experimentally determined fluxes of network model. Net ($\longmapsto$) and exchange ($\longleftrightarrow$) rates, including 95% confidence interval for internal biochemical reactions of parental, negative control and anti-466h-miRNA cell line.

Glyc1	*gluc.c ->G6P.c*	243.2654	[225.4, 261.1]	209.7773	[199.2, 220.3]	202.7344	[193, 212.5]
Glyc2 net	*G6P.c <->F6P.c*	181.268	[137.5, 260.1]	127.5352	[112.1, 160.7]	151.0286	[128.1, 224.8]
Glyc2 exch	*G6P.c <->F6P.c*	1.00E+07	[0, Inf]	1.15E+06	[0, Inf]	9.49E+05	[0, Inf]
Glyc3	*F6P.c ->F16BP.c*	214.4009	[191.3, 256.4]	176.5759	[166.3, 190.4]	178.4007	[166.1, 224.8]
Glyc4 net	*F16BP.c <->DHAP.c + GAP.c*	214.4009	[191.3, 256.4]	176.5759	[166.3, 190.4]	178.4007	[166.1, 224.8]
Glyc4 exch	*F16BP.c <->DHAP.c + GAP.c*	3.4171	[0, Inf]	7.2537	[0, Inf]	2.0505	[0, Inf]
Glyc5 net	*DHAP.c <->GAP.c*	211.5029	[188.4, 253.5]	174.5302	[164.2, 188.3]	175.8915	[163.6, 199.7]
Glyc5 exch	*DHAP.c <->GAP.c*	1.00E+07	[0, Inf]	4.42E+05	[0, Inf]	5.95E+05	[0, Inf]
Glyc6 net	*GAP.c <->G3P.c*	442.4703	[403.3, 508.1]	375.6264	[355.3, 396.9]	367.9783	[346.6, 391]
Glyc6 exch	*GAP.c <->G3P.c*	5.4522	[0, Inf]	1.00E-07	[0, Inf]	1.24E+00	[0, Inf]
Glyc7 net	*G3P.c <->PEP.c*	418.1757	[381.1, 508.1]	360.4847	[340.8, 381.8]	352.3033	[330.4, 391]
Glyc7 exch	*G3P.c <->PEP.c*	1.00E-07	[0, Inf]	1.00E-07	[0, Inf]	7.27E-01	[0, Inf]
Glyc8	*PEP.c ->Pyr.c*	418.1757	[381.1, 535.7]	360.4847	[340.8, 413.6]	352.3033	[330.4, 380.8]
Lac Prod	*Pyr.c ->Lac.c*	442	[415, 469]	335	[316.8, 353.2]	370.0042	[352.8, 387.2]
TCA1	*Pyr.m ->CO2.m + AcCoA.m*	81.309	[76.9, 89]	62.9501	[57.9, 69]	66.2459	[60.4, 72.3]
TCA2 net	*AcCoA.m + Oxa.m <->Cit.m*	81.309	[76.9, 89]	62.9501	[57.9, 69]	66.2459	[60.4, 72.3]
TCA2 exch	*AcCoA.m + Oxa.m <->Cit.m*	1.00E-07	[0, Inf]	1.00E-07	[0, Inf]	1.00E-07	[0, Inf]
TCA3	*Pyr.m + CO2.m ->Oxa.m*	3.3941	[0.7, 5.6]	9.4358	[6.6, 11.8]	5.4464	[2.5, 7.9]
TCA4 net	*Cit.m <->Ict.m*	19.2385	[-13.4, 25.3]	-7.4086	[-11.5, 22.2]	-4.5875	[-10.5, 15.8]
TCA4 exch	*Cit.m <->Ict.m*	49.822	[0, 656]	10.5973	[0, Inf]	13.9712	[0, Inf]
TCA5 net	*Ict.m <->AKG.m + CO2.m*	19.2385	[-13.4, 25.3]	-7.4086	[-11.5, 22.2]	-4.5875	[-10.5, 15.8]
TCA5 exch	*Ict.m <->AKG.m + CO2.m*	15.247	[0, 27.7]	1.00E-07	[0, Inf]	1.00E-07	[0, Inf]

		WT		NC		F9	
Flux ID	***Biochemical Reaction***	**Flux Value**	**Interval**	**Flux Value**	**Interval**	**Flux Value**	**Interval**
TCA6	*AKG.m ->Suc.m + CO2.m*	66.2656	[60.6, 75.2]	63.9685	[58, 70.7]	33.2895	[27.5, 39.4]
TCA7 net	*Suc.m <->Fum.m*	66.2656	[60.6, 75.2]	63.9685	[58, 70.7]	33.2895	[27.5, 39.4]
TCA7 exch	*Suc.m <->Fum.m*	300.7024	[0, Inf]	24.7724	[0, Inf]	33.0995	[0, Inf]
TCA8 net	*Fum.m <->Mal.m*	66.2656	[60.6, 75.2]	63.9685	[58, 70.7]	33.2895	[27.5, 39.4]
TCA8 exch	*Fum.m <->Mal.m*	1.00E+07	[0, Inf]	1.00E-07	[0, Inf]	1.00E-07	[0, Inf]
TCA9 net	*Mal.m <->Oxa.m*	66.2656	[10.2, 133.6]	6.36E-12	[-15.1, 70.8]	3.96E-13	[0, Inf]
TCA9 exch	*Mal.m <->Oxa.m*	1.00E+07	[0, Inf]	1.00E-07	[0, 15]	1.00E-07	[0, Inf]
TCA10	*Mal.m ->Pyr.m + CO2.m*	1.00E-07	[0, 13.4]	1.00E-07	[0, 12.2]	4.69E+00	[0, 10.4]
R20	*Oxa.c ->PEP.c + CO2.c*	1.00E-07	[0, 32.7]	1.00E-07	[0, 32.3]	1.00E-07	[0, 10.7]
R21	*G6P.c ->Ru5P.c + CO2.c*	55.188	[0, 97.8]	77.4354	[45, 92.2]	45.8102	[0, 67.7]
R22 net	*Ru5P.c <->R5P.c*	22.0551	[5.3, 36.3]	28.3947	[17.6, 33.3]	18.4381	[3.1, 25.7]
R22 exch	*Ru5P.c <->R5P.c*	3.7306	[0, Inf]	0.0348	[0, Inf]	2.8286	[0, Inf]
R23 net	*Ru5P.c <->X5P.c*	33.133	[-3.9, 61.1]	49.0407	[27.4, 58.9]	27.3721	[-3.3, 41.7]
R23 exch	*Ru5P.c <->X5P.c*	1.00E+07	[0, Inf]	1.00E-07	[0, Inf]	7.86E+00	[0, Inf]
R24 net	*X5P.c + R5P.c <->GAP.c + S7P.c*	16.5665	[-1.9, 30.5]	24.5203	[13.7, 29.4]	13.686	[-1.6, 20.9]
R24 exch	*X5P.c + R5P.c <->GAP.c + S7P.c*	1.00E-07	[0, Inf]	2.97E+03	[0, Inf]	1.00E-07	[0, Inf]
R25 net	*X5P.c + E4P.c <->GAP.c + F6P.c*	16.5665	[-1.9, 30.5]	24.5203	[13.7, 29.4]	13.686	[-1.6, 20.9]
R25 exch	*X5P.c + E4P.c <->GAP.c + F6P.c*	106.6349	[0, 172.7]	103.6777	[0, 151.5]	54.0305	[0, 106.7]
R26 net	*S7P.c + GAP.c <->F6P.c + E4P.c*	16.5665	[-1.9, 30.5]	24.5203	[13.7, 29.4]	13.686	[-1.6, 20.9]
R26 exch	*S7P.c + GAP.c <->F6P.c + E4P.c*	1.00E-07	[0, Inf]	1.00E-07	[0, Inf]	1.00E-07	[0, Inf]
R29 net	*Cit.c <->Ict.c*	3.9112	[0.6, 39.2]	29.3042	[0.5, 33.8]	20.4786	[-0.7, 35.7]

		WT		NC		F9	
Flux ID	***Biochemical Reaction***	**Flux Value**	**Interval**	**Flux Value**	**Interval**	**Flux Value**	**Interval**
R29 exch	*Cit.c <-> Ict.c*	1.00E-07	[0, Inf]	1.00E-07	[0, Inf]	1.00E-07	[0, Inf]
R30 net	*Ict.c <-> AKG.c + CO2.c*	3.9112	[0.6, 39.2]	29.3042	[0.5, 33.8]	20.4786	[-0.7, 41.7]
R30 exch	*Ict.c <-> AKG.c + CO2.c*	1.00E-07	[0, Inf]	3.3184	[0, Inf]	3.652	[0, Inf]
R31	*Cit.c -> AcCoA.c + Oxa.c*	58.1593	[55.6, 60.8]	41.0544	[39.2, 42.9]	50.3547	[48.5, 52.2]
R32 net	*Oxa.c <-> Mal.c*	5.01E-09	[-55.2, 66.9]	-63.9685	[-80.3, 6.3]	-28.5951	[0, Inf]
R32 exch	*Oxa.c <-> Mal.c*	103.2322	[0, Inf]	-7.42E-06	[0, Inf]	4.06E+05	[0, Inf]
R33	*Gln.m -> Glu.m*	62.2028	[58.7, 302.7]	130.1476	[55.7, 148.8]	79.1754	[32.1, 121.5]
R34	*Glu.c -> Gln.c*	1.00E-07	[0, 196.3]	71.5613	[0, 89.3]	45.4056	[0, 87.6]
R35 net	*AKG.m <-> Glu.m*	-62.2028	[-259.3, 96.4]	-73.1096	[-148.8, 12.4]	-39.6287	[-121.9, 31.7]
R35 exch	*AKG.m <-> Glu.m*	2.84E+03	[0, Inf]	124.8959	[0, Inf]	132.1067	[0, Inf]
R36 net	*Ser.c <-> Gly.c + C1.c*	3.182	[3, 3.3]	2.2462	[2.1, 2.3]	2.755	[2.7, 2.9]
R36 exch	*Ser.c <-> Gly.c + C1.c*	54.7196	[38.9, 71.8]	53.984	[33.9, 84.2]	54.9155	[38.9, 77.6]
R37 net	*Ser.c <-> Pyr.c*	174.8975	[103.8, 193.6]	121.1117	[106.6, 133.1]	137.3575	[125.8, 165]
R37 exch	*Ser.c <-> Pyr.c*	1.00E-07	[0, 4.2]	0.0634	[0, 2.7]	1.00E-07	[0, 27.5]
R38 net	*Ala.m <-> Pyr.m*	-66.3701	[-129.4, -13.9]	-74.2105	[-111.2, -40.8]	-52.6587	[-102.1, -12]
R38 exch	*Ala.m <-> Pyr.m*	1.00E-07	[0, Inf]	288.2099	[0, Inf]	204.8268	[0, Inf]
R39	*Asp.c -> Asn.c*	6.7865	[6.5, 7.1]	4.7906	[4.6, 5]	5.8758	[5.7, 6.1]
R40 net	*Asp.c <-> Oxa.c*	-58.1593	[-113.5, 23.1]	-105.0229	[-121.5, -19.1]	-78.9498	[0, Inf]
R40 exch	*Asp.c <-> Oxa.c*	1.4283	[0, Inf]	2.9802	[0, Inf]	4.4059	[0, Inf]
CO2 Ex 1 net	*CO2.m <-> CO2.c*	163.419	[125.6, 196.2]	110.0741	[98.8, 150]	94.1959	[78.2, 120.7]
CO2 Ex 1 exch	*CO2.m <-> CO2.c*	1.00E-07	[0, Inf]	1.46E+06	[262.3, Inf]	3.52E+05	[0, Inf]

		WT		NC		F9	
Flux ID	***Biochemical Reaction***	**Flux Value**	**Interval**	**Flux Value**	**Interval**	**Flux Value**	**Interval**
CO2 Ex 2	*CO2.c -> CO2.e*	219.8539	[146.8, 272.2]	214.933	[174.6, 243.3]	158.1778	[96.8, 187.2]
Glucose Uptake	*gluc.e -> gluc.c*	243.2654	[225.4, 261.1]	209.7773	[199.2, 220.3]	202.7344	[193, 212.5]
Ala Secr	*Ala.c -> Ala.e*	52.2337	[0, 115.3]	64.2317	[30.7, 101.2]	40.4193	[0, 82.8]
Asp Secr	*Asp.c -> Asp.e*	28.6093	[0, 33.3]	38.8726	[6.5, 43.4]	2.6518	[0, 5.8]
Glutamate Secr	*Glu.c -> Glu.e*	9.9938	[9.4, 10.5]	10.0947	[9.4, 10.8]	8.4986	[8.1, 8.9]
Arg Uptake	*Arg.e -> Arg.c*	8.8838	[8.5, 9.3]	6.271	[6, 6.6]	7.6916	[7.4, 8]
R50	*Cys.e -> Cys.c*	3.4165	[3.3, 3.6]	2.4117	[2.3, 2.5]	2.958	[2.8, 3.1]
Glutamine Uptake	*Gln.e -> Gln.c*	69.7886	[66.3, 73.3]	63.9412	[61, 66.9]	40.3376	[38.7, 42]
Gly Uptake	*Gly.e -> Gly.c*	13.9499	[13.3, 14.6]	9.8472	[9.4, 10.3]	12.0779	[11.6, 12.5]
His Uptake	*His.e -> His.c*	3.3693	[3.2, 3.5]	2.3784	[2.3, 2.5]	2.9171	[2.8, 3]
Ile Uptake	*Ile.e -> Ile.c*	7.6353	[7.3, 8]	5.3897	[5.1, 5.6]	6.6107	[6.4, 6.9]
Leu Uptake	*Leu.e -> Leu.c*	13.2876	[12.7, 13.9]	9.3796	[9, 9.8]	11.5045	[11.1, 11.9]
Lys Uptake	*Lys.e -> Lys.c*	13.4284	[12.8, 14]	9.4791	[9, 9.9]	11.6264	[11.2, 12.1]
Met Uptake	*Met.e -> Met.c*	3.2513	[3.1, 3.4]	2.2951	[2.2, 2.4]	2.815	[2.7, 2.9]
Phe Uptake	*Phe.e -> Phe.c*	5.1613	[4.9, 5.4]	3.6433	[3.5, 3.8]	4.4686	[4.3, 4.6]
Pro Uptake	*Pro.e -> Pro.c*	7.3727	[7, 7.7]	5.2043	[5, 5.4]	6.3833	[6.1, 6.6]
Ser Uptake	*Ser.e -> Ser.c*	164.5985	[109.9, 181.1]	115.8494	[85.1, 126.6]	133.7999	[101.6, 158.8]
Tyr Uptake	*Tyr.e -> Tyr.c*	4.2896	[4.1, 4.5]	3.028	[2.9, 3.2]	3.714	[3.6, 3.9]
Trp Uptake	*Trp.e -> Trp.c*	461.4831	[0, Inf]	43.7456	[0, Inf]	16.5037	[0, Inf]
Thr Uptake	*Thr.e -> Thr.c*	9.0931	[8.7, 9.5]	6.4188	[6.1, 6.7]	7.8729	[7.6, 8.2]

		WT		NC		F9	
Flux ID	***Biochemical Reaction***	**Flux Value**	**Interval**	**Flux Value**	**Interval**	**Flux Value**	**Interval**
Val Uptake	*Val.e ->Val.c*	9.8011	[9.4, 10.2]	6.9185	[6.6, 7.2]	8.4858	[8.2, 8.8]
Lac Secretion	*Lac.c ->Lac.e*	442	[415, 469]	335	[316.8, 353.2]	370.0042	[352.8, 387.2]
Pyr Mit Ex	*Pyr.c ->Pyr.m*	151.0732	[90.5, 268.5]	146.5964	[108, 181.5]	119.6566	[73.2, 166.9]
Cit Mit Ex	*Cit.m ->Cit.c*	62.0705	[58.3, 97.9]	70.3586	[40.7, 75]	70.8333	[49.1, 92.3]
Mal Mit Ex net	*Mal.m <->Pyr.c*	50.9	[-6.9, 55.3]	63.9685	[-6.3, 80.3]	28.5951	[0, Inf]
Mal Mit Ex exch	*Mal.m <->Mal.c*	1.00E-07	[0, Inf]	1.00E-07	[0, Inf]	5.17E+05	[0, Inf]
Gln Mit Ex net	*Gln.c <->Gln.m*	62.2028	[58.7, 302.7]	130.1476	[55.7, 148.8]	79.1754	[32.1, 121.5]
Gln Mit Ex exch	*Gln.c <->Gln.m*	0.0556	[0, Inf]	1.00E-07	[0, Inf]	1.00E-07	[0, Inf]
Glu Mit Ex net	*Glu.m <->Glu.c*	2.30E-12	[-174.3, 177.4]	57.038	[-81.3, 71.3]	39.5467	[-64, 75.4]
Glu Mit Ex exch	*Glu.m <->Glu.c*	1.00E-07	[0, 174.3]	1.00E-07	[0, 81.3]	1.00E-07	[0, 72]
R000 net	*Asp.m <->Oxa.m*	11.6492	[-55.2, Inf]	53.5143	[-15.3, 70.8]	60.7995	[0, Inf]
R000 exch	*Asp.m <->Oxa.m*	1.03E-07	[0, Inf]	1.00E-07	[0, Inf]	1.00E-07	[0, Inf]
R001 net	*AKG.c <->Glu.c*	19.0869	[-175.6, 215.4]	31.0368	[-54.7, 105.7]	22.2304	[-49.1, 104]
R001 exch	*AKG.c <->Glu.c*	1.08E-06	[0, Inf]	0.0037	[0, Inf]	1.00E-07	[0, Inf]
Ala Mit Ex net	*Ala.m <->Ala.c*	66.3701	[13.9, 129.4]	74.2105	[40.8, 111.2]	52.6587	[12, 102.1]
Ala Mit Ex exch	*Ala.m <->Ala.c*	1.00E-07	[0, Inf]	-2.50E-07	[0, Inf]	1.00E-07	[0, Inf]
Asp Mit Ex net	*Asp.m <->Asp.c*	-11.6492	[0, 55.2]	-53.5143	[-70.8, 15.3]	-60.7995	[0, Inf]
Asp Mit Ex exch	*Asp.m <->Asp.c*	1.00E-07	[0, Inf]	0.4836	[0, Inf]	2.2119	[0, Inf]
AKG Mit Ex net	*AKG.m <->AKG.c*	15.1756	[-174.3, 177.4]	1.7326	[-81.3, 77]	1.7517	[-71.9, 77.1]
AKG Mit Ex exch	*AKG.m <->AKG.c*	1.00E-07	[0, 174.3]	1.00E-07	[0, 81.3]	1.00E-07	[0, 72]

		WT		NC		F9	
Flux ID	***Biochemical Reaction***	**Flux Value**	**Interval**	**Flux Value**	**Interval**	**Flux Value**	**Interval**
Biomass	*144.2*R5P.c + 83.6*C1.c +70*CO2.c + 76.14*DHAP.c + 178.9*G6P.c + 1528*AcCoA.c + 371.4*Ala.c +233.4*Arg.c + 292*Asp.c + 178.3*Asn.c + 89.76*Cys.c + 199.3*Gln.c + 238.9*Glu.c + 450.1*Gly.c + 88.52*His.c + 200.6*Ile.c + 349.1*Leu.c + 352.8*Lys.c + 85.42*Met.c + 135.6*Phe.c + 193.7*Pro.c + 284.1*Ser.c + 238.9*Thr.c + 27.24*Try.c + 112.7*Tyr.c + 257.5*Val.c ->Biomass*	0.0381	[0.0364, 0.04]	0.0269	[0.026, 0.028]	0.033	[0.032, 0.034]
R002	*G3P.c ->Ser.c*	24.2946	[0, 27.2]	15.1417	[0, 17.1]	15.675	[0, 19]